McGILL UNIVERSITY

FLUID STRUCTURE INTERACTION (FSI) BASED WIND LOAD MODELING FOR DYNAMIC ANALYSIS OF OVERHEAD TRANSMISSION LINES

Hooman KEYHAN

Department of Civil Engineering and Applied Mechanics
McGill University
Montréal, Québec, Canada August 2012
Ph.D. Thesis

A manuscript-based thesis submitted to McGill University in partial fulfilment of the requirements of the degree of Ph.D. in Civil Engineering

Fluid Structure Interaction (FSI) Based Wind Load Modeling for Dynamic Analysis of Overhead Transmission Lines

Hooman KEYHAN

Supervisors:
PROFESSOR GHYSLAINE MCCLURE
Department of Civil Engineering and Applied Mechanics,
McGill University, Montréal, QC, Canada

PROFESSOR WAGDI G. HABASHI
Department of Mechanical Engineering,
McGill University, Montréal, QC, Canada

Department of Civil Engineering and Applied Mechanics
McGill University
Montréal, Québec, Canada 2012
Ph.D. Thesis

Fluid Structure Interaction (FSI) Based Wind Load Modeling for Dynamic Analysis of Overhead Transmission Lines

Hooman KEYHAN

Ph.D. Thesis
Department of Civil Engineering and Applied Mechanics
McGill University
Room 492, Macdonald Engineering Building, 817 Sherbrooke Street West
Montréal, Québec, H3A 2K6
Canada
Tel.: 514-398-6860
Fax: 514-398-7361

Cover:
4 circuit 230/132 kV line heavy angle split tower located in Tabriz, Iran, designed and constructed by Pars Sakhtar Inc.

Dedicated to my parents: Mahboubeh & Mahmoud & my beloved spouse Elnaz

For their everlasting love and devotion

Hooman KEYHAN
Department of Civil Engineering and Applied Mechanics
McGill University

ABSTRACT

Electricity is a crucial form of energy in our societies, and transmission lines are key elements to ensure the reliability of electric power grids. Continuity of service is the main preoccupation of electric utilities, and this continuity may be disrupted by a large variety of sources and accidents. Transmission lines, by their intrinsic topology, remain the grid components that are the most exposed to climatic sources of disruption.

The most common and important source of dynamic loads on transmission lines results from wind effects on the towers and conductors. Conductors are particularly sensitive to wind effects as they are long and relatively flexible (compared to their supports) and are literally wind-catching structures in the power grid infrastructure. In cold climates, wind and ice have compounding effects on lines and give rise to the most severe design loading conditions. Therefore accurate prediction of the wind pressure on overhead conductors is essential to conduct a reliable assessment of the line response, in terms of both electrical clearances and conductor loads transferred to supports. Spatial randomness of wind loads on overhead lines has already been addressed by stochastic analysis methods and is now taken into account in design with the use of so-called span factors. Further reasonable gains in wind load accuracy can be obtained by examining the physics of wind effects on conductors, in both non-iced and iced conditions, with improved predictions of lift and drag forces determined from fluid-structure interaction (FSI) analysis.

The traditional design method to apply wind load on transmission lines is to convert the design wind speed to a static pressure through Bernoulli's equation where the pressure is proportional to the air density and the squared wind speed. In this approach the fluid-structure interaction of wind and line components is ignored: wind is considered as a quasi-static load on conductors and supports, while special instability effects due to

particular wind conditions such as vortex shedding (Aeolian vibrations) and flutter (cable galloping) are accounted for separately with specific mitigation solutions if necessary.

In gusty wind conditions with high turbulence intensity, conductors may experience large horizontal displacements that affect their surrounding wind flow. A physically accurate wind load evaluation on conductors is possible by computational wind-structure interaction analysis. To date, largely due to its high computational cost and the lack of experimental data to validate computational models, an advanced fluid-structure analysis framework for wind-cable interaction has not been developed.

In this study a new approach based on FSI analysis to evaluate equivalent wind loads on conductors is developed. The first step in such an approach is accurate evaluation of wind pressure on conductor. For this purpose the FSI analysis is carried in two dimensions where the detailed bare and iced conductor section geometry and surrounding air flow are modeled, considering a given incident wind speed. The conductor cross section is assumed to be supported on flexible supports to study the interaction between the conductor motion and the air flow. FSI analysis yields both the fluid and structure response. Of particular interest is the wind pressure field on the conductor section, which allows the computation of the resultant drag and lift forces. This process is repeated for several cross sections along the span and the resulting forces provide the effective span wise wind load distribution on the conductor. This wind loading is then used as input in a separate 3-D computational nonlinear dynamic analysis model to predict the line response. This dynamic analysis of the line section can be detailed to represent very realistic line sections including conductors, suspension links and supporting towers.

It should be emphasized that the author does not advocate the "complexification" of overhead line wind analysis with the introduction of FSI and dynamic computational simulations in engineering offices. It is rather proposed to use these advanced computational methods, in a research and development context, to evaluate and possibly improve current wind analysis methods. Another very interesting application of this computational technique relates to optimized cross-sectional design of conductors, in terms of geometry and surface roughness. Detailed FSI analysis also enables the

evaluation of aerodynamic damping of various cable geometries. As many Canadian utilities are reassessing the reliability levels of their transmission infrastructure and making difficult investment decisions, a more realistic wind loading model could be of high value.

Key words: Overhead transmission line wind loading; fluid-structure interactions; computational fluid dynamics; conductor lift and drag coefficients; interactive wind and ice effects; overhead line conductors

RÉSUMÉ

Nos sociétés sont fortement dépendantes de l'électricité, et il ne fait pas de doute que la fonctionnalité des lignes de transport est déterminante pour assurer la fiabilité des réseaux électriques modernes. En effet, la continuité de l'approvisionnement en électricité reste la préoccupation majeure de toutes les compagnies d'électricité, et cette continuité du service peut être compromise par une multitude d'incidents ou d'accidents sur l'ensemble du réseau. Les lignes de transport sont toutefois les composants du réseau qui sont les plus exposés aux charges climatiques ou environnementales susceptibles de déclencher des pannes.

Parmi toutes les sources possibles de charges dynamiques sollicitant les lignes de transport, celles provenant des effets du vent sur les pylônes et les conducteurs restent les plus fréquentes. Les conducteurs de lignes sont particulièrement vulnérables aux effets du vent car les portées sont longues et flexibles (comparé aux pylônes) et leur présence physique dans le réseau en font des structures exposées à toutes les intempéries qui peuvent survenir sur le territoire couvert. Cette vulnérabilité est encore plus grande dans les climats nordiques où les effets combinés du givrage atmosphérique et du vent créent des scénarios de charges de conception parmi les plus critiques et donc susceptibles de contrôler la conception finale des lignes. Il nous apparait donc essentiel de comprendre la dynamique des fluides des effets du vent pour prédire avec réalisme et un degré de précision raisonnable la pression du vent exercée sur les conducteurs. Une meilleure évaluation des charges dues au vent permettrait par le fait même des prédictions plus réalistes de la réponse des lignes aux charges de vent, non seulement en terme de déplacements et dégagements électriques mais aussi en terme des charges nettes transférées aux pylônes par les conducteurs. La nature aléatoire des effets du vent sur les conducteurs a déjà fait l'objet de nombreuses études scientifiques et les méthodes d'analyse stochastique modernes permettent de cerner la question : les méthodes de conception simplifiées qui sont suggérées dans les normes et guides tiennent compte de ces effets en utilisant un coefficient de portée global qui ajuste à la baisse les efforts calculés au pylône sous des charges supposées synchrones et uniformes le long des conducteurs. Cette recherche ne concerne pas cet aspect de la question. Nous croyons que

des gains de précision appréciables dans la prédiction des charges de vent sur les lignes sont possibles par une meilleure modélisation de la physique des effets du vent sur les conducteurs, dans les conditions givrées ou non, en utilisant les techniques d'analyse qui tiennent compte des interactions dynamiques fluide-structure. Ces interactions sont ignorées dans les méthodes d'analyse conventionnelles qui consistent simplement à calculer une pression statique proportionnelle à la vitesse carrée du fluide selon l'équation classique de Bernouilli. Bien sûr, les concepteurs ne négligent pas la considération des vibrations éoliennes ou du galop des conducteurs, mais ces phénomènes sont traités séparément et n'influencent pas le calcul des charges sur les pylônes. Dans cette recherché, nous nous intéressons aux conditions de vent de rafale avec grande turbulence qui caractérisent les tempêtes de vent. Ces vents forts et turbulents créent de grands déplacements des conducteurs qui modifient les conditions d'écoulement d'air. Une évaluation plus précise de ces conditions est possible par analyse computationnelle des interactions vent-conducteur. Les bases théoriques de la physique des phénomènes en présence sont connues mais aucun cadre d'application numérique n'a été proposé à date, en partie à cause des coûts numériques élevés mais aussi dû au manque de données expérimentales pouvant valider ces modèles computationnels. Nous avons développé un tel cadre d'analyse computationnelle dans cette recherche et l'avons illustré dans un cycle complet, du calcul des charges au calcul de la réponse d'une section de ligne, avec plusieurs exemples pratiques à chacune des étapes de développement.

L'étape initiale consiste à déterminer précisément le champ des pressions exercées à la surface d'un conducteur de ligne à partir de modèles en deux dimensions qui rendent la réponse détaillée d'une section de conducteur sur supports flexibles dans un écoulement d'air à vitesse de vent incidente donnée. Une analyse CFD (dynamique des fluides computationnelle) du domaine fluide, l'air en mouvement entourant le conducteur, procède interactivement avec une analyse des déplacements de la section de conducteur, pour déterminer les forces nettes (trainée et portance) agissant à l'interface air-conducteur. Le processus est répété à volonté pour différentes conditions de support du conducteur (correspondant à diverses positions le long de la portée) et pour une série temporelle de conditions de vitesse de vent incident. Au final, on peut ainsi calculer un historique des forces dues au vent sur une portion tributaire de la portée jugée

représentative et utiliser ces forces comme des charges externes sur des modèles d'analyse dynamique non linéaire de sections de lignes en trois dimensions. Ces analyses peuvent être détaillées à souhait pour déterminer la réponse dynamique des conducteurs, accessoires d'attache et pylônes sous vents turbulents.

Nous insistons sur le fait que nous ne suggérons pas une complexification de l'analyse des lignes de transport sous les effets du vent dans les bureaux d'études à l'aide de modèles dynamiques sophistiqués combinant les interactions des domaines fluides et solides. Nous proposons plutôt d'utiliser le cadre computationnel mis à l'épreuve dans cette recherche dans un contexte de recherche et développement pour évaluer et possiblement améliorer les méthodes statiques conventionnelles. Une autre application intéressante concerne la conception optimisée de la géométrie des conducteurs de lignes en termes de propriétés aérodynamiques.

Mots clés: vent sur les lignes aériennes de transmission; interactions fluide-structure ; dynamique des fluides computationnelle ; coefficients de trainée et de portance des conducteurs ; interactions vent et givre.

Statement of Original Contributions

To the author's best knowledge, the original contributions of this research include:

- The first computational study of the aerodynamic properties (lift and drag coefficients and aerodynamic damping) of overhead transmission line conductors by wind-structure interaction analysis;
- The numerical study of the effects of conductor cross-sectional geometry (as defined by stranding pattern, angle of attack of wind, and accreted ice shape and thickness) on its aerodynamic properties;
- The development of a new wind load calculation method for the dynamic analysis of overhead line conductors that accounts for wind-conductor dynamic interaction effects;
- The evaluation of the accuracy of the current quasi-static method to evaluate wind loading on transmission line conductors, which excludes wind-conductor interaction effects.

Preface

This dissertation is submitted in partial fulfilment of the requirements for the degree of Doctor of Philosophy in Civil Engineering at McGill University.

First of all I would like to express my deepest gratitude to Professor Ghyslaine McClure of the Department of Civil Engineering and Applied Mechanics of McGill University for her continuous support, precise and regular supervision, invaluable and critical suggestions and contributions in the course of this study. Her financial support, friendly treatment and care in the last four years made it a pleasant and joyful experience for me and my family. I also like to express my sincere appreciation to Professor Wagdi G. Habashi, Director of the Computational Fluid Dynamics Laboratory, Department of Mechanical Engineering of McGill University from whom I have learned a great deal, for his enthusiasm, guidance and friendship throughout this research. Most pleasing was to discover the "big person" who fills up the "big name".

I would like to thank everyone at CLUMEQ, especially Dr. Vladimir Timochevski who enabled us to take advantage of Krylov and Guillimin computational platform during this research. The partial financial support provided by *Fonds québécois de la recherche sur la nature et les technologies (FQRNT)* is gratefully acknowledged.

I would also like to thank my close colleague and friend, Dr. Seyed Ali Ghafari Oskoei who was most helpful from the first day I arrived in Canada up to this point. His academic advice and help have saved me great efforts. I also like to thank my close friends Dr. Ali Shirazi, Dr. Farshad Habibi, Dr. Sadegh Gholparvar and Dr. Abolfazl Keyghobadi whose continuous support and friendship made the past four years so pleasant. In addition I'd like to thank my close friend and colleague Mr. Amir Borna for all his help during this research specially in helping me to understand the Computational Fluid Dynamics intricacies at the early stage of this research.

Last, but certainly not least, my special gratitude goes to my family. I'd like to take this opportunity to express my deepest gratitude to my parents Mahboubeh and Mahmoud for all their unconditional love and support during my entire life, certainly I could not go this far without their sacrifices. Most deserving of special recognition is my wife, Elnaz. My deepest appreciation and thanks for her unconditional love, sacrifice and support. Her love, devotion and patience made it all possible. Without her sacrifices WE couldn't get here.

Vancouver, 15 August 2012
Hooman Keyhan

LIST OF FIGURES

LIST OF TABLES

Table of Contents

1 Introduction

1.1 General

Electricity is a crucial form of energy in our societies, and the reliability of overhead transmission lines is key to ensure the overall reliability of electric power grids. Continuity of service is the main preoccupation of electric power utilities, and this continuity may be disrupted by a large variety of accidents caused by environmental loads.

The most common and important source of dynamic loads on transmission lines results from wind effects on the towers and conductors. Conductors are particularly sensitive to wind as they are long and relatively flexible (compared to their supports) and are literally wind-catching structures in the power grid infrastructure. In cold climates, wind and ice have compounding effects on lines and give rise to the most severe design loading conditions.(Farzaneh 2008)

The traditional design method to calculate wind loads on transmission lines is to convert the design wind speed to a static pressure through Bernoulli's equation where the pressure is proportional to the air density and the squared wind speed. The vertical profile of this static pressure is calculated using an exponential function according to the boundary layer wind model, and a gust effect factor is applied to the static pressure to yield the equivalent wind pressure. (Davenport 1979b) In this approach the fluid-structure interaction of wind and the motion of line components is ignored: wind is simply considered as a quasi-static load on conductors and supports, while special instability effects due to particular wind conditions such as vortex shedding (Aeolian vibrations) and flutter (cable galloping) are accounted for separately with specific mitigation solutions if necessary.

In this research the dynamic effects of gusty wind on overhead line conductors are evaluated and the description of wind-conductor interaction effects is studied using computational models. In order to achieve such evaluation, a new wind-load model is

developed which accounts for fluid-structure interactions (FSI) between the wind and the suspended conductors. The proposed approach is compared with current wind-resistant design methods for assessing the wind loads transferred by the line conductors on their supporting towers using a case study.

1.2 Research Objectives

The main goal of this research is to provide more insight in the dynamic nature of the wind loads transferred from conductors to supporting towers with a view to assess and improve the accuracy of static design approaches. This study examines wind effects on conductors only. For precise evaluation of turbulent wind effects on conductors, the drag and lift coefficients of iced and bare conductors with different cross sections and iced thicknesses and subject to various flow conditions were evaluated by taking into account the wind-conductor dynamic interactions. A new wind load model is proposed and is compared to other current methods using a case study of a line section.

The more specific research objectives can be summarized as follows:

- To evaluate conductor aerodynamic properties (lift and drag coefficients and aerodynamic damping) using fluid-structure interaction analysis;
- To evaluate the effects of conductor geometry as defined by stranding pattern and accreted ice shape and thickness on conductor aerodynamic properties;
- To describe wind-conductor dynamic interaction effects on the wind pressure field on conductors;
- To assess the variation of wind-conductor interactions along the span;
- To determine whether including wind-conductor interaction effects is important when evaluating the line response to gusty wind.

1.3 Methodology

In this research, the following methodology is used to evaluate turbulent wind effects on overhead conductors considering wind-conductor interactions.

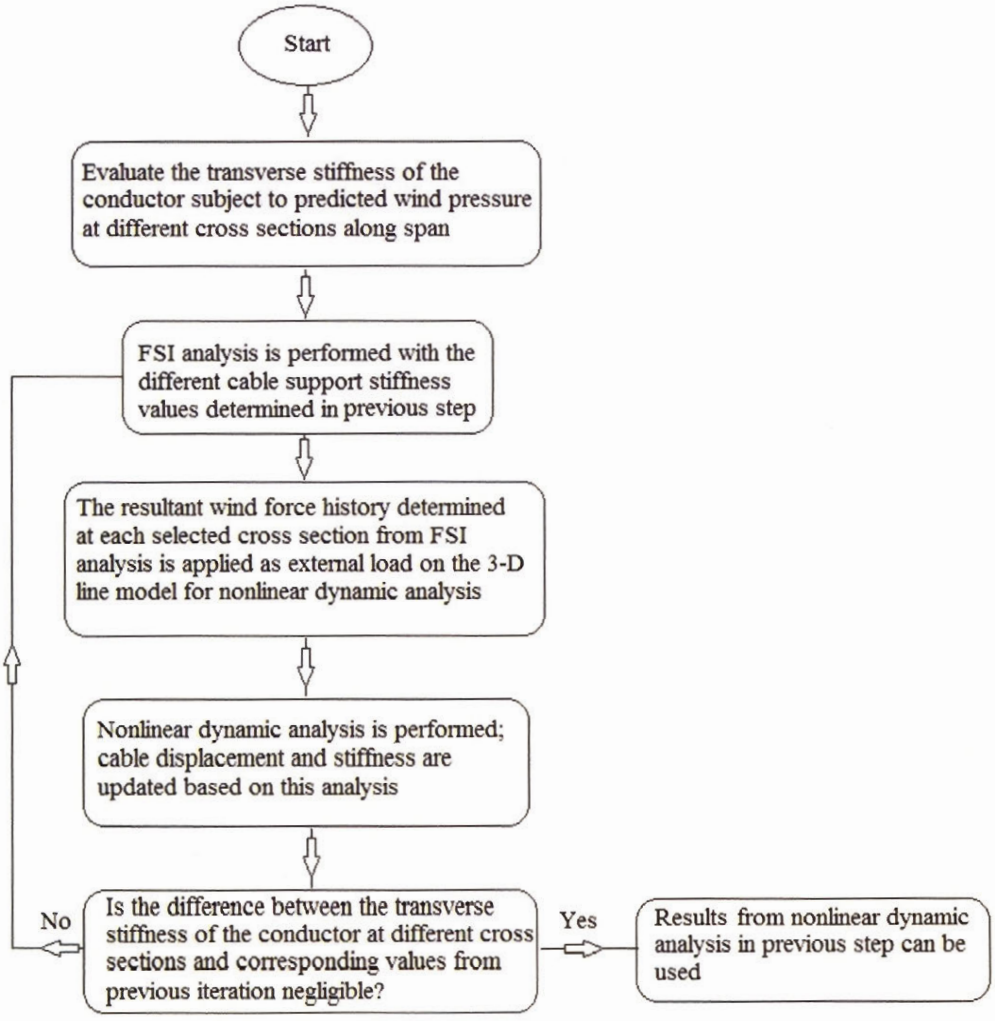

Figure 1.1 Wind load modeling and dynamic analysis procedure.

To study the interaction between the conductor motion and the air flow, the conductor cross section is assumed to rest on flexible supports. For this purpose the conductor horizontal and vertical stiffness values are evaluated along the span: cross sections closer to the anchor and suspension points are therefore assigned stiffer support conditions than cross sections further inside the span. Then, FSI analysis is carried out in two dimensions

where the detailed conductor section geometry and surrounding air flow are modeled, considering a given incident wind speed. Various cross sections of bare and iced conductors are studied to evaluate the influence of conductor stranding pattern and ice thickness on the wind pressure field surrounding the conductor. FSI analysis yields both the fluid and structure responses. This process is repeated for several cross sections along the span and the resulting forces provide the effective span wise wind load distribution on the conductor. This wind loading is then used as input in a separate 3-D computational nonlinear dynamic analysis model to predict the line response. Because this loading differs from the static loading used in the first step to evaluate the lateral stiffness of the cable, the conductor will experience slightly different displacements which in turn provide different values of conductor lateral stiffness. So the FSI analysis of Step 2 in Figure 1.1 is repeated with the new stiffness values and after a few iterations a very good estimate of lateral stiffness of the conductor is obtained. The dynamic analysis of the line section can be detailed to represent very realistic line sections including conductors, suspension links and supporting towers.

In this research four different natural wind records have been applied on the ACSR 54/7 conductor to evaluate the wind lift and drag forces that account for wind-cable interactions. ACSR 54/7 is the conductor used in the double-circuit line which is modeled as a case study in this research: it is widely used on Hydro Québec's transmission network. The wind pressures obtained from this analysis are compared against pressures predicted by standard OHL wind calculation practice based on Bernoulli's equation. To demonstrate the complete wind analysis procedure, the resultant wind forces obtained from FSI analysis are used as input loads along the conductor span for three-dimensional dynamic analysis of a detailed numerical model of a 120 kV double-circuit line section comprising five spans supported by four tangent suspension lattice supports and two straining towers at both ends. The suspension towers have been modeled in detail (every member of the lattice tower is modeled) while the straining towers are simply represented by fixed supports. The results obtained from these analyses are compared against results obtained from the existing method (which neglects FSI), to assess the influence of wind-conductor interactions on the line response. The results such as conductor tension,

conductor horizontal displacement and internal forces in the main members of towers are compared. This example serves as a case study to demonstrate the application of the proposed method, with the understanding that the trends observed in the results are mostly indicative and may not be valid to describe all possible cases.

1.4 Organization of the thesis

The thesis consists of 8 chapters, using the manuscript format for chapters 3 to 7.

Chapter 1 includes a general introduction to the research topic, its objectives, methodology and organization of the dissertation.

Chapter 2 presents a summary of the background and literature review. A brief review of relevant published studies (in English) of the last 30 years on wind loading of transmission line conductors is presented. This chapter is divided into two subsections where experimental and numerical studies are reviewed. Then some of the most recent research findings on transmission line response to wind loading are discussed. Finally, current calculation methods for wind loading of transmission line conductors are presented as used in Canadian and American standards.

The first step of this computational research is described in **Chapter 3,** Keyhan H., McClure G. and Habashi W.G. (2011). On computational modeling of interactive wind and icing effects on overhead line conductors. International Workshop on Atmospheric Icing of Structures (IWAIS), May 8-13, 2011, Chongqing, China: B-5-1-28.(Keyhan H. et al. 2011b)

This paper describes how wind and conductor are represented computationally in different domains and how the interaction between these two domains is performed. The influence of the flexibility of conductor supports (i.e. position of the cross section along the span) is explained and finally results of FSI analysis of a few cases of bare and iced conductors are presented and discussed.

In **Chapter 4**, the published journal paper citation is:

Keyhan, H., McClure G., Habashi W.G. (2011). "Computational study of surface roughness and ice accumulation effects on wind loading of overhead line conductors." International Review of Civil Engineering 2(2): 207-214. (Keyhan H. et al. 2011a)

In this paper FSI analyses of three models with different cross sections are performed to study the influence of the cross-sectional shape and surface roughness on the fluid flow around the conductor, and in particular the fluid pressure in the boundary layer at the air-conductor interface is studied. The effects of different pressure distributions on drag and lift are investigated and compared in different conditions. Among different results, the aerodynamic damping of conductors was of particular interest.

In **Chapter 5** a comprehensive study of wind load on conductors is presented. The manuscript of this paper is currently under review:

Keyhan, H., McClure G., Habashi W.G. (2012). "Fluid-Structure Interaction analysis of wind effects on overhead transmission line conductors." Journal of Wind Engineering & Industrial Aerodynamics, Manuscript number: INDAER-D-12-00062, submitted in March 2012.(Keyhan H. et al. 2012c)

This manuscript comprises results of computational FSI analysis of 15 different models each with four different incident wind velocities. The studied parameters are wind velocity, conductor stranding size and pattern, ice accretion, support stiffness and angle of attack, and their effects on drag and lift coefficients are discussed.

Chapter 6 demonstrates how the results from 2-D FSI analysis are integrated and applied on 3-D transmission line model. This manuscript is also under review:

Keyhan, H., McClure G., Habashi W.G. (2012). "Dynamic analysis of an overhead transmission line subject to gusty wind loading predicted by wind-conductor interaction." Computers & Structures, Manuscript number: CAS-D-12-00549, submitted in June 2012). (Keyhan H. et al. 2012b)

In this chapter a case study of a 5-span transmission line section is presented where the latticed suspension towers and conductors are modeled in details. Four different natural

wind records are used as loading scenarios. The results from these analyses are compared against results from another set of dynamic analysis results which were based on pressure loads predicted by Bernoulli's equation. Comparing the results from these two approaches shows how including FSI can affect the predicted stress and deflection levels and consequently transmission line structural design.

In **Chapter 7,** the case study of Chapter 6 is used to compare results which are important in overhead transmission line design. This part of the work is to be presented in September 2012 at the Cigré Canada conference:

Keyhan H., McClure G. and Habashi W.G. (2012). Advances in wind load modelling on overhead transmission lines. 2012 CIGRÉ Canada (International Council on Large Electric Systems), 24-26 September 2012, Montreal, Canada.(Keyhan H. et al. 2012a) Response indicators like conductor maximum tension, conductor displacement and internal forces in tower members predicted by the proposed method are compared against those from the design method used in engineering practice. Comparing the results from these two approaches shows how including FSI can affect the predicted stress and deflection levels and consequently transmission line structural design.

The **last chapter** of this thesis summarizes the main conclusions of the research followed by recommendations for future studies and a brief statement of the limitations of this research.

2 Background literature

2.1 General

Our survey of the published studies in the last 30 years on dynamic analysis of transmission line supports has shown that none of them has addressed the dynamic nature of gusty (buffeting) wind effects on conductors transferred to towers. Note that this survey does not include a review of publications on conductor galloping (there is

abundance of such studies) because galloping happens in steady wind conditions while the main objective is this research is studying gusty wind effects.

Some studies covered seismic analysis (El-Attar 1997; Khedr 1998) and others were concerned with dynamic behaviour under various transient loads such as shock loads due to cable rupture and sudden ice shedding. (McClure et al. 1987; Roshan Fekr et al. 1998; McClure et al. 2003; Kálmán et al. 2007; McClure et al. 2008). The only published studies on wind loading of transmission lines considered direct wind on towers. Previous research on dynamic wind effects on cable structures and transmission lines has mostly been dedicated to wind-induced instability phenomena like cable galloping or Aeolian vibrations rather than investigating the gusty wind fluctuations and their effects on transmission lines as a system. (Liao 1996; EPRI 2006; Krishnan 2006; Zhan et al. 2008) Other work relates to the experimental collection of meteorological data and their statistical analysis for the development of stochastic models for site-specific wind speed and directionality (Fikke et al. 2005; Lozowski et al. 2009).

The relatively recent availability of commercial finite element software enabling coherent fluid-structure interaction (FSI) modeling has made it possible to study the large kinematics of overhead line conductors in gusty wind fields. In turn, the lack of research in this area could explain in part why most utilities still rely on simplified static methods. The following sections summarize previous research specifically addressing wind loading on overhead lines.

2.2 Evaluation of wind pressure on conductors

One important parameter which has a direct effect on the evaluation of wind effects on a line conductor is the drag coefficient of the conductor's cross section. The drag on conductors has been the subject of numerous experimental studies in the past few decades. Most of these studies were dedicated to the evaluation of various conductors' drag coefficients in wind tunnel tests or field measurements (Ball et al. 1992; Shan et al. 1992; Tabatabai M. et al. 1992). They are very few numerical studies (Panneer et al. 1993) on this subject which have modeled stranded conductors with their realistic outer

surface pattern; most have used a smooth circular cylinder geometry to determine the drag coefficient. All the reviewed experimental and numerical studies on drag coefficients of conductors have considered the conductor on a fixed support, which prevents the study of cable-wind interactions. As will be presented next, only a few wind tunnel tests have modeled the conductor on flexible supports to study instability phenomena like galloping and Aeolian vibrations.

2.2.1 Experimental studies

Numerous wind tunnel studies have measured the aerodynamic properties of line conductor in the 1970s. The quality of many of these results was compromised by excessive scatter in measurements (Ball et al. 1992), and advances in the wind tunnel and the measurement methods provided more reliable results in the 1990s.

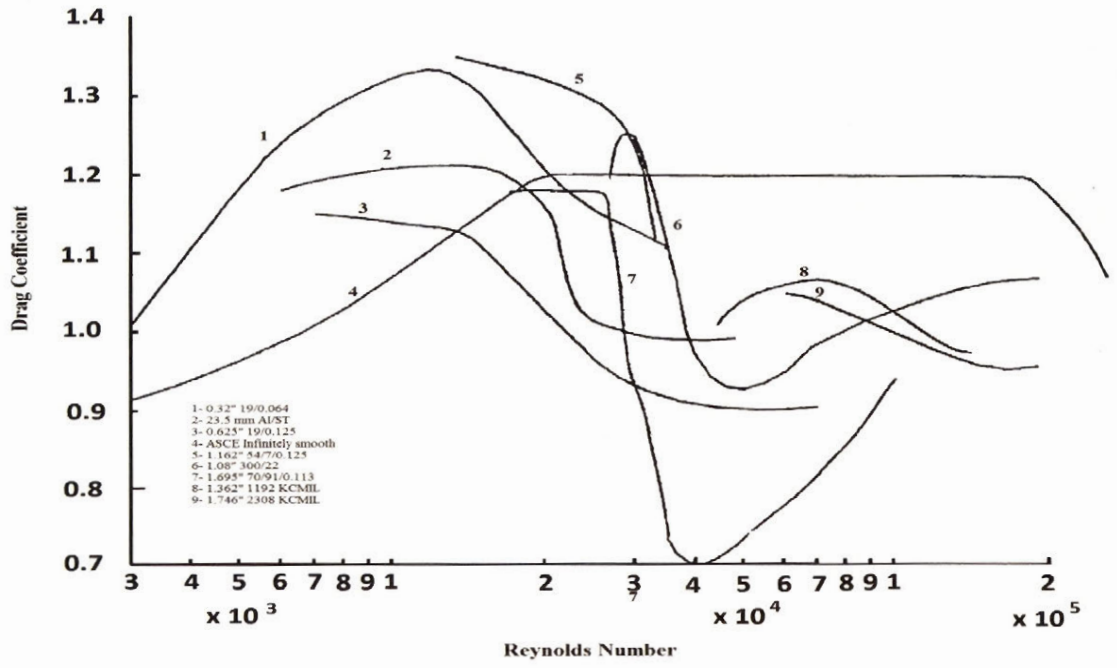

2-1 Drag coefficient for different conductors based on different wind tunnel tests adapted from (ASCE 2010)

Tabatabai and his collaborators (Tabatabai M. et al. 1992) have conducted several test series in the National Research Council of Canada wind tunnel to measure and compare the drag coefficient of stranded and trapezoidal conductors on fixed supports in different wind speeds ranging from 5.5 m/s to 52.8 m/s. After comparing their results with some earlier studies of the 1970s, they have identified that the main sources of scatter (see figure 2.1) were background turbulence in the wind tunnel, surface roughness of conductors and aspect ratio (Specimen length to diameter) of conductor specimens. They have also noticed that fluctuations in the air temperature affected the results by changing the air density as well as disturbing the calibration of the measuring instruments such as force transducers. The critical Reynolds number for conductors with larger strands was found to be smaller than for smooth surfaces, which resulted in a reduction of the drag coefficient at lower wind speeds ranging between 20 to 25 m/s. Also the drag coefficients of conductor in the sub-critical and super critical ranges were found to depend on the ratio of strand diameter to conductor diameter. These findings are consistent with results from previous studies and those obtained in the present computational research.

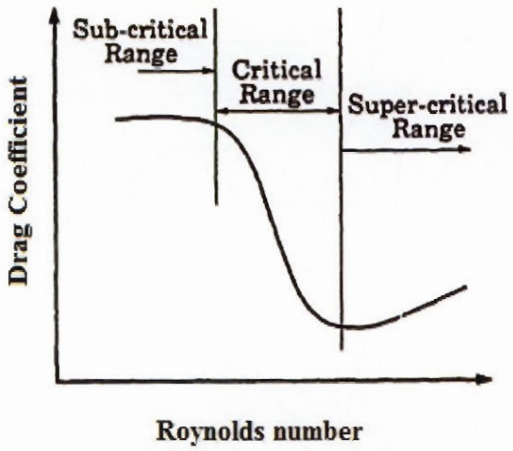

Figure 2.2 Typical drag coefficient curve for two- dimensional cylinder (Tabatabai M. et al. 1992)

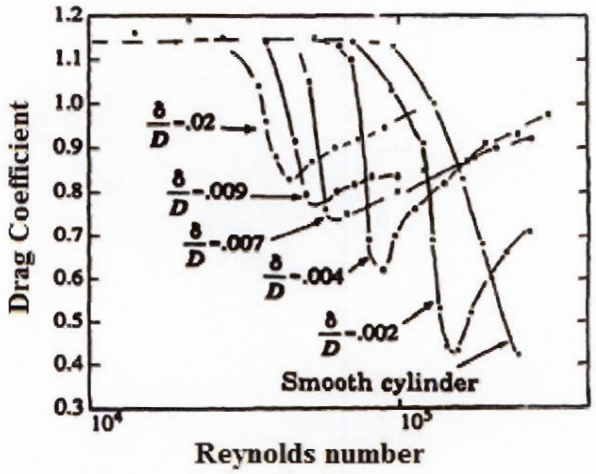

Figure 2.3 Effect of surface roughness on drag coefficient (D is cylinder diameter, δ is strand diameter) (Tabatabai M. et al. 1992)

The drag coefficients of stranded and trapezoidal (Figures 2.4 & 2.5) conductors were reported to be very close for wind speeds under 85 km/h. Compact trapezoidal conductors were found to experience reduced drag at increased wind speeds, a reduction of the order of as much as 30% at the speed of 44.4 m/s. Comparing the results from this study with results from our numerical simulation shows that the aerodynamic properties of compact conductors are closer to smooth cylinders than stranded conductors. This is discussed in detail in chapter 5.

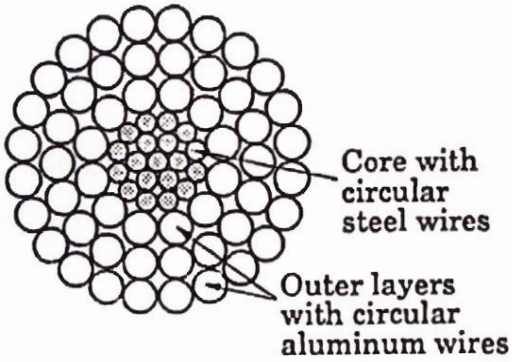

Figure 2.4 Cross-section of stranded ACSR conductor (Tabatabai M. et al. 1992)

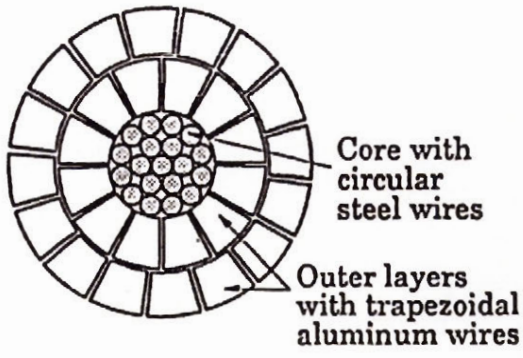

Figure 2.5 Cross-section of ACSR conductor with trapezoidal wires (compact conductor) (Tabatabai M. et al. 1992)

Variability in wind tunnel measurements was also addressed by (Shan et al. 1992) who conducted field measurements in the open air using a tunnel-like test setup. Because of the differences in the test environments, the drag coefficients measured in wind tunnel and open air could be affected by several parameters such as wind turbulence, yaw angle, swing angle, wind distribution profile and wind-conductor interactions which happen in the field measurements where conductor spans of a few hundred meters and can experience large horizontal displacements away from the end supports. So in their study, Shan and his colleagues have tried to identify the effect of turbulence of natural wind on drag coefficients.

In their field measurements, the measurement devices have been mounted on a 20 m tower to give the specimen the elevation comparable to the conductor in the existing line. The conductor length was chosen to be comparable to the conductors used in the wind tunnel test. Since it is very hard to obtain long straight conductor sections from a conductor on a reel, the conductors used in this study had been modeled by wrapping strands around an aluminum bar with similar diameter and stranding of Chukar and Bluebird conductors. To achieve a higher Reynolds number in the existing flow conditions another model was fabricated with larger diameter, 69.75mm.

Shan *et al.* have reported drag coefficients for each conductor based on measurement with 10-second average. About 200 results are reported for each conductor for Reynolds numbers ranging from 13000 to 50000 except for the largest conductor where the Reynolds number reaches 90000. Reported results show that the drag coefficients for smooth cylinders remain almost unchanged, over 1.2, in the range of Reynolds numbers used in this test, but the drag coefficients of stranded conductors drop from about 1.3 to 0.8 when the Reynolds numbers increase from 20000 to 40000. And finally the authors reported a good agreement between the field-determined drag coefficients and wind tunnel drag data and concluded that the results from wind tunnel tests can be considered as a reliable source for wind load calculations on conductors.

Because of the differences in the conductor size, strand configuration, support condition and air flow parameters the results from Shan's study could not be compared to those presented in this thesis, but the general trend of drag coefficient variation with increasing Reynolds numbers is consistent with the results from our numerical models which is discussed in detail in chapter 5. While every effort has made by Shan to simulate the wind tunnel conditions in the field measurement, some parameters remain hard to control in field studies (such as turbulence intensity) and this can affect any comparison between field measurements and wind tunnel test results.

Ball et al. (Ball et al. 1992) have conducted a series of wind tunnel tests to measure the drag coefficient of conductors. In their research, they have tried to identify the main sources of errors in drag measurements to address the large discrepancy between field

measurements and wind tunnel test results. Among different source of errors, they have focused on model aspect ratio and the end conditions present at the junction of the cable model and the wind tunnel wall. Two different wind tunnels ($2m \times 3m$ for low wind speed and $9m \times 9m$ for higher wind speed) are used and a drag coefficient of ACSR is measured with different aspect ratios. The ACSR conductor has 57.2 mm diameter and 24 outer strands each 6.25mm in diameter. The aspect ratio has been adjusted by adding mid span supports which aerodynamically divide the conductor to shorter spans. The aspect ratio has been varied from 5:1 to 294:1. The authors concluded that there was no truly two-dimensional flow in any of the tests observed and the measured drag is significantly affected by the lack of flow uniformity. Different issues like the air leakage through the gaps at the ends of the model contributed to the span wise pressure gradients. They have observed a strong aspect ratio effect on drag coefficient measurement up to an aspect ratio of 60:1 but this effect becomes negligible in tests with aspect ratio of 294:1. Results from this study showed a need for great care in measuring drag coefficients of conductor. Finally the authors compared the test results of this study with results from few other wind tunnel tests and conclude that the discrepancies in the results from wind tunnel and field measurements could partly be attributed to errors in the field measurements. There are several parameters which are varying in time and not easy to control or record in real time such as turbulence of air flow or oscillating angle of incidence arising from the unsteady nature of the wind direction.

These findings confirm the necessity of numerical modeling of the conductor subject to wind which gives the possibility of modeling a 2-D flow and controlling different parameters of air flow to study how they can affect the aerodynamic properties of conductors.

2.2.2 Computational modeling

To the authors knowledge there is no published research on the study of conductor's aerodynamic properties using advanced numerical modeling including conductor-wind dynamic interactions. All reviewed numerical studies have considered conductors as fixed objects in the wind flow. Most of these studies have examined the aerodynamic

properties of smooth circular cylinders and they are very few numerical studies that properly modeled the stranded configuration of conductors. One of those studies which are more relevant to this thesis is discussed next.

Panneer and his colleagues (Panneer et al. 1993) have tried to compute conductor drag coefficients using large eddy simulation. Their main objective was to compare the computed drag coefficients with available field measurements. They have employed a hybrid procedure, using the finite difference method to integrate the momentum equation and the finite element method to integrate the pressure. Although wind is modeled as a laminar flow and no turbulence model is used, Joel (Joel H 1990) and Rodi (Rodi 1993) refer to this type of work as one form of large eddy simulation (LES) because they consider that the fourth derivative error terms of the numerical scheme used in that method play a similar role as the LES model. The flow was assumed as viscous, incompressible and unsteady.

Panneer et al. (Panneer et al. 1993) have computed drag coefficients in different Reynolds numbers and they have tried different grid sizes. They have reported that the grid which fulfills the requirements to model the flow in the boundary layer was not fine enough for this type of simulation and resulted in much lower values for drag coefficients comparing to field measurements. They reported results with better agreement with field measurements by refining the mesh size and reducing the time increment from 0.2 to 0.002 sec. in the higher Reynolds numbers. They finally compared the computed drag coefficients with field measurements for Reynolds number ranging from 2×10^4 *to* 4×10^4, and the reported value for drag coefficient , C_D=1.20, is in good agreement with field measurements in the Reynolds number of 2×10^4 but the drag coefficient from field measurements dropped to 0.95 and 0.75 in the Reynolds numbers of 3×10^4 *and* 4×10^4 respectively while the computed value remained at 1.20.

We believe that the time step used in their study was appropriate for small Reynolds numbers and by increasing Reynolds number, especially with refined grid in the boundary layer, smaller time steps are required to model the fluid appropriately; this can explain the discrepancy between results from this study and wind tunnel test results. So

with a smaller time step Panneer (Panneer et al. 1993) could have seen the drop in drag coefficient in the critical Reynolds numbers which are expected around 3×10^4.

2.3 Overhead transmission line behaviour subjected to wind loading

In this section, some of the few published studies on overhead transmission line response to wind loading is summarized. All these studies have used wind pressure predicted by either Bernoulli's equations or wind tunnel tests, which do not include effects of wind-conductor interactions.

Loredo-Souza (Loredo-Souza 1996) has completed a comprehensive review of the work done in the field of transmission line wind loading, starting as early as 1963. He has concluded from his review that: the behaviour of transmission lines is significantly affected by turbulent wind and that statistical methods combined to influence lines (a method to predict structural response under spatially variable loads) provide a better description of wind load effects than traditional deterministic static methods (Loredo-Souza et al. 2003). He has also concluded that transmission line response to strong gusty winds was not fully understood due to the lack of coherent data in both full-scale field measurements and wind tunnel tests. It is noteworthy that none of the work surveyed addressed the wind-structure interaction effects.

The main research contribution of Loredo-Souza was to introduce a new scaling boundary layer wind tunnel test model which is called distorted model. In this method the cable length is reduced by a distortion factor so a longer conductor section can be represented in wind tunnel tests. However, his work has not accounted for the interaction between conductors and supports during their dynamic response and has not explained how these two systems with different range of dominant natural frequencies could damp or amplify the other system's response. Our review of the published studies does not show whether the method proposed by Loredo-Souza has indeed been used in later wind tunnel tests, but his study nonetheless confirmed that to understand conductor behaviour under wind loading, turbulent wind needs to be modeled properly.

Battista and his collaborators (Battista et al. 2003) were among the first few researchers to study the wind effects on transmission lines considering the towers and conductors together as a system. They have used the finite element method to build a three-dimensional model of a central tower and its adjacent spans of conductors. The adjacent towers and the line continuity are simulated by applying representative boundary conditions involving elastic, inertial and kinematical characteristics. They have used frame elements instead of the more common pre-stressed truss elements to discretize the cables to provide improved numerical stability. However, this becomes an important modelling consideration when the cables experience tension variation along with large displacements. A geometric non-linear static analysis was first conducted to find the initial equilibrium configuration of the line system under the self weight and pre-tension loadings of the suspended conductors and insulator strings. Afterwards, an eigenvalue analysis of the initial configuration was conducted to identify the dominant swaying modes of the conductors that will affect the towers. Then, the linear time-history response of the structure under wind action is obtained by modal superposition of the major sway modes of the structure and the conductors. In this study the wind speed at each point comprised two parts: The first part is the mean wind speed which varies with height, and the second part is the turbulent component which is represented as a statistical function of the mean wind velocity, the roughness length and the altitude above ground level. Then the drag force was obtained from Bernoulli's formula using the wind speed. The roughness length was defined as the height where the mean wind speed becomes zero if the wind velocity profile has a logarithmic variation with height. Essentially, Battista's model accounted for the inertia forces induced on the towers by the wind-excited sway motion of the conductors. Using a simple double pendulum model with the suspension insulator rods, the dynamic properties of coupled conductor-tower system could be approximated. His analysis was also limited by a small kinematics assumption which cannot be realistically applied to large gusty wind effects on overhead lines. Although the line model of this study was considering both the line supports and conductors and looked promising to simulate the line behaviour under wind load, the wind-conductor interactions were not considered and the aerodynamic properties of the conductor were assumed to be remain constant during the analysis. One parameter which could affect the

results of this analysis considerably is the aerodynamic damping of the conductor. In chapter xx, our numerical FSI analysis shows that aerodynamic damping is larger than structural damping for the conductor so it should be considered in dynamic analysis of overhead transmission lines subjected to wind.

Bartoli and his collaborators (Bartoli et al. 2006) have performed a series of wind tunnel tests, exposing cables to wind action both in laminar and turbulent flows to investigate the stochastic characteristics of dynamic behaviour of cable, such as axial load variation . The wind tunnel employed in these tests had cross section of 2.4 m by 1.6 m and the length of 24 m. In the laminar tests, the mean wind velocity ranged between 10 to 30 m/s with the turbulence intensity less than 1% while in the turbulence test cases the mean wind speed varied between 10 to 20 m/s and the turbulence intensity was increased to 14% in the along wind direction. The tested cable was been built by connecting 48 cylinder, each with 40mm in diameter and 40mm in length, by a 0.7 mm-diameter steel strand. The tension in the tested cable was 23.5 N with the sag of about 1/10 of span which is typical of transmission line. The drag coefficient variation pattern obtained from this test did not follow the same pattern as in other previous tests especially in the lower Reynolds numbers and the researchers attributed this to the surface roughness and turbulence intensity. The drag coefficient evaluation was not the main purpose of the study, and the spectral density of measured data on support reactions and cable tensions were compared with analytical results. Good agreement was reported between several peaks obtained from the power spectral density of the conductor tension and the frequencies of the natural modes of the cable obtained from analysis.

Monitoring the dynamic response of conductor while subjected to wind inside a wind tunnel seems a promising research method because it provides a better evaluation of the real wind action on the conductor rather than the estimation provided by Bernoulli's equation. However, important parameters such as the conductor's surface roughness and the ratio of conductor tension to conductor drag force are not matching real conditions. Nonetheless, the drag coefficients obtained from this study are compared to results from our numerical models of smooth cylinder (discussed in chapter 5) and they show good agreement in high Reynolds number.

Cluni et al. (Cluni et al. 2008) have developed finite element models for dynamic analysis of conductor under wind loading which accounted for nonlinear geometrical effects. The wind loading used in their numerical model was based on wind tunnel test results (Bartoli et al. 2006) and scaled to the cable model. Finally results such as support reaction and mid-span displacement predicted by numerical model and wind tunnel results were compared. In this study the cable had been discretized by two-node truss elements and the incremental form of the equations of motion was solved using a modified Newton–Raphson algorithm.

To validate the numerical model, a quasi-static wind load based on Bernoulli's equation was applied on each node of cable and the results were compared against analytical and experimental results. A dynamic analysis was performed where the numerical model was loaded with the results of wind tunnel test based on the following assumptions

1) The time history of the along-wind reaction at the end supports represented the time history of the overall drag force applied on the cable model.
2) The overall drag force was distributed uniformly on the nodes of the cable mesh.

Finally the results of these analyses were compared against those of wind tunnel tests in terms of the mean value and coefficient of variation of cable tension and agreement was generally good. Because the type of conductor and wind speed time history are different from what is used in our numerical analysis, it was not possible to compare these results with ours.

2.4 Design guidelines for wind loads

The definition of wind loading on transmission lines is similar in most design codes and standards worldwide, and it is based on the Davenport method presented in introduction. Only slight differences arise from the definition and evaluation of some coefficients as described next for the design procedure recommended by the Canadian standard, which is essentially the International Electro-technical Commission (International Electrotechnical Commission (IEC) 2003) and for the American approach

described in ASCE Manual 74 (ASCE 2010). These two methods cover most of the international design practice.

2.4.1 CAN/CSA-C22.3 No. 60826-10 Design criteria of overhead transmission lines

Canadian design criteria of overhead transmission lines (Canadian Standards Association (CSA) 2010), which are adapted from international design criteria of overhead transmission lines design defined by the (International Electrotechnical Commission (IEC) 2003), define V_R (m/s) as the reference wind speed based on return period T which is determined from a statistical analysis of relevant wind speed data measured at 10 m above ground with an averaging period of 10 minutes. Some countries like the United States have adopted the 3-second averaging period, which means that their reference velocity is already representing the mean-value of a strong wind. The IEC 60826 procedure for evaluating wind effects on a transmission line is to find out the unit action, ***a***, of the wind speed and then apply it to all components exposed to wind pressure. The following equation determines the dynamic wind pressure, q_0, for a reference wind speed. (International Electrotechnical Commission (IEC) 2003; Canadian Standards Association (CSA) 2010)

$$q_0 = \frac{1}{2}\,\tau\mu\,(K_R\,V_{RB})^2 \qquad 2.1$$

Where, V_{RB} is the reference wind speed in the area with terrain of Category B (open country with very few obstacles) modified by a terrain roughness factor K_R and multiplied by μ, the air mass per unit volume, and τ the air density correction factor – this latter factor is assumed to be one unless the temperature and altitude are significantly different from the assumptions of 15 °C and sea level. Then the value of the unit action of wind on line components is given by:

$$a = q_0\,C_x\,G \qquad 2.2$$

Where C_x is the drag coefficient and G is the combined wind factor, taking into account the influences of the height of the element above ground level, terrain category, wind gusts and dynamic response. To obtain the load on tower attachment points due to wind acting on the whole span, the wind action should be multiplied by the projected area of cable and by the span factor which accounts for the spatial variability of the wind pressure along the span. Figures 2.6 and 2.7 are the charts provided by CAN/CSA-C22.3 No. 60826-10 to evaluate combined wind factor and span factor.

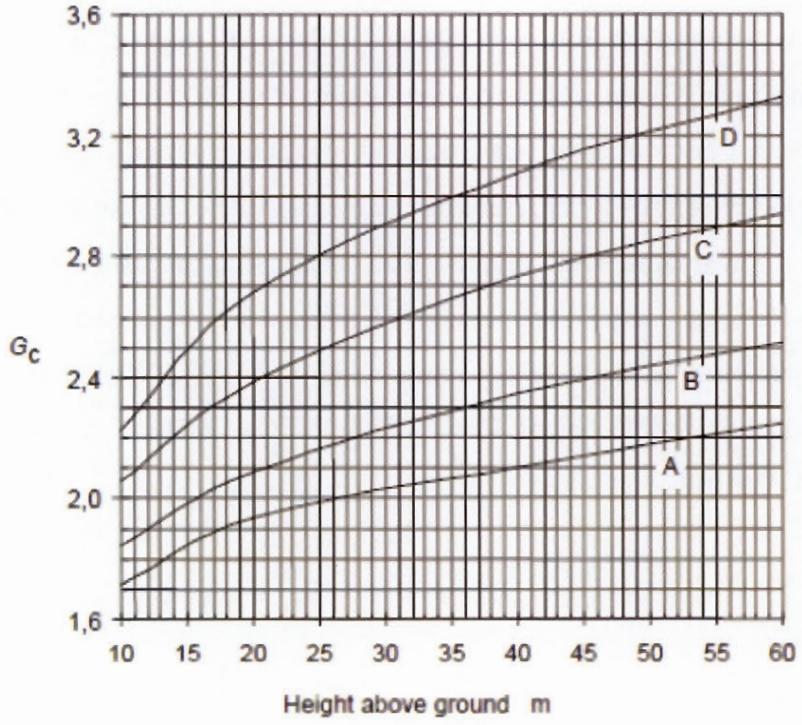

Figure 2.6 Combined wind factor G_c for conductors for various terrain categories and heights above ground (Canadian Standards Association (CSA) 2010)

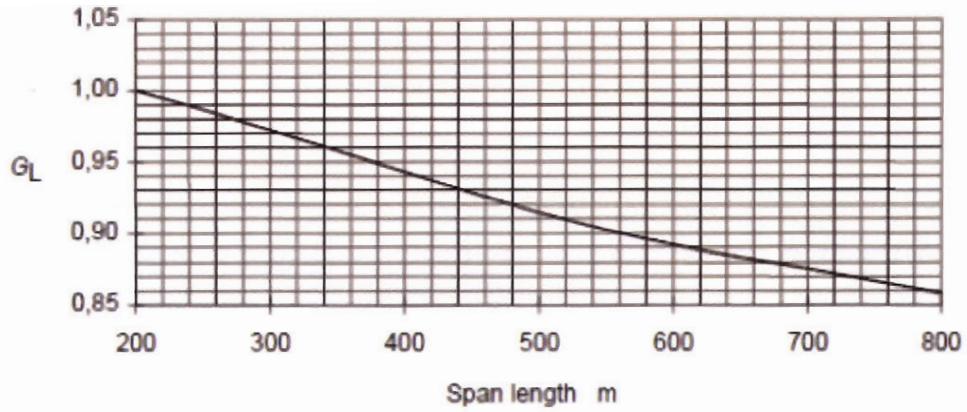

Figure 2.7 Span factor G_L (Canadian Standards Association (CSA) 2010)

It is seen that the CAN/CSA-C22.3 No. 60826-10 method is relatively simple, especially when compared with the ASCE Manual 74 method presented next.

2.4.2 ASCE Manual No.74, Guidelines for Electrical Transmission Line Structural Loading

ASCE Manual 74 (ASCE 2010) uses the following expression to calculate the wind load on line components:

$$F = \gamma_w Q K_z K_{zt} (V_{50})^2 G C_f A \qquad 2.3$$

Where, F is the wind force (in N/m) in the direction of wind, γ_w is the load factor to adjust the force to the desired return period, V_{50} is the basic wind speed of the 3-sec gust for a 50-year return period, K_z is the velocity pressure exposure coefficient to modify the basic wind speed according to height above ground (equation 2.4). K_{zt} Takes the topographical effects in to account, Q is a numerical constant equal to $0.613\ kg/m^3$ to convert the kinetic energy of moving air into the potential energy of pressure. It is obtained by dividing the air density by 2. A is the area projected on a plane normal to the wind direction, C_f is the drag coefficient which has been called force coefficient in this manual, and finally G is the gust response factor which is explained in detail in the following paragraph.

$$K_z = 2.01(\frac{Z_h}{Z_g})^{\frac{2}{\alpha}} \quad 2.4$$

Z_h is the height of the center of pressure of wind load from ground and it is called the effective height; it is always taken as $\frac{2}{3}$ of the tower's height for wind on towers and it is the average value of the conductor's height in the span for wind on conductors; Z_g is the thickness of the atmospheric boundary layer, also called gradient height.

The gust response factor accounts for the load effects due to dynamic amplification of towers and cables as well as wind turbulence when the average wind speed is used for quasi static analysis of lines. To determine the appropriate gust response factor for the conductors and towers, ASCE Manual No.74 provides equations 2.5 And 2.6 respectively, in which the numerators are taken directly from Davenport's method(Davenport 1979b), and tare divided by the square value of the wind speed conversion factor, Kv ,which is the ratio of the 3-sec gust wind speed to the 10-min average wind speed (ASCE 2010). ASCE Manual No.74 simplifies these equations by neglecting the resonant response of tower and conductor (R_w, R_t). Neglecting the resonant response terms in the Davenport equation is based on assessment of field-test data and theoretical appraisal of transmission line response as well as the hypothesis that it is very unlikely to have peak vibration response of conductor and tower simultaneously. Also the aerodynamic damping of conductors and tower which is not accounted for in the quasi-static wind can play an important role in reducing the resonant response of towers and conductors.

$$G_w = (1 + g_s \varepsilon E(B_w + R_w)^{0.5})/{K_v}^2 \quad 2.5$$

$$G_t = (1 + g_s \varepsilon E(B_t + R_t)^{0.5})/{K_v}^2 \quad 2.6$$

In equations 2.5 and 2.6 g_s is a statistical peak factor which depends on the frequency characteristics of the response and sampling intervals, ε is the approximate coefficient for separation of the conductor and structure response terms, E is exposure factor reflecting the terrain type and object height on the gust effect factor and B is a dimensionless response term corresponding to the quasi-static background wind loading, and R is the resonant response term.

It is seen that the ASCE Manual 74 method is relying on several parameters determined with empirical equations derived from experiments and engineering judgment.

2.5 Fluid-Structure Interaction (FSI) in Finite Element Analysis

Up until now, a wide range of studies have been performed in FSI to determine structural response to wind effects, but a thorough understanding of the nonlinear interactions between wind and these structures has not yet been achieved (Wu et al. 2008). However, the topic can now be explored with wind tunnel tests and computer modeling. Due to recent developments in technology and numerical computational methods, it is possible to integrate computational structural dynamics (CSD) and computational fluid dynamics (CFD) to model structures and their surrounding air flow simultaneously. Clearly this CFD-CSD modeling approach presents the promise of the best simulation results of the real conditions. Wind tunnel experiments are still necessary for model validation purposes, but the advantages of modeling are far reaching, including its low cost, wider accessibility, and easier control of variables like fluid properties or flow conditions.(Glück et al. 2001)

Exploring the recent literature, they are many studies on fluid-structure interaction from aerospace (Guruswamy 1990) to medical sciences (Tambaca et al. 2005). Few of these studies are based on FSI modeling using commercial software but in most cases the authors have defined a formulation for the fluid and structure domains with discretization using FEM to solve these domains. Many of these studies explore different numerical methods and issues related to mesh generation and optimization, stabilizing solutions or

means of achieving faster convergence.(Forster 2007; Wall et al. 2007) Some examples of implementation of these methods are discussed for vibrations of thin-walled structures in contact with a fluid. (Lee et al. 2007)

To the author's knowledge there is no published work on FSI modeling of wind loads on overhead transmission lines. Although the above-mentioned studies provide background knowledge for FSI studies, each FSI problem has its own characteristics and difficulties which have to be addressed in detail. The closest related work to the proposed study was reported by Wu (Wu et al. 2008) who have used FEM to simulate the wind–structure interaction on cables used in a suspension roof. They have adopted a partitioned solution procedure, which includes three independent modules: the computational structural dynamics CSD module, the computational fluid dynamics CFD module and the computational mesh dynamics module which links the CSD and the CFD. For the CFD module, they have adopted the moving boundary formulation based on the Arbitrary Lagrangian–Eulerian (ALE). In the CSD domain, the updated Lagrangian formulation is used to describe the large kinematics of the structural motion.

In this study modeling fluid-structure interaction consists of modeling three domains. The first domain is the solid structure (the transmission line system) where the main solution variables are displacements. The second domain is the fluid part and typically its solution is consisting of velocity, pressure and temperature fields. The third domain is the moving air-conductor interface where all the above-mentioned variables are considered; therefore the fluid and solid models share this domain.

In FSI modeling, it is essential to map all the physical quantities from one mesh domain to the other. ADINA, the commercial software used in this study,(ADINA R&D Inc. 2009) does this mapping by some operators which interpolate the nodal point properties from both domains to the interface domain. The way the interface conditions are imposed is playing a crucial role in coupling the discretized fluid equations to the governing equations of motion of the structure. At the interface of these two domains, the traction equilibrium and compatibility of displacements should be satisfied. The first

condition of surface traction equilibrium at the interface requires stress resultant balance which is shown in the following equation (ADINA R&D Inc 2009).

$$\int_{Sf} \tau_f . n . dA_f + \int_{Sf} \tau_s . n . dA_s = 0 \qquad 2.7$$

Where, n is the normal vector to the interface, τ_f is the stress tensor acting on the fluid interface surface dA_f and τ_s is the stress tensor acting on the solid interface surface dA_s. To determine the force applied on the solid by the fluid, the fluid nodal stress is interpolated onto the solid nodes then integrated into solid nodal forces.

The force applied on the solid boundary is a function of the fluid pressure and velocity so the discretized structure equations contain fluid solution variables. Another boundary condition to apply is the displacement compatibility which can be enforced on the entire interface or only along the normal direction of the interface. To apply the displacement condition on the entire interface, the displacement is written in Lagrangian coordinate system where d_f is the vector of nodal point displacements of the fluid domain at the interface and d_s is the vector of nodal point displacements of the solid domain:

$$d_f = d_s \qquad 2.8$$

3 On Computational Modeling of Interactive Wind and Icing Effects on Overhead Line Conductors

The essential prerequisite for developing a new wind loading model for overhead transmission line conductors based on FSI analysis is to have a thorough understanding of wind-conductor interactions and how the pressure field is developed around flexible conductors. To model the interaction numerically, both the solid domain (cable) and fluid domain (wind) have to be represented with proper mathematical representation of the actual physics of the problem. This chapter describes how wind and conductor are represented computationally in these two different domains and how the interaction between these two domains is modeled. The influence of the flexibility of conductor supports (i.e. position of the cross section along the span) is explained and finally results of FSI analysis of a few cases of bare and iced conductors are presented and discussed to illustrate the approach.

This first part of the research was summarised into a conference publication that was presented by the author. The full citation is: Keyhan H., McClure G. and Habashi W.G. (2011). On computational modeling of interactive wind and icing effects on overhead line conductors. International Workshop on Atmospheric Icing of Structures (IWAIS), May 8-13, 2011, Chongqing, China: B-5-1-28.(Keyhan H. et al. 2011b). The following section presents the paper as it is published in the conference proceedings.

ON COMPUTATIONAL MODELING OF INTERACTIVE WIND AND ICING EFFECTS ON OVERHEAD LINE CONDUCTORS

Hooman Keyhan[1], Ghyslaine McClure[1], Wagdi G. Habashi[2]
[1]Department of Civil Engineering and Applied Mechanics, McGill University
[2]Computational Fluid Dynamics Laboratory, Department of Mechanical Engineering, McGill University
Montreal, Quebec, Canada
Hooman.Keyhan@mail.McGill.ca

Abstract: Transmission line analysis methods generally consider wind effects on conductors and supports as quasi-static loads, despite the dynamic nature of wind loading. In this paper, the authors explore wind-cable interactions using a 2-D fluid-structure interactive model using linear dynamic finite element analysis. The numerical simulation results reported show the effect of ice accretion thickness and bare conductor roughness on the resultant aerodynamic forces induced on the iced section.

Introduction

Design wind loads on overhead transmission line systems are usually considered as quasi-static horizontal loading resulting from a static pressure adjusted to account for drag effects. Hence, aerodynamic wind-cable interaction effects are only roughly approximated in design. Even though fluid-structure interaction (FSI) analysis is becoming fairly common in several engineering fields such as aerospace, automotive and biomedical applications, it has not been as frequently used in transmission line engineering. In this work, FSI analysis is used to study the wind-cable interactions in overhead transmission conductors and to explore the variation in the aerodynamic properties of conductors due to glaze ice accumulation. In current analysis methods, the wind-on-conductor load for iced conductors is simply obtained by adjusting the bare conductor load to account for the additional windward area. This approach negates the effects of the accretion on the drag and lift coefficients of the iced conductor. The general goal of this research is thus to develop a rational gusty wind load model for overhead conductors, in both iced and bare conditions, that will serve to determine the resultant wind forces acting at the tower attachment points. As a first step, the main focus of this paper is to illustrate how the conductor aerodynamic properties (drag and lift coefficients) change with ice thickness accumulated on the conductor.

RESULTS and DISCUSSION

Figs. 3.1 and 3.2 display the effect of ice accumulation on the resulting drag and lift force coefficients of conductors with ice accumulation at the bottom edge, taking an ovoid shape with the major axis normal to the incident wind flow.

These force coefficients are determined from integration of the surface tractions exerted by the fluid flow on the interface between the fluid and solid domains. As vortices are shed in the wake, the aerodynamic forces fluctuate in time and the range of the calculated drag and lift is shown in the figures. The detailed paper presents the simulation results obtained for five different cable-ice geometries.

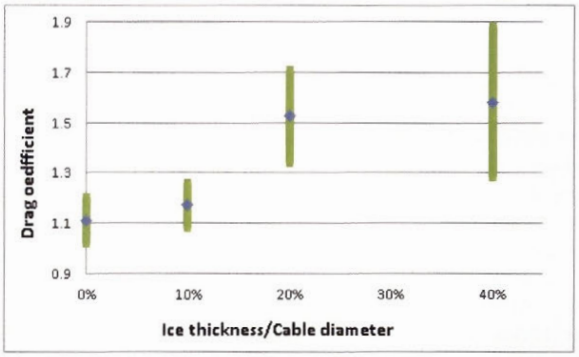

Figure 1: Effect of ice thickness accretion on drag coefficient

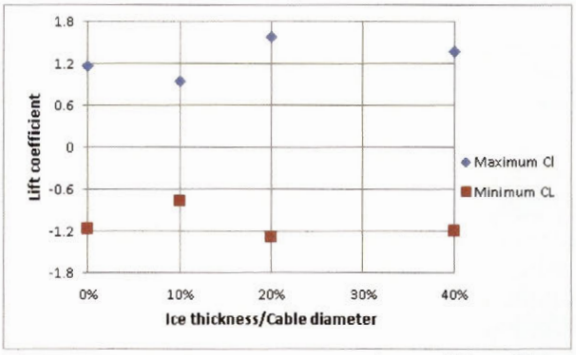

Figure 2: Effect of ice thickness accretion on lift coefficient

CONCLUSION

The study confirms that the shape of the iced cable is a significant factor on the effective wind loading, as the eccentric iced profile is subjected to larger net forces and motion. The eccentricity of the iced cable shape contributes significantly to the additional aerodynamic damping.

The smooth round and the stranded conductor shapes differ in their response with the stranded shape, experiencing drastically less forces and motion especially in vertical direction.

REFERENCES

[1] ADINA Inc (2009). ADINA theory and modeling guide. 71 Elton Ave, Watertown, MA 02472, USA.

[2] Bathe, K.-J. and H. Zhang (2002). "A flow-condition-based interpolation finite element procedure for incompressible fluid flows. *Computers & Structures*, **80**(14-15): 1267-1277.

ON COMPUTATIONAL MODELING OF INTERACTIVE WIND AND ICING EFFECTS ON OVERHEAD LINE CONDUCTORS

Hooman Keyhan[1], Ghyslaine McClure[1]
Department of Civil Engineering and Applied Mechanics
McGill University
Montreal, Quebec, Canada

Wagdi G. Habashi[2]
[2]*Computational Fluid Dynamic Laboratory, Department of Mechanical Engineering*
McGill University
Montreal, Quebec, Canada

***Abstract*— Current transmission line analysis methods generally consider wind effects on conductors and supports as quasi-static loads, despite the dynamic nature of wind loading. In this paper, the authors explore wind-cable interactions using a two-dimensional dynamic fluid-structure interactive model using linear dynamic finite element analysis. The numerical simulation results reported show the effect of ice accretion thickness and bare conductor roughness on the resultant aerodynamic forces induced on the iced cable section.**

Keywords- computational fluid dynamics; interactive wind and ice effects; overhead line conductors, conductor lift and drag coefficients; fluid-structure interactions

3.1 Introduction

Design wind loads on overhead transmission line systems are usually considered as quasi-static horizontal loading resulting from a static pressure adjusted to account for drag effects. Hence, aerodynamic wind-cable interaction effects are only roughly approximated in design. Even though fluid-structure interaction (FSI) analysis is becoming fairly common in several engineering fields such as aerospace, automotive and biomedical applications, it has not been as frequently used in transmission line engineering. In this work, FSI analysis is used to study the wind-cable interactions in overhead transmission conductors and to explore the variation in the aerodynamic properties of conductors due to glaze ice accumulation. In current analysis methods, the wind-on-conductor load for iced conductors is simply obtained by adjusting the bare conductor load to account for the additional windward area. This approach negates the effects of the accretion on the drag and lift coefficients of the iced conductor.

The general goal of this research is thus to develop a rational gusty wind load model for overhead conductors, in both iced and bare conditions, that will serve to determine the resultant wind forces acting at the tower attachment points. As a first step, the main focus of this paper is to illustrate how the conductor aerodynamic properties (drag and lift coefficients) change with ice thickness accumulated on the conductor.

3.2 Modeling Approach

The conductor used in the numerical simulations is a stranded ACSR 26/7 (Aluminum Conductor Steel Reinforced) with 29.5-mm outside diameter (D). As shown in Fig.3.1, five different shape conditions are modeled: (a) a circular smooth cylinder, (b) the realistic wavy surface profile of the bare stranded cable, (c) the stranded cable with a thin layer of ice accumulated at the bottom, (d) a smooth cylinder of oval shape representing a 6-mm thick layer of ice at the bottom, and (e) a smooth cylinder of oval shape with 12-mm ice thickness.

Model (a) serves to compare the results from this study with existing experimental test results that are mostly obtained on smooth circular cylinders. In model (b), the cable outline takes the shape of the contour of the 16 aluminum outer wires of 5-mm diameter each. In model (c) the maximum ice thickness is 3 mm (10% of the cable diameter) and the cable strands are still represented at the top surface. In models (d) and (e) the maximum ice thickness is increased to 20% and 40% of the cable diameter, respectively, at the bottom and the top surface of the conductor is assumed to be completely covered by ice, resulting in a smooth oval cross-sectional shape. As shown schematically in Fig. 3.1, the incident wind flow is assumed uniform and horizontal.

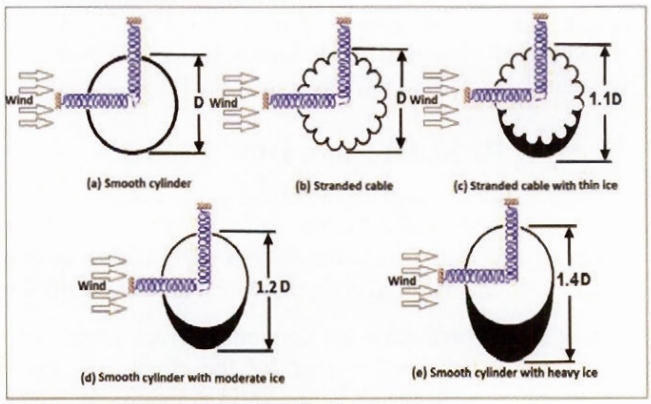

Figure 3.1. Five different cable sections under study .

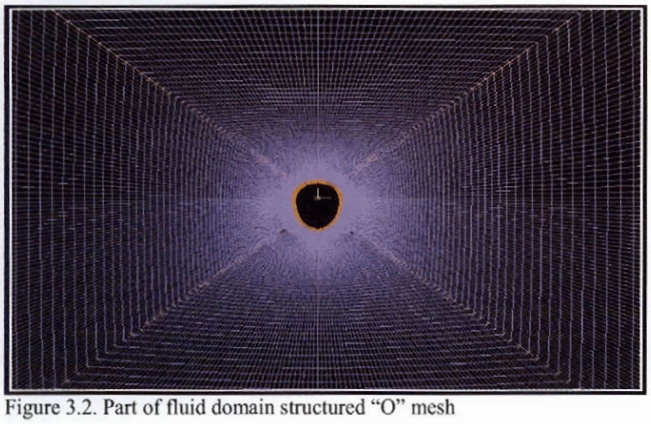

Figure 3.2. Part of fluid domain structured "O" mesh

The equivalent vertical and horizontal linearized stiffnesses of the conductor section are modeled by linear springs at the cable's centroid. These equivalent spring stiffness properties were determined for a mid-span cross-section using nonlinear elastic static analysis of a level 356-m span suspended in still air with fixed ends, with a horizontal tension of 19.2 kN in the bare condition (cable self-weight 14.9 N/m), and 22.5 kN in the iced condition (iced cable weight 17.9 N/m). A small viscous damping constant (equivalent to 1% of critical) is also assigned at the support in each orthogonal direction to approximate internal material damping effects in the conductor.

As previously reported [2], the overall dimensions of the fluid domain had to be optimized for CFD and FSI analyses to ensure that the computational domain is large enough for the fluid boundaries to have negligible effects on the calculated cable response, and yet attempt to reduce the computational cost. The fluid domain (see Fig. 3.2) has a horizontal length of 60xD and a vertical depth of 40xD. Further fluid modeling considerations are discussed next.

3.3 Detailed Modeling Considerations

To keep the cable cross-sectional model simple, only the outer cable boundary is modeled using stiff two-dimensional Bernoulli beam elements with appropriate tributary mass. To get a smooth geometric profile and retain reasonable accuracy in FSI analysis, the perimeter of the conductor is modeled with beam elements of length varying between 0.30 to 0.32 mm (300 to 380 elements in total) in the different models. In the solid domain, the incremental form of the nonlinear equations of motion (updated Lagrangian formulation) of the cable cross section on spring supports with dashpots is solved by direct integration using the classical unconditionally stable Newmark method, and the equilibrium iterations are carried out using the Full Newton method for stiffness updates [1].

The fluid domain is discretized with quadrilateral FCBI-C elements [3] using a structured "O" shape mesh, as shown in Fig.3.2 for cable section (e). Using the FCBI-C elements, the degrees of freedom of the fluid elements are defined at the centroid and the solution variables are piecewise constant. The final solution is interpolated at corner nodes for post-processing purpose. Discretizing the fluid domain with these elements helps reach stability for different Reynolds number without setting any artificial numerical parameters [3].

The fluid mesh geometry that provided optimal computational performances differs for each case, ranging from 90 × 75 to 120 × 106 elements at the external boundaries for the circular cylinder (a) and the more heavily iced cylinder (e), respectively. The fluid mesh is gradually refined to a resolution of 300 to 380 elements at the air-cable interface. The refined mesh in a ring zone of about 1xD thickness around the cable surface (see Fig. 3.2) is able to capture the response with reasonable accuracy. Cell thicknesses around the solid domain are small enough to allocate about 5 mesh layers with a Y^+ under 10.

The CFD analysis proceeds with direct time integration of the unsteady Reynolds-averaged Navier-Stokes equations using the Euler α - method of first order, and a constant time step of 0.1 ms was found optimal for the problem at hand. The iterative solver for the linearized incremental equations is the Algebraic Multigrid method (AMG). Airflow turbulence is modeled with the Spalart-Allmaras one-equation model and vortex-shedding effects are introduced with the Detached Eddy Simulation (DES) algorithm. In FSI analysis, the Arbitrary-Lagrangian-Eulerian (ALE) formulation is used to allow for compatible mesh deformations and displacements for the fluid surrounding the cable in motion in each solution step. [1]

3.4 Results

For the sake of brevity, only the salient features of the results obtained for the five models with incident wind speeds of 20 and 10 m/s are presented next. Fig. 3.3 shows the calculated pressure fields developed around the cable in the five models subjected to the same incident flow conditions at time t = 2 s. The pressure fields show the largest fluctuations in the heavy iced cylinder case (Fig. 3.1e) and the smallest for the bare stranded cable (Fig. 3.1b), while the smooth circular cylinder (Fig. 3.1a) yields intermediate results. The maximum pressure developed at the stagnation point reaches 266 Pa in the heavily iced cylinder, 235 Pa and 232 Pa in the bare stranded cable and smooth circular cylinder, respectively.

The negative pressure on the leeward side of the heavily iced cylinder reaches -942 Pa compared to -654Pa in the bare stranded cable. The pressure fields are significantly different for the five models considered: the heavily iced cylinder experiences the largest area of the negative pressure zone, from the flow separation point to the leeward side followed by the iced and stranded cable, and finally the bare circular cylinders profile experiences the smallest suction area. The stranded cable shows round improved aerodynamic behavior compared to cylinder, as its corrugated surface enables a more gradual flow separation [2]. These differences in pressure explain the trends observed in cable response, which are discussed next.

Figs. 3.4 and 3.5 present time history plots of the ne cable force response calculated from the integration of the pressure field at the air-cable interface. The force respons

of the five models is shown in terms of drag (C_D in Fig. 3.4) and lift (C_L in Fig. 3.5) coefficients. The heavily iced cable model, with its eccentric shape, experiences the largest drag coefficient with a value of 1.82 in the steady state; followed by the moderately iced cylinder with 1.5, and the circular cylinder has the smallest value, slightly below 1.2. The drag forces oscillate with a frequency of 59 Hz, which corresponds to a Strouhal number value of about 0.18.

Fig. 3.5 compares the vertical force response and it is seen that the heavily and moderately iced cylinders present similar behavior (C_L= +1.2 ~ C_L= -1.0), while the stranded cable is significantly less loaded with $C_L \approx \pm 0.7$.

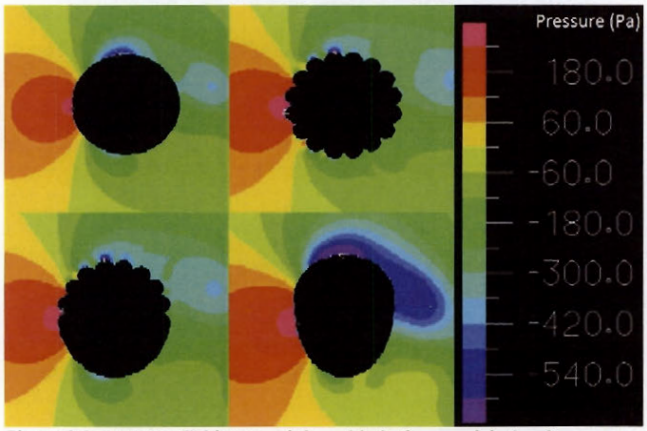

Figure 3.3. Pressure fields around the cable in four models (t = 2 s; incident wind speed = 20 m/s; ρ = 1.22 kg/m^3, and μ = 1.7×10-5 kg/m.s)

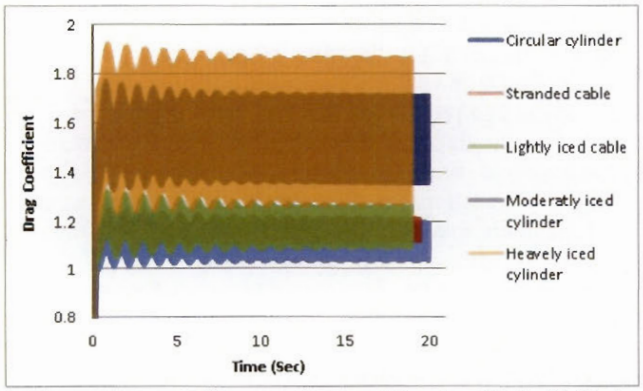

Figure 3.4. Drag coefficient obtained from different models for V=10m/s

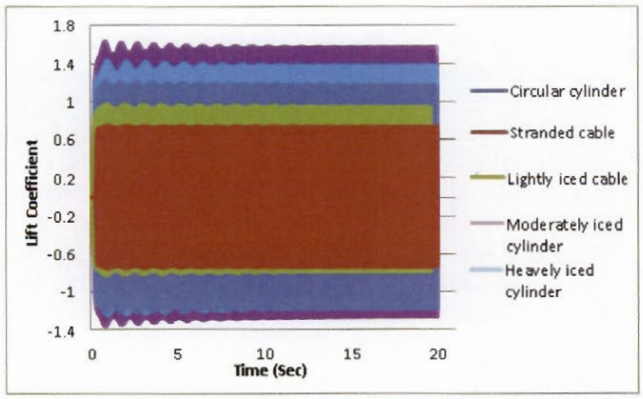

Figure 3.5. Lift coefficient obtained from different models for V=10m/s

3.5 Effect of Ice Accretion On Drag and Lift Coefficients

Analysis results for all five models with different ice thickness values confirm that the aerodynamic properties change significantly with ice thickness. Of course, the orientation of the incident wind flow is also an important factor, but the results discussed here are strictly for the wind flow direction indicated in Fig. 3.1. Figs 3.6 and 3.7 display the variations in drag and lift coefficients, respectively, for different amounts of ice accumulation.

As expected, the drag and lift coefficients increase with ice accumulation, particularly when the ice thickness is increased from 10% of cable diameter to 20%, but this also includes the influence of the change in the top surface roughness (see Fig. 3.1c and d). In most experimental works, the drag and lift coefficients are reported as constant values developed at the steady-state. However, the numerical results show that the magnitude of the drag and lift forces is fluctuating by as much as 30% depending on ice thickness and wind velocity. As shown in Figs. 3.4 and 3.6, the amplitude of the drag force fluctuations increases with ice thickness because of the larger fluctuations induced in the pressure field for the more asymmetric profiles. Fig.3.7 shows that the lift coefficient seems to stabilize with the increased ice thickness when the iced shape takes similar eccentric ovoid profiles (see Fig. 3.1 d and e).

Fig. 3.8 displays the cable horizontal displacement history for the five different models. It is seen that the steady state is reached after about 15 s and the transient amplitude is about twice the steady-state value. Again, in keeping with the preceding results, the heavily iced cable experiences the largest motion and the stranded cable, the smallest. Fig. 3.8 also provides useful information on the amount of aerodynamic damping present in the five models when the logarithmic decrement of the amplitude of the transient motion is calculated. In the particular flow conditions of the cases reported here, the viscous damping ratios are approximately 3.5% for the iced cylinder, 2.3% for the stranded cable and 1.6% for the smooth bare cylinder.

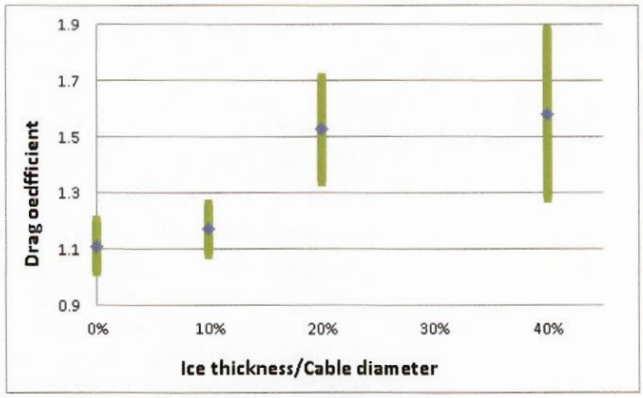

Figure 3.6: Cable drag coefficient for different ice accumulations

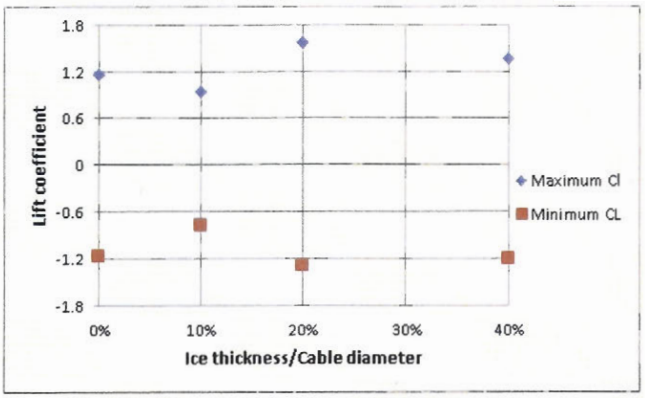

Figure 3.7: Cable lift coefficient for different ice accumulations

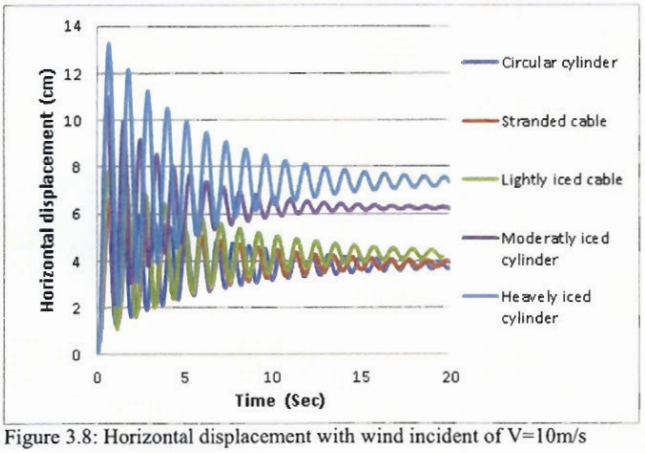

Figure 3.8: Horizontal displacement with wind incident of V=10m/s

Recalling that the cable elastic supports already accounted for the presence of dashpots with viscous damping ratio of 1%, it is seen that the eccentricity of the iced cable shape contributes greatly to the additional aerodynamic damping.

3.6 Conclusion

A computational study of the dynamic wind-cable interactions on two-dimensional models of five bare and iced cable cross-sectional shapes reveals that, unlike most of the results reported from experimental studies and used in design, drag and lift coefficients are not constant for the cable as resultant forces fluctuate due to both wind-cabl interaction and vortices in the flow around the cable Depending on cable movement, wind speed and cabl shape, the amplitude of these fluctuations may be as large a 50% of its maximum value. In this study, the incident win direction was fixed and it was confirmed the cable shap alone is a significant factor on the wind-induced cabl response. As expected, the eccentric iced shape is subjecte to larger net forces and motion. The presence of a thin laye of ice causes a significant increase on lift forces but whe the ice thickness exceeds 40% of the cable diameter the lif remains almost unchanged (the asymmetric aerodynami shape remains similar) while the drag force still increase significantly due to the increased drag coefficient and th larger windward area of the iced cable.

Overall, the smooth round cylinder and the bare strande conductor shapes differ significantly in their response, wit the stranded conductor experiencing significantly less force and motion than the smooth round cylinder, especially in th vertical direction. Although the results obtained for othe incident wind velocities were not presented, similar trend have been observed and the differences in respons observed here were found to be exacerbated at lower win speeds.

ACKNOWLEDGMENT

A research team grant from the Fonds québécois d la recherche sur la nature et les technologies (FQRNT) i kindly acknowledged.

REFERENCES

[1] ADINA Inc (2009). ADINA theory and modeling guide. 71 Elto Ave, Watertown, MA 02472, USA.

[2] Keyhan, H., McClure, G., Habashi,W.G. (2010). Computation study of surface roughness and ice accumulation effects on win loading of overhead line conductors. 13th International Conferenc on Wind Engineering (ICWE13). Amsterdam, The Netherlands, 1(15 July 2011.

[3] Bathe, K.-J. and H. Zhang (2002). A flow-condition-base interpolation finite element procedure for incompressible fluid flow *Computers & Structures*, **80**(14-15): 1267-1277.

4 Computational Study of Surface Roughness and Ice Accumulation Effects on Wind Loading of Overhead Line Conductors

Overhead transmission line conductors are exposed to different weather conditions and experience different wind pressures depending on their cross-sectional geometry, surface condition and incident wind velocity. In this chapter FSI analyses of three models with different cross sections, namely a bare ACSR stranded conductor, a smooth circular cylinder, and an iced smooth cylinder, are performed to study the influence of the cross-sectional shape and surface roughness on the fluid flow around the conductor, and in particular the fluid pressure in the boundary layer at the air-conductor interface is studied. The effects of different pressure distributions on drag and lift are investigated and compared in different conditions. Variation of conductor aerodynamic properties with wind speed is studied in this part of research as well. Among different results, the aerodynamic damping of conductors was of particular interest.

This part of the research was summarised into a scientific paper published last year in a peer-reviewed journal: Keyhan, H., McClure G., Habashi W.G. (2011). "Computational study of surface roughness and ice accumulation effects on wind loading of overhead line conductors." International Review of Civil Engineering 2(2): 207-214. (Keyhan H. et al. 2011a). The following section presents the paper as published.

Computational study of surface roughness and ice accumulation effects on wind loading of overhead line conductors

Hooman Keyhan [1], Ghyslaine McClure [2], Wagdi G. Habashi [3]

Abstract – *Current transmission line analysis methods generally consider wind effects on conductors and supports as static loads, despite the dynamic nature of wind loading. In this paper, the authors explore wind-cable dynamic interactions using a two-dimensional fluid-structure interaction (FSI) model and finite element analysis. The numerical simulation results reported show the effects of ice accretion and bare conductor roughness on the resultant aerodynamic forces induced on the cable section.*

Keywords: *computational fluid dynamics, conductor lift and drag coefficients; fluid-structure interactions, interactive wind and ice effects, overhead line conductors*

4.1 Introduction

With the exception of conductor galloping and Aeolian vibration effects, design wind loads on overhead transmission line systems are usually considered as a static pressure resulting from a synoptic ground boundary-layer wind velocity profile adjusted with elevation and terrain roughness. Therefore, aerodynamic wind-structure interaction effects are only roughly approximated in transmission tower analysis. Although fluid-structure interaction (FSI) analysis is becoming rather common in several engineering fields, namely in automotive, aerospace and biomedical applications, it has not been widely applied to transmission line engineering, for several practical reasons. One of them is the lack of a simplified framework to account for these loading interactions in stress analysis models used to study line sections comprising several conductor spans and supports, with reasonable engineering accuracy. Even if one could argue that the computational burden of full nonlinear dynamic FSI analysis is no longer an issue when a supercomputing platform is available, this is far from realistic in practice. The goal of this study is thus to develop a rational gusty wind load model for overhead line conductors that will serve to determine the resultant wind forces acting at the tower attachment points. Note that this work excludes the effects of wind-induced instability phenomena, and the results presented herein are limited to two-dimensions; the spatial and time randomness of wind pressure fluctuations will be introduced at a later stage of the research.

The study makes use of computational fluid dynamics (CFD) and recent advances in FSI analysis to simulate the pressure fields around a conductor cross section subjected to a laminar incident wind velocity of constant intensity. The writers are reporting results obtained with detailed two-dimensional models created with the commercial finite element software ADINA [1]. The main focus is to illustrate how the conductor aerodynamic properties (drag and lift coefficients) change with the conductor's shape and the incident wind speed.

4.2 General Modeling Approach

The study considers an ACSR (Aluminum Conductor Steel Reinforced, widely used in North America) conductor with 30-mm diameter (D), with three variants in shape: (a) a smooth circular cylinder, (b) a smooth cylinder of oval shape representing some ice accumulation at the bottom face, and (c) the realistic wavy surface profile of the bare stranded conductor (See Figure 4.1). The maximum ice thickness in model (b) is 6 mm (20% of the cable diameter). In model (c) the cable surface shows the outline of 30 outer layer strands of 3-mm diameter each. In all three models, the equivalent vertical and horizontal linearized stiffnesses of the conductor section are modeled by linear springs supported at the cable centroid, represented schematically in Figure 4.1. The equivalent spring stiffness properties were determined for a mid-span cross section using nonlinear elastic static analysis of a level 356-m span suspended in still air with fixed ends, with a horizontal tension of 19.2 kN in the bare condition (cable self-weight 14.9 N/m), and 22.5 kN in the iced condition (iced cable weight 17.9 N/m). A small viscous damping constant (equivalent to 1% of critical) is also assigned at the support in each orthogonal direction to approximate internal material damping in the conductor.

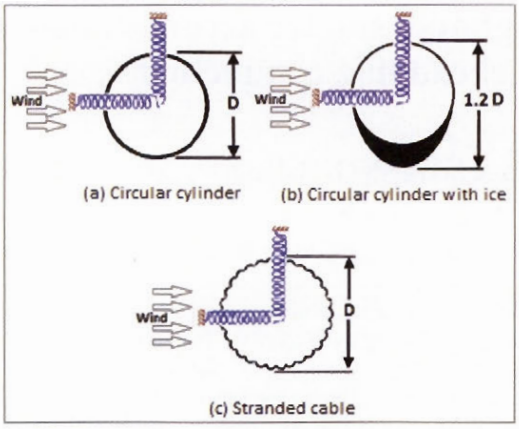

Fig. 4.1. Three fluid-cable sections under study

Optimizing the overall dimensions of the fluid domain for CFD and FSI analyses is imperative to ensure that the computational domain is large enough for the fluid boundaries to have negligible effects on the calculated cable response and yet attempt to reduce the computational cost. The total fluid domain (See Figure 4.2) has a horizontal length of 60xD and a vertical depth of 40XD. Further fluid modeling considerations are discussed in Section III. All three models were analyzed using four different horizontal wind velocities ranging from 5 m/s to 40 m/s, to study the aerodynamic cable response at different Reynolds numbers. The incident wind velocity profile is kept constant and uniform throughout, and so are the air properties.

4.3 Detailed Modeling Considerations

To keep the cable cross-sectional model simple, only the outer cable boundary is modeled using stiff two-dimensional Bernoulli beam elements with appropriate tributary mass. To obtain a realistic geometric profile and retain reasonable accuracy in FSI analysis, the cable perimeter is modeled with beam elements of length 0.31 mm (300 elements in total), 0.32 mm and 0.35 mm in configurations (a), (b) and (c), respectively. In the solid domain, the incremental form of the nonlinear equations of motion (updated Lagrangian formulation) of the cable cross section on linear spring supports and dashpots (see equation4.1)is solved by direct time-step integration using the classical Newmark method, and the equilibrium iterations are carried using the Full Newton method for stiffness updates. [1] In this equation M, C and K are mass, damping and stiffness matrixes respectively and u is the cable displacement and $F_{t+\Delta t}$represents the fluid force applied on cable at time $t + \Delta t$.

$$M\Delta\frac{d^2u}{dt^2} + C\Delta\frac{du}{dt} + K\Delta u = F_{t+\Delta t} - M\frac{d^2u}{dt^2} - C\frac{du}{dt} - Ku \quad (4.1)$$

The fluid domain is discretized with quadrilateral FCBI-C elements [2], using a structured "O" shape mesh, as shown in Fig.4.2 for the smooth round cylinder. The mesh geometry that provided optimal computational performances for this case comprises 75 × 75 elements at the external boundaries, and is gradually refined to a resolution of 300 elements at the air-cable interface. As indicated in Fig.4.2, the refined mesh in a ring zone of about 1xD thickness around the cable surface is able to capture the response with reasonable accuracy. The CFD analysis is based on the direct time-step integration of the unsteady Reynolds-averaged Navier-Stokes equations (See equation 4.2) using the Euler α - method of first order, and a constant time-step size of 0.1 ms was found optimal for the problem at hand. The iterative solver for the linearized incremental equations is the Algebraic Multi-Grid method (AMG). Airflow turbulence is modeled with the Spalart-Allmaras one-equation approach and vortex-shedding effects are introduced with the Detached Eddy Simulation (DES) algorithm. In FSI analysis, the Arbitrary-Lagrangian-Eulerian (ALE) formulation is used to allow for compatible mesh deformations and displacements for the fluid surrounding the cable in motion in each solution step. [1]

$$\rho\bar{u}_j\frac{\partial\bar{u}_i}{\partial x_j} = \rho\bar{f}_i + \frac{\partial}{\partial x_i}\left[-\bar{p}\delta_{ij} + \mu\left(\frac{\partial\bar{u}_i}{\partial x_j} + \frac{\partial\bar{u}_j}{\partial x_i}\right) - \rho\overline{\acute{u}_i\acute{u}_j}\right] \quad (4.2)$$

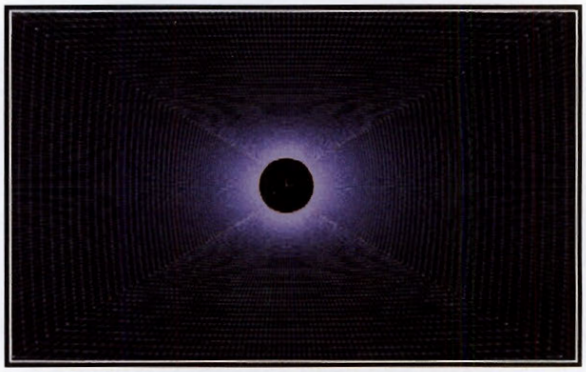

Fig. 4.2. Fluid domain structured "O" mesh

4.4 Results

For the sake of conciseness, a selection is made among the different model simulations in different flow conditions to illustrate the salient features of the results for the smooth, stranded and iced cross-section models with the incident wind speed of 5 m/s. Figure 4.3 depicts the pressure fields developed around the cable in the three models subjected to the same incident flow conditions at time t = 8 s. In general, the pressure field shows larger fluctuations in the iced cylinder case (Figure 4.3b) and smaller fluctuations in the stranded cable with wavy surface geometry (Figure 4.3c), while the circular cylinder case yields intermediate results. The maximum pressure developed at the stagnation point reaches 18.3 MPa in case (b) and 16.8 MPa in case (c), while the negative pressure on the leeward side of the

iced cylinder drops to -49 MPa in case (b) compared to -35 MPa in the stranded cable (c). Looking at the pressure fields developed around each model, it can be seen that both the pressure values and field patterns differ in the three cross-sectional models. The iced cable experiences the largest area of the negative pressure zone, from the flow separation point to the leeward side, followed by the smooth circular cylinder, and finally the stranded cable experiences the smallest suction area. The results indicate that the stranded cable shows improved aerodynamic behavior compared to the smooth round cylinder, as the corrugations of the stranded cable surface enable a more gradual flow separation. These pressure field differences will explain the trends observed in cable response in Figures 4.4 and 4.5 discussed next. [3]

Figures 4.4 and 4.5 present the time history of the drag (C_D) and lift (C_L) coefficients, respectively, resulting from the integration of the surface tractions exerted by the fluid on the cable-air interface. The results in Figure 4.4 show that the iced cylinder experiences the largest drag coefficient with a value of 1.55 in the steady state; the smooth round cylinder follows with 1.1, and the stranded cable has the smallest value, slightly above 1.0. The time fluctuations of the drag forces oscillate with a frequency of 32 Hz, which corresponds to a Strouhal number of approximately 0.2 for the wind speed of 5 m/s. The lift coefficients for the three models are compared in Figure 4.5 which shows that the smooth cylinder and stranded cable models are experiencing zero lift in average while the average coefficient is approximately 0.2 upward for the iced cylinder (with ice accretion at the bottom face). It is also observed that the stranded cable surface roughness, which enables a more gradual flow separation than the smooth surfaces, has reduced the lift force amplitude from 1.25 in the smooth cylinder to 0.7, which can significantly lower the amplitudes of vibration and, as a result, generate less fatigue and wear at conductor-hardware joints.

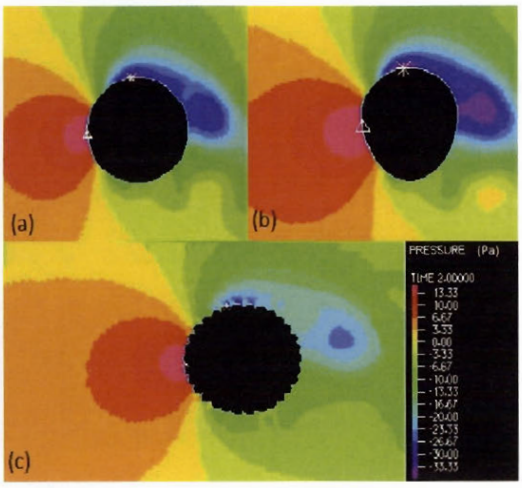

Fig. 4.3. Pressure fields around the cable in three models (t = 2 s; incident wind speed = 5 m/s; Re = 10600, ρ = 1.22 kg/m^3, and μ = 1.7×10^{-5} kg/m.s) a) Circular cylinder, b) Circular cylinder with ice c) Stranded cable

Figure 4.6 shows the cable horizontal displacement time history for the three different models. Depending on the incident wind speed (5 m/s is reported here) and the internal cable damping, the different models reach a steady state after about 10 s to 15 s. The transient amplitude is about twice the steady-state value in the three models and, as expected, the iced model experiences larger displacements due to its higher wind loading reported in Figure 4.4.

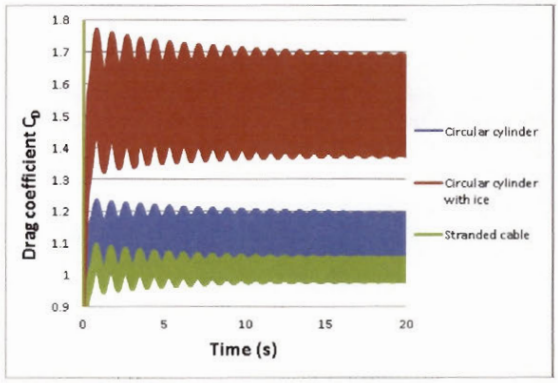

Fig. 4.4. Drag coefficients obtained for the three models

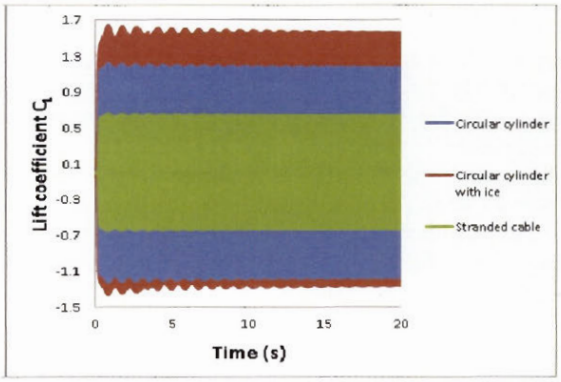

Fig. 4.5. Lift coefficients obtained for the three models

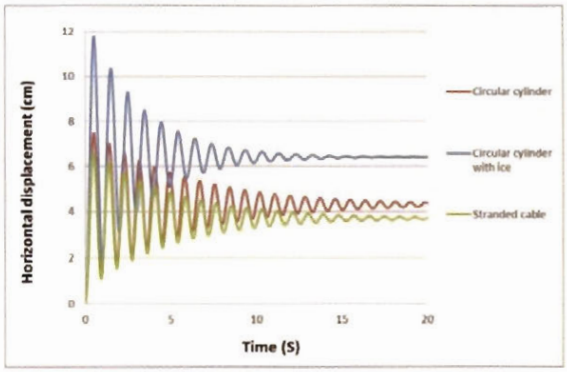

Fig. 4.6. Cable horizontal displacements

The horizontal displacements of the two bare cable models (smooth and stranded) are in the same range, as the drag coefficients are close for these two cases, and they oscillate with the same frequency, while the frequency of the motion of the iced section is lowered by the added mass of ice. Another interesting result of practical significance obtained in this study is the aerodynamic damping generated in the different models. The total equivalent viscous damping ratio corresponding to each displacement time history has been calculated using the logarithmic decrement. This total damping ratio consists of the predefined value of structural damping (set to 1% here) and the aerodynamic damping provided by the fluid-structure interaction.

For the set of results shown in Figure 4.6, the calculated viscous damping ratios are approximately 4.0% for the iced cylinder, 2.2% for the stranded cable and 1.7% for the smooth bare cylinder. This suggests that the eccentricity of the iced cable shape contributes greatly to the additional aerodynamic damping.

4.5 Effect of Wind Velocity on Drag and Lift Coefficients

Running numerical simulations for all three models with different incident wind velocities (5 m/s to 40 m/s) has shown that the aerodynamic properties of the models change with wind velocity, and the rate of these changes is different for each cable model. Figures 4.7 and 4.8 display the variations in drag and lift coefficients, respectively, for the smooth circular cylinder in different wind velocities (and corresponding Reynolds numbers). As expected, both the drag and lift coefficients decrease when wind speed increases and the largest drop is observed when the wind speed increases from 20 m/s to 30 m/s. Another point that is worthy of note relates to drag force oscillations. In most of the published experimental studies (See [4], and [5]), the drag and lift coefficients are reported as constant for a given wind speed. However, the numerical results obtained in this study show that the drag and lift coefficients oscillate in time and the range of the amplitude of these oscillations can be as large as 25% of the maximum value, depending on wind velocity.

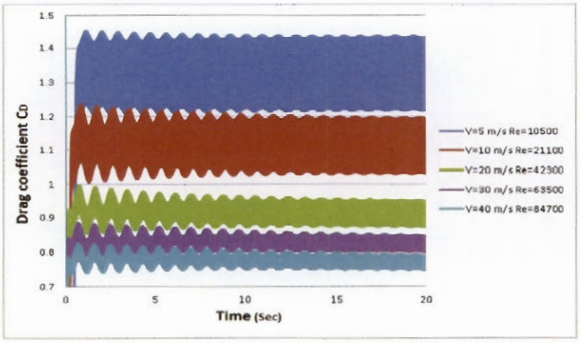

Fig. 4.7. Drag coefficient for circular cylinder at different wind speeds.

As shown in Figure 4.7, the amplitude of the drag oscillations decreases when the wind velocity increases due to the reduction in the pressure field fluctuations obtained at higher wind velocities. To illustrate this point with an example, Figure 4.9 shows two snapshots of the pressure field developed around the smooth circular cable for two values of incident wind speed (5 m/s and 30 m/s) at comparable conditions at t = 5 s. The pressure fields for V = 5 m/s are displayed on the left side and show that the zero pressure point moves by as much as 13.2° while it is only about 3.6° when the wind speed increases to 30 m/s. So it is seen that at higher wind velocity, the pressure field fluctuates less and therefore causes smaller drag oscillations. Another observation relates to the magnitude of the pressure changes during vortex shedding. Fluctuations as large as 25% of the maximum are simulated when the wind speed is 5 m/s but this value decreases to approximately 15% when the wind speed increases to 30 m/s.

Figures 4.10 and 4.11 summarize the results obtained for the three models showing the variation of the drag and lift coefficients, respectively, with increasing wind speed (and Reynolds numbers).

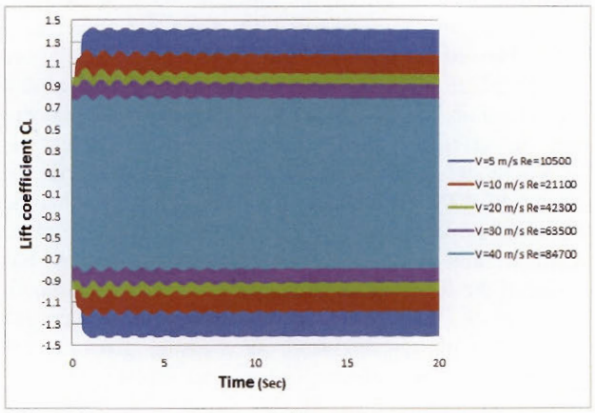

Fig. 4.8. Lift coefficient for circular cylinder at different wind speeds.

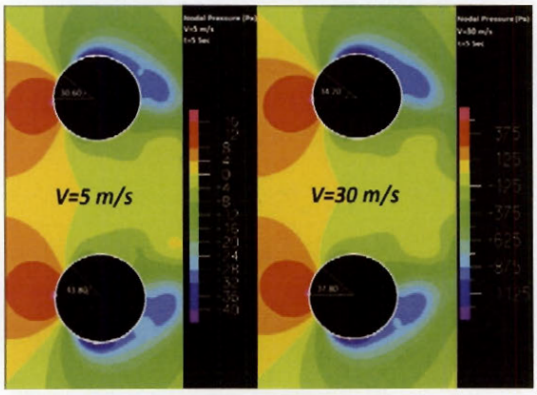

Fig. 4.9. Pressure fields around the smooth circular cylinder.

For the drag coefficients (Figure 4.10), each vertical bar indicates the two extreme values and the darker dash

line corresponds to the average. Comparing the simulated drag behavior of the bare circular cylinder and the stranded cable, it is seen that using a drag coefficient based on the smooth cylinder model to predict the wind force on the bare stranded cable will overestimate the wind drag force for wind speeds under 30 m/s but will underestimate it at the higher wind speed of 40 m/s.

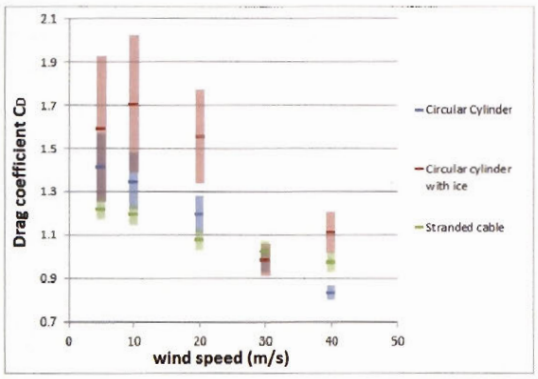

Fig. 4.10. Variations in drag coefficients with wind speed.

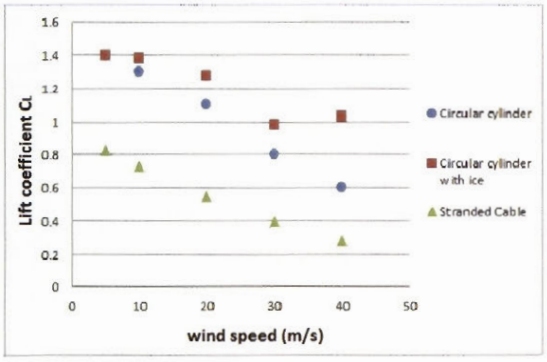

Fig. 4.11. Variations in lift coefficients with wind speed.

When comparing Figures 4.10 and 4.11, one should keep in mind that the results shown are for drag and lift coefficients and not effective wind loads on the cable cross section. The resultant cable forces in horizontal and vertical directions depend on wind speed, force coefficients (C_D and C_L) and projected area of conductor. To see how these parameters influence the effective wind loads, Figures 4.12 and 4.13 show plots of the average drag and lift forces (in N/m) as a function of wind speed, respectively.

In Figure 4.12, the comparison shows that the drag forces calculated in the three models are almost the same for the wind speed of 30 m/s. At lower speeds, the drag force on the stranded cable is about 10% less than that on the smooth circular cylinder while the force applied on the iced cylinder is about 25% higher. At 40 m/s, the iced cable experiences 36% more drag force than the smooth bare cylinder.

Figure 4.13 shows that the lift force applied on the stranded cable is about half the lift force applied on the bare smooth cylinder. As mentioned earlier, this is due to the effect of surface roughness, which causes the flow to separate in a different fashion in the stranded and smooth models as the corrugated surface enables a more gradual flow separation. One can also see that the rate of increase of the lift force with wind speed is higher for the iced cross section with unbalanced profile, while the models with symmetric profiles exhibit a steady rate.

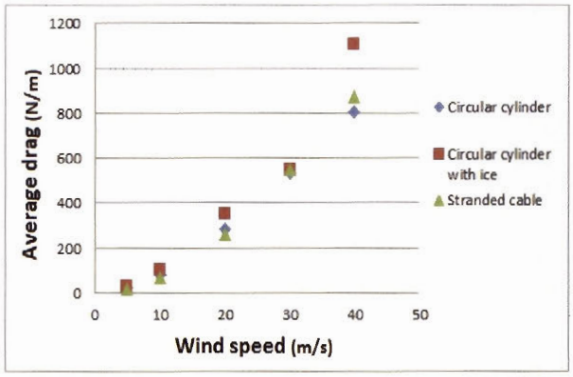

Fig. 4.12. Variations in drag forces with wind speed.

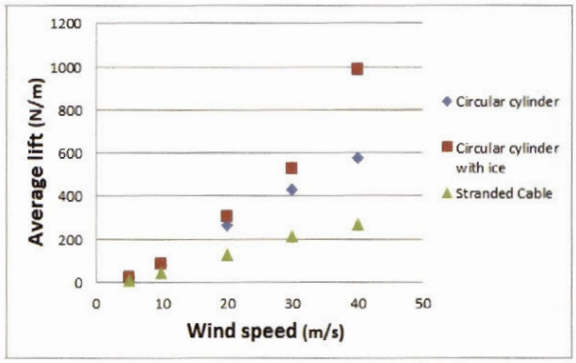

Fig. 4.13. Variations in lift forces with wind speed.

4.6 Effect of Incident Wind Velocity on Aerodynamic Damping

To study the effect of incident wind speed on the conductor's aerodynamic damping, the conductor motion is monitored in the time domain and the logarithmic decrement is calculated and translated into its equivalent viscous damping ratio. The variation of this ratio (in % of critical) with wind speed is plotted in Figure 4.14 for the three studied models. These results are very interesting in showing how the stranded cable shape is efficient in generating aerodynamic damping compared to the bare circular cylinder. The iced cylinder generates significant damping at wind speeds of 10 and 20 m/s but the ratio tends to saturate after 30 m/s. This saturation is also observed in the smooth circular cylinder but not in the stranded conductor, which exhibits a linear relation between wind speed and aerodynamic damping ratio in the wind speed range considered in the study. A time

history of conductor horizontal displacement for the three models is shown in Figure 4.15 to illustrate the aerodynamic damping effects calculated at high wind speed (V = 40m/s). Considering it takes several seconds for the displacement to reach a steady-state value, one can anticipate that aerodynamic damping plays a significant role in reducing the cable motion in buffeting wind conditions.

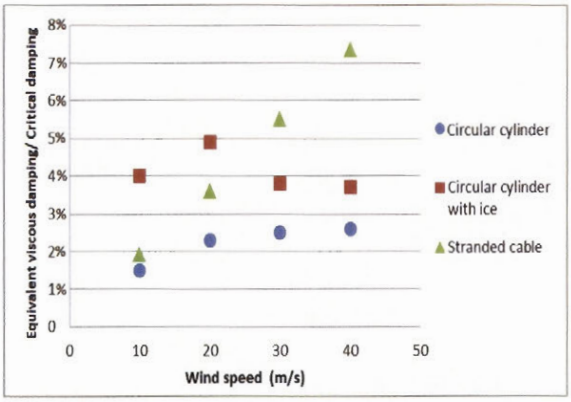

Fig.4.14.Variation of equivalent viscous damping ratio with wind speed

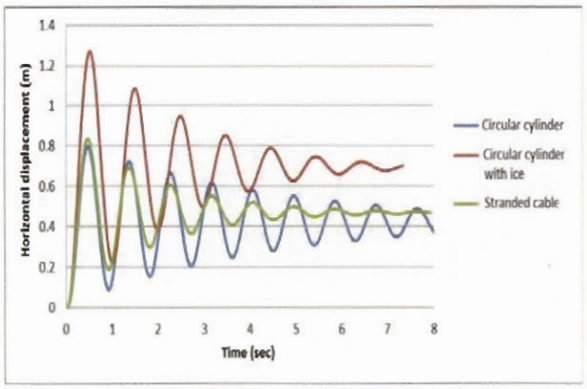

Fig. 4.15. Time history of cross-sectional horizontal displacements for an incident wind velocity of 40m/s

4.7 Conclusion

A computational study of dynamic wind-cable interactions using two-dimensional models of three cable cross-sectional shapes confirms that shape alone is a significant factor on cable response to wind. As expected, the eccentric iced shape is subjected to larger net forces and motion. However, the smooth round cylinder and the stranded conductor shapes differ significantly in their response, with the stranded conductor experiencing significantly less forces and motion than the smooth round cylinder. These findings are of high significance for overhead line design. Although the results obtained for other incident wind velocities were not presented herein, similar trends have been observed and the differences in response discussed here were found to be exacerbated at lower wind speeds. This study is the first step in the development of a rational conductor wind load model for overhead line supports which would account for wind-structure interaction effects in dynamic simulations of overhead line response.

ACKNOWLEDGEMENTS

A research team grant from the Fonds québécois de la recherche sur la nature et les technologies (FQRNT) is gratefully acknowledged.

REFERENCES

[1] ADINA Inc. 2009. ADINA theory and modeling guide. 71 Elton Ave, Watertown, MA 02472, USA.

[2] Bathe KJ and Zhang H. 2002. A flow-condition-based interpolation finite element procedure for incompressible fluid flows. Computers & Structures, 80:1267-77.

[3] Keyhan H, McClure G, and Habashi WG. 2011. "On computational modeling of interactive wind and icing effects on overhead line conductors". Proceedings of the International Workshop on Atmospheric Icing of Structures (IWAIS), Chongqing, China, May 8-13, Paper B-5-1-28.

[4] Zdravkovich MM. 1997. Flow around circular cylinders : a comprehensive guide through flow phenomena, experiments, applications, mathematical models, and computer simulations: Oxford University Press.

[5] Shih WCL, Wang C, Coles D, and Roshko A. 1993. Experiments on flow past rough circular cylinders at large Reynolds numbers. Journal of Wind Engineering and Industrial Aerodynamics. 49:351-68.

[6] Keyhan H, McClure G and Habashi, WG. 2011. "Fluid-Structure Interaction Wind Load Model for Dynamic Analysis of Overhead Transmission Lines Subjected to Glaze Icing and Gusty Winds", Sixth M.I.T. Conference on Computational Fluid and Solid Mechanics, Cambridge, MA, USA June 15-17 (Oral presentation and abstract P.94).

[7] Shan L, Jenke LM, and Cannon DD. 1992. Field determination of conductor drag coefficients. Journal of Wind Engineering and Industrial Aerodynamics, 41:835-46.

[8] Kadab RR. 1998. Response of electrical transmission conductors to extreme wind using field data. Ph.D. thesis, May 1988, 142 p. Texas Tech University, USA.

[9] Zdero R, and Turan OF. 2010. The effect of surface strands, angle of attack, and ice accretion on the flow field around electrical power cables. Journal of Wind Engineering and Industrial Aerodynamics, 98:672-8.

[10] Breuer M. 1998. Numerical and modeling influences on large eddy simulations for the flow past a circular cylinder. International Journal of Heat and Fluid Flow, 19:512-21.

[11] Battista RC, Rodrigues RS, and Pfeil MS. 2003. Dynamic behavior and stability of transmission line towers under wind forces. Journal of Wind Engineering and Industrial Aerodynamics, 91:1051-67

[12] Forster C. 2007. Robust methods for fluid-structure interaction with stabilised finite elements. Ph.D. thesis, 2007, 184 p. University of Stuttgart, Germany.

[13] Bathe KJ. 2006. Finite Element Procedures. Prentice Hall.

[14] Hughes TJR, Liu WK, and Zimmermann TK. 1981. Lagrangian-Eulerian finite element formulation for incompressible viscous flows. Computer Methods in Applied Mechanics and Engineering, 29:329-49.

5 Fluid-Structure Interaction analysis of wind effects on overhead transmission line conductors

Following the computational studies presented in the previous chapters, which revealed that conductor aerodynamic properties could vary considerably depending on their surface geometry and roughness, a more comprehensive study was conducted consisting of 15 different models each with four different incident wind velocities. This part of the research examines the detailed effects of conductor strand size and number, ice accretion shape and thickness, conductor motion, incident wind velocity as well as angle of attack, on the conductor aerodynamic properties.

The main results were summarised into a manuscript that is currently under review: Keyhan, H., McClure G., Habashi W.G. (2012). "Fluid-Structure Interaction analysis of wind effects on overhead transmission line conductors." Journal of Wind Engineering & Industrial Aerodynamics, Manuscript number: INDAER-D-12-00062, submitted on March 22nd 2012.(Keyhan H. et al. 2012c).

Fluid-Structure Interaction analysis of wind effects on overhead transmission line conductors

Hooman Keyhan[1] [a], Ghyslaine McClure [a], and Wagdi G. Habashi [b]

[a] *Department of Civil Engineering and Applied Mechanics, McGill University, 817 Sherbrooke Street West, Montreal, Quebec, Canada*
[b] *Computational Fluid Dynamics Laboratory, Department of Mechanical Engineering, McGill University, 688 Sherbrooke Street West, Montreal, Quebec, Canada*

Abstract

Transmission line analysis methods generally consider wind effects on conductors and supports as quasi-static loads, despite the dynamic nature of wind loading and wind-cable interactions. In the present study, the authors explore wind-cable interactions via a 2-D fluid-structure interactive model based on linear dynamic finite element analysis. The numerical simulation results provide additional insight, not available from experimental procedures, on the effects of ice accretion thickness, bare conductor roughness, wind velocity and angle of attack on the resultant aerodynamic forces induced on the conductor. This information is used to develop a new wind-load model for 3-D overhead line conductors, which is illustrated with a numerical example of a single span model. The results indicate that disregarding wind-cable interactions tends to overestimate wind loads and conductor response.
Keywords: Computational fluid dynamics; fluid-structure interaction; overhead line conductors; Conductors drag and lift coefficient; interactive wind and ice effects.

5.1 Introduction

The most common and important source of dynamic loads on overhead transmission lines comes from wind effects on the towers and conductors. (Davenport, 1979) Conductors are particularly sensitive to wind effects as they are long and relatively flexible compared to their supports, and are literally wind-catching structures in the power grid infrastructure. Since the aerodynamic properties of transmission line conductors are known to play an important role in transmission line loading, they should be evaluated precisely and carefully. This had traditionally been done based on wind tunnel experiments that are not easily available and are expensive, with overhead line load monitoring and experimental line tests providing additional useful information. On the other hand, a Fluid-Structure Interaction (FSI) analysis of wind and conductors is becoming possible by coupling computational structural dynamics (CSD) and computational fluid dynamics (CFD) to model structures and their surrounding air flow in a more complete and realistic fashion . Experimental studies will always remain necessary for model validation, but the advantages of numerical modelling are far reaching, including low cost, wider accessibility, and easier control of variables like fluid properties, conductor surface condition or flow conditions. In this study, a smooth cylinder and two conductors with different strand configurations, in bare and iced conditions, are analysed in detail in their surrounding airflow using a commercial finite element

[1] Corresponding author Tel:+1-514-452-7797; Fax: +1-514-398-7361; E-mail address: Hooman.Keyhan@mail.mcgill.ca

software.(ADINA R&D Inc, 2009) The objectives of this paper are thus to study the effect of different parameters such as strand configuration, ice accretion, angle of attack and wind velocity, on the aerodynamic properties of overhead conductors, with a view to develop a more modern, more realistic, gusty-wind loading model for transmission line analysis.

5.2 General modelling approach

To study the aerodynamic properties of conductors in different conditions, three geometries are selected for a 30-mm diameter conductor: a smooth circular cylinder; an ACSR 26/7 (Aluminium Conductor Steel Reinforced conductor with 26 aluminium and 7 steel strands) with 16 outer layer aluminium strands of 5-mm diameter each; and an ACSR 54/7 conductor with 30 outer layer aluminium strands of 3-mm diameter each. A total of 15 different conditions are analysed, as illustrated schematically in Figure 5.1 and summarized in Table 5.1.

Table 5.1. Studied conductor models

Model	Support condition	Surface condition	Ice thickness	Angle of attack
a	Fixed	Smooth	0	90°
b	Flexible	Smooth	0	90°
c	Flexible	Stranded	0	90°
d	Flexible	Stranded	0	90°
e	Flexible	Stranded	0.1D (3mm)	90°
f	Flexible	Smooth	0.2D (6mm)	90°
g	Flexible	Smooth	0.4D (12mm)	90°
h	Flexible	Stranded	0.1D (3mm)	0°
i	Flexible	Stranded	0.1D (3mm)	45°
j	Flexible	Stranded	0.1D (3mm)	135°
k	Flexible	Stranded	0.1D (3mm)	180°
l	Flexible	Smooth	0.1D (3mm)	0°
m	Flexible	Smooth	0.1D (3mm)	45°
n	Flexible	Smooth	0.1D (3mm)	135°
o	Flexible	Smooth	0.1D (3mm)	180°

Model (a), a smooth cylinder on fixed supports, serves to compare the results from this study with experimental wind tunnel results (Shih et al, 1993; Zdravkovich, 1997), while Model (b) is on flexible supports. Models (c) and (d) are used to study the effects of surface roughness provided by the outer layer strand geometry. In Model (e) the maximum ice thickness is only 3 mm (10% of the cable diameter) and the cable strands are not completely covered with ice, while in models (f) and (g) the maximum ice thickness is increased to 20% and 40% of the cable diameter, respectively, such that the conductor is assumed iced on its entire surface and represented by a smooth cylinder of oval shape.(Keyhan et al, 2011c) All models are exposed to four different wind speeds, ranging from 10m/s to 40m/s, in increments of 10 m/s. The incident wind speed is assumed constant, despite the fact that wind speed naturally fluctuates in time: this is to limit the number of variables when observing the influence of wind speed on the aerodynamic properties of the fluid-cable system. A natural wind time history record is considered in the last section of this paper to illustrate the development of a 3D loading model.

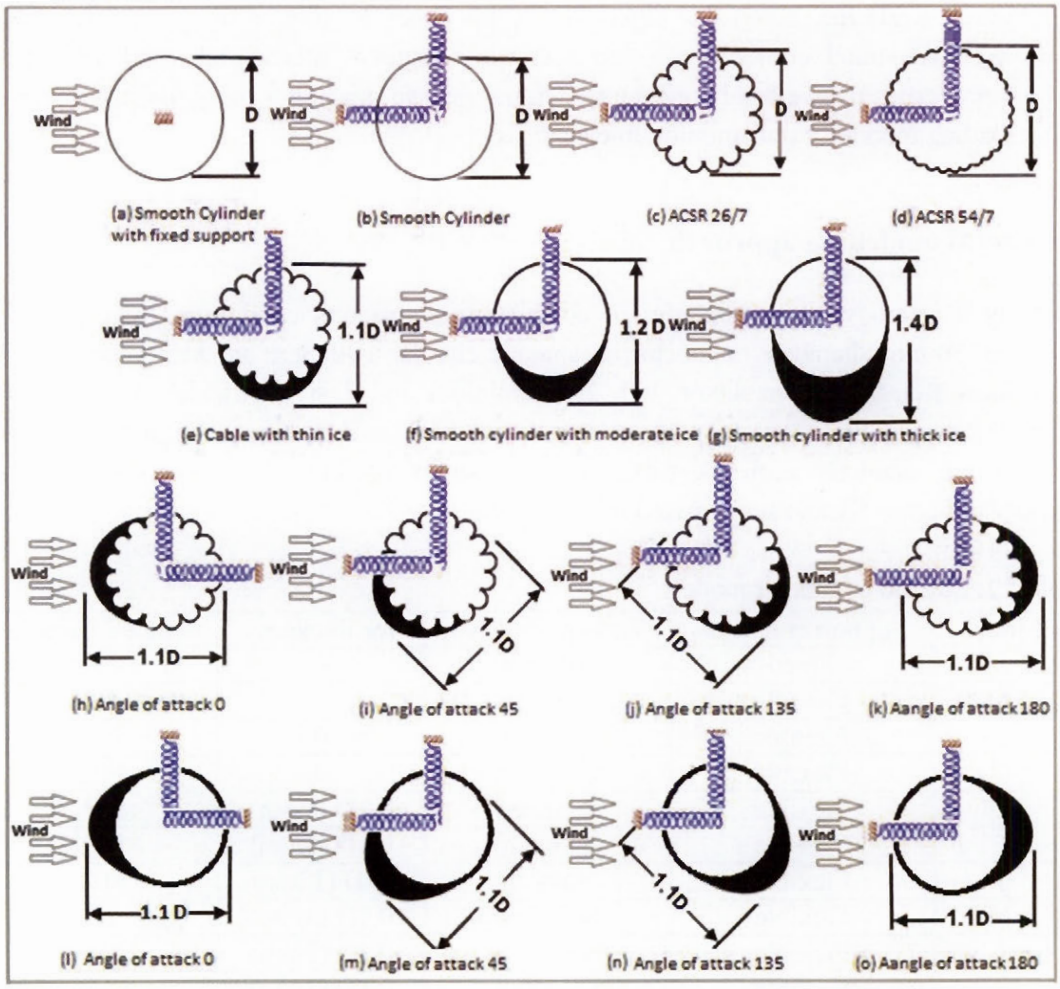

Figure 5.1 Studied conductor models

In all the models (except the reference case (a) that is completely fixed), the equivalent vertical and horizontal linearized stiffnesses of the conductor section are modelled by linear springs at the cable centroid, represented schematically in Figure 5.1. The equivalent spring stiffness properties were determined for a mid-span cross section using nonlinear elastic static analysis of a level 355-m span suspended in still air, with a horizontal tension of 19.2 kN in the bare condition (cable self-weight 14.9 N/m), and 22.5 kN in the iced condition (iced cable weight 17.9 N/m). A small viscous damping constant is also assigned at the support in each orthogonal direction to approximate internal material damping in the conductor.(Keyhan et al, 2011a) Introducing such damping filters the spurious high frequency response resulting from discretization of the continuous physical problem. The damping constant for the bare cable is assigned a fixed value corresponding to 1% of the critical linear viscous damping. Cable manufacturers do not supply this information and little research has been carried out on conductors' structural damping properties; most of the published data report total damping, combining both structural and aerodynamic damping effects.

The fluid domain mesh (seeFigure 5.2) has a horizontal length of 60xD and a vertical depth of 40xD. This overall size was determined based on several trial simulations using the smooth cylinder model (a) to ensure that the computational domain is large enough for the fluid boundaries to have negligible effects

on the calculated cable response, and yet strive to reduce the computational cost. Further essential fluid modelling considerations are discussed next.

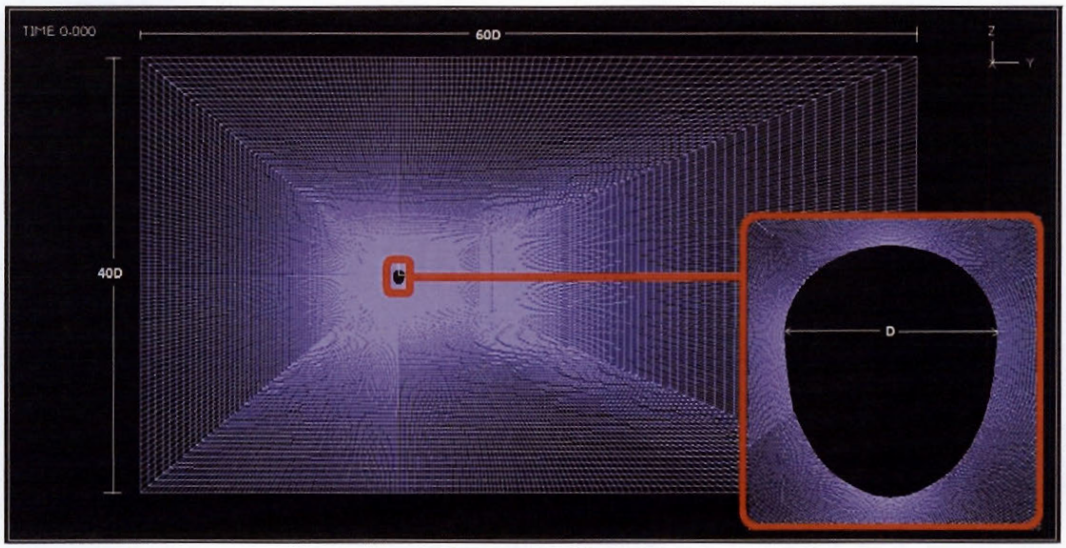

Figure 5.2 Fluid domain mesh for CFD analysis for model (f)

5.3 Detailed modelling considerations

To keep the conductor cross-sectional models simple, two-dimensional stiff Bernoulli beam elements are used to model the outer cable boundary and an appropriate tributary lumped mass is assigned to beam element nodes. Several cable mesh models have been tested and optimal results were obtained with 400 to 580 elements to represent the cable contour, depending on the geometry of the fluid-structure interface. The analysis in the solid domain proceeds with the time-accurate solution of the incremental form of the nonlinear equations of motion (using the updated Lagrangian formulation) of the cable cross-section on spring/dashpot supports: the direct integration operator selected is the classical Newmark method with a time step of 0.1s, and the equilibrium iterations are carried using the Full Newton method with an energy-based convergence criterion.

Quadrilateral FCBI-C elements (Bathe and Zhang, 2002) are used to discretize the fluid domain, using the structured "O" shape mesh of Figure 5.2. Since all FCBI-C's degrees of freedom are defined at the centre of the element, the solution variables are assumed to be piecewise constant during computations, while the final solution is interpolated at corner nodes for post-processing. Depending on the conductor cross-sectional model, different fluid mesh layouts are used to provide optimal computational performance, varying from 50 × 150 to 90 × 200 elements at the external boundaries, for the ACSR model (d) and the heavily iced cylinder case (g), respectively; this mesh is gradually refined to a resolution of 400 to 580 elements at the air-conductor interface. To capture the fluid response with reasonable accuracy, a refined mesh is used in a ring zone of about 1xD thickness around the cable surface. The CFD analysis proceeds with direct time-accurate integration of the unsteady Reynolds-averaged Navies-Stokes (URANS) equations using the Euler α - method of first order. A constant time step of 0.1to 0.025 ms, depending on wind speed, was found optimal for the problems at hand. The

iterative solver for the linearized incremental URANS equations is the Algebraic Multi-Grid method (AMG). Airflow turbulence is modelled with the Spalart-Allmaras one-equation technique and vortex-shedding effects are introduced with the Detached Eddy Simulation (DES) algorithm. In FSI analysis, the Arbitrary-Lagrangian-Eulerian (ALE) formulation is used to allow for compatible mesh deformations and displacements of the fluid surrounding the cable in motion in each solution step.(ADINA R&D Inc, 2009; Hughes et al, 1981)

5.4 Results

5.4.1 Air pressure fields

Before discussing the results obtained for the aerodynamic properties of the conductors in different models, a presentation of the computed pressure fields developed around the conductor will help in interpreting the results. This presentation is made for the incident flow conditions with $V = 20\ m/s, \rho = 1.292\ kg/m^3, \mu = 1.7 \times 10^{-5}\ Ns/m^2$, at time t = 5 s (see Figure 5.3).

As shown in the figure, the pressure fields developed around the cable in each model are significantly different depending on the geometry of the cross-section. The positive pressures on the upstream side are only slightly different: the smooth cylinder (model (b)) and ACSR 54/7 (model (d)) experience a maximum of approximately 237 Pa, while the pressure increases to 256 Pa for ACSR 26/7 (model (c)) due to its larger strand diameter which leads to a higher pressure at a stagnation point between two strands. The iced models experience higher pressure on their upstream side reaching 263 Pa in the moderately iced model (f), and 286 Pa in the heavily iced model (g). The largest pressure differences are experienced on the downstream side and at the separation points where the negative pressure of the heavily iced cylinder (model (g)) drops to -930 Pa, compared to -588 Pa in the ACSR 26/7 model (c). The overall pressure field patterns are also significantly different in the three models: the heavily iced cylinder experiences the largest area of negative pressure followed by the iced and bare circular cylinders, and finally the ACSR 26/7 cable experiences the smallest suction area. An interesting observation is that the stranded cables show different aerodynamic behaviour compared to the smooth round cylinder, because the surface corrugations provided by the strands enable a more gradual flow separation; this effect is observed to be more pronounced in cables with larger strands.

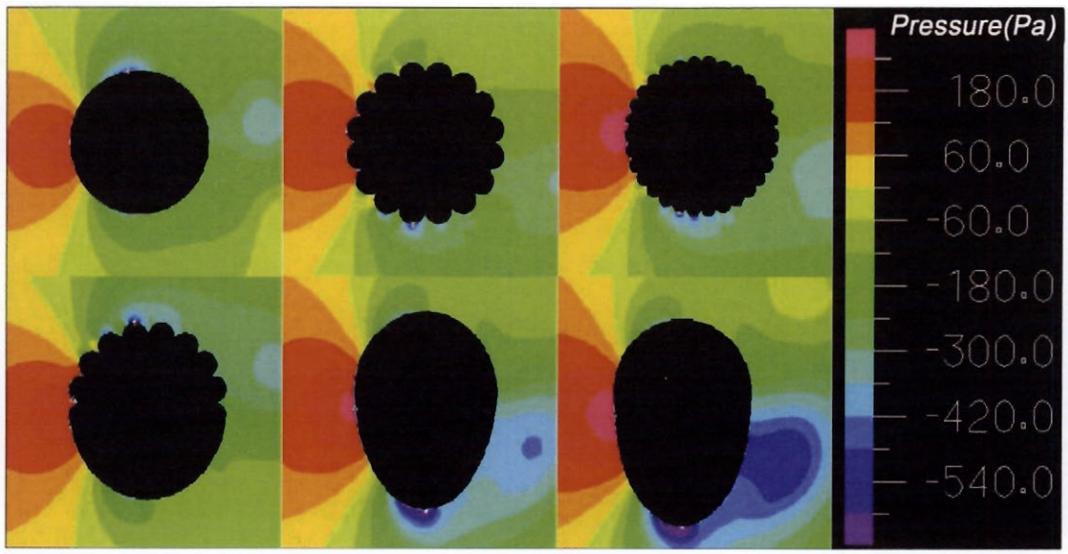

Figure 5.3Pressure field developed around conductors at $V = 20\ m/s\,, \rho = 1.292\ kg/m^3\,, \mu = 1.7 \times 10^{-5}\ N.s/m^2$

5.4.2 Fluctuations in drag and lift coefficients

Among the interesting features observed in the computational results, which are missed in experimental studies, is the fluctuation in drag and lift coefficients with two different frequencies for a give incident wind speed. This is illustrated in Figure 5.4 for V = 10 m/s. The transient oscillation with lower frequency that produces a wavy pattern in the initial portion of the drag and lift coefficient time history plots is eventually flattened. The second higher frequency oscillation in drag and lift is caused by the air flow around the conductor (vortex shedding). The shedding frequency is known to depend on parameters such as Reynolds number and surface roughness, to list the most important (Kadab, 1998; Shih et al, 1993; Zdravkovich, 1997). For the smooth cylinder with V = 10 m/s, the vortex shedding frequency is approximately 63 Hz. The change in flow pattern leads to a change in the pressure field around the conductor, as can be seen in Figure 5.3, causing variations in drag and lift: the pressure field is asymmetric about the horizontal axis and the negative pressure field moves between the separation points in each period. These fluctuations of the pressure field induce cyclic changes of lift direction, which can be seen in Figure 5.4, but have less effect on the drag.

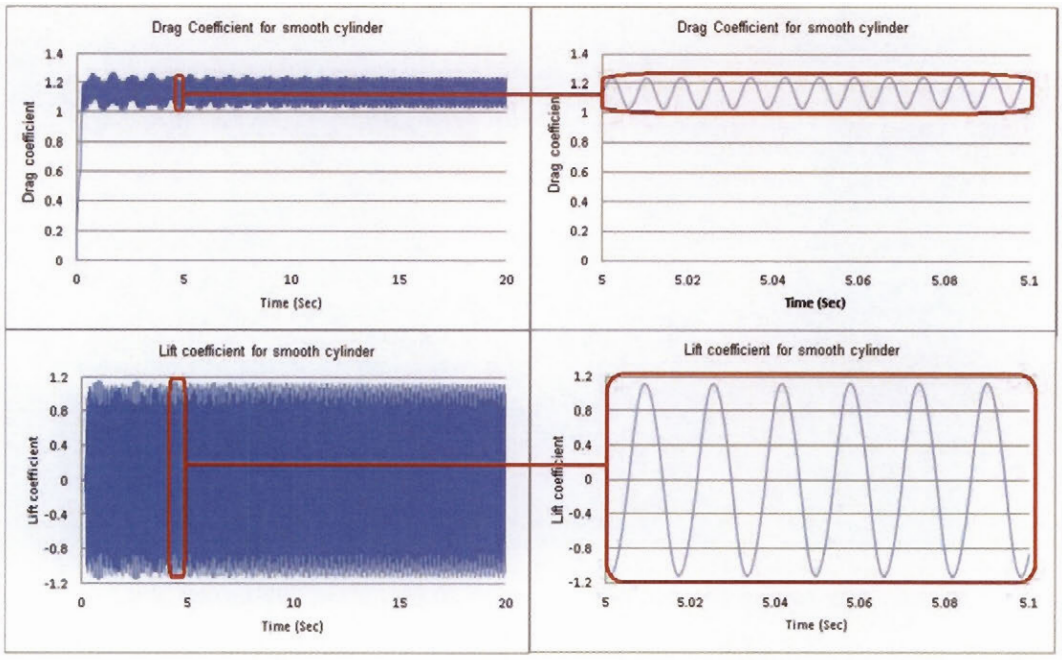

Figure 5.4Drag and lift oscillations due to vortex shedding (Model (b) with V = 10 m/s).

5.4.3 Effects of wind velocity on conductor drag and lift coefficients

Several published works have studied the variation of drag and lift coefficients on a smooth circular cylinder for different Reynolds numbers (Shih et al, 1993; Zdravkovich, 1997), but to the authors' knowledge there is no published numerical study of the effect of wind velocity, and consequently Reynolds number, on the drag and lift coefficients of stranded conductors with wavy surface patterns. Although there have been some wind tunnel studies and field measurements to determine the drag coefficient of overhead line conductors in bare (non-iced) condition, the results obtained from these tests show a large scatter (Shan et al, 1992; Tabatabai et al, 1992) that complicates their interpretation. Indeed, several wind characteristics and parameters are difficult to be controlled in physical tests such as background turbulence, air temperature variations (which can affect both air density and instruments calibration), aspect ratio of conductor specimens, surface roughness, etc. Taking these issues into consideration, a comparison between the results from this numerical study and published experimental values is attempted whenever possible.

Depicts the variation of drag coefficients in the different bare cable models when the wind velocity (and corresponding Reynolds number) is increased. The velocity range considered (10 to 40 m/s) corresponds to that used in transmission line design. A bar graph is used, as the drag coefficient oscillates between two values, and the darker shape indicates the mean value. The amplitude of oscillation is largest for the smooth cylinder and smallest for ACSR 26/7, as its surface corrugations enable a more gradual flow separation. Figure 5.5 also illustrates that the variations in drag coefficient occur at a different rate in the various models, which is explained by the fluctuations in pressure fields discussed in section 4.1 To further illustrate this observation, displays, for a wind velocity of 10 m/s in the top part and 20 m/s in the bottom part, the pressure field developed around the three cable models. For V = 10 m/s, the fluctuations in positive pressure are small (less than 2 Pa on a reference of 60 Pa) while they are more significant in

negative pressure (ranging from-134 Pa to -151 Pa). When the fluid velocity is increased to 20m/s, the positive pressure experiences the largest increase in the smooth cylinder at 266 Pa, compared to 256 Pa in ACSR 26/7. The smooth cylinder also experiences the largest drop in negative pressure with -716 Pa compared to -588 in ACSR 26/7 and -568 Pa in ACSR 54/7. This is in agreement with previous observations that stranded surfaces experience a "drag crisis" in the range of 20,000< Re< 40,0000 while it happens around $Re = 10^5$ in smooth cylinders(Shan et al, 1992; Tabatabai et al, 1992; Zdravkovich, 1997) . For the fixed smooth cylinder, although the calculated drag coefficient of approximately 1.2 is comparable with most reported values (Shih et al, 1993; Zdravkovich, 1997), drag effects increase when the same shape is on flexible supports: this effect is exacerbated at lower wind speeds.

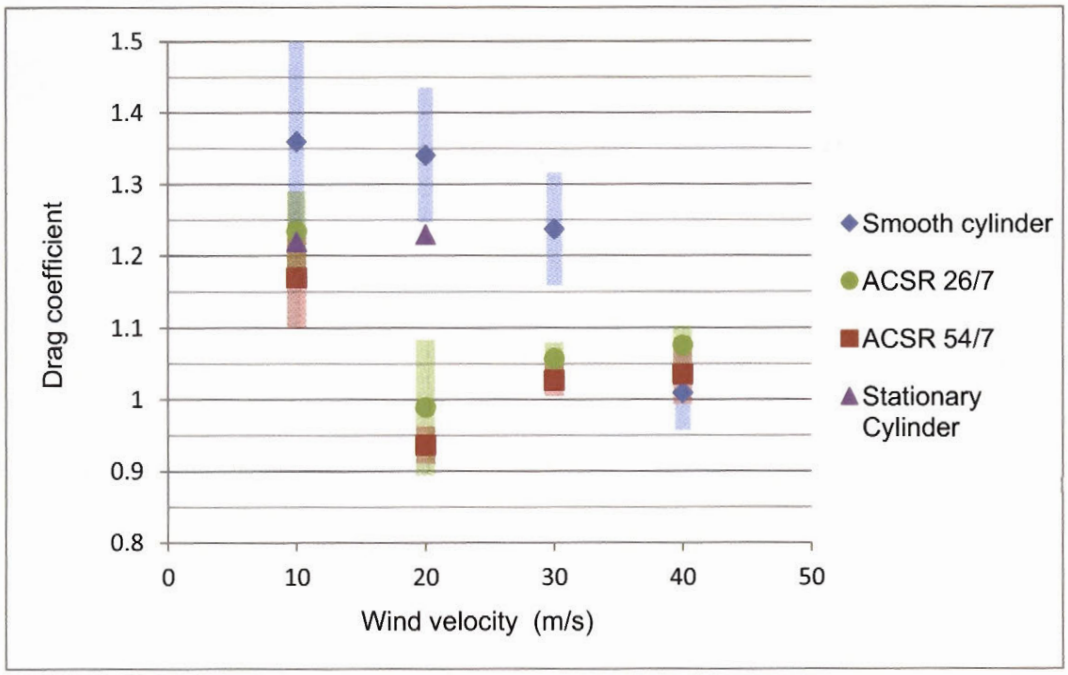

Figure 5.5Variation of drag coefficient with incident wind velocity

Another observation from the results of Figure 5.5 relates to the variation in amplitude of the drag coefficients at any given wind speed. Spatial pressure field variations, as well as time pressure changes in each cycle of vortex shedding, causes the drag coefficient to oscillate with decreased amplitude when the wind velocity increases. The reduced fluctuation in pressure field at higher wind velocities is illustrated in Figure 5.7for the smooth circular cylinder. The pressure fields developed around the cylinder with V = 5 m/s are displayed on the left for two selected extreme conditions: it is seen that the stagnation point moves by about 13.2° (from 30.6 °to 43.8°) in each vortex shedding cycle. On the right, for V = 30 m/s, the stagnation point moves by only 3.6°.

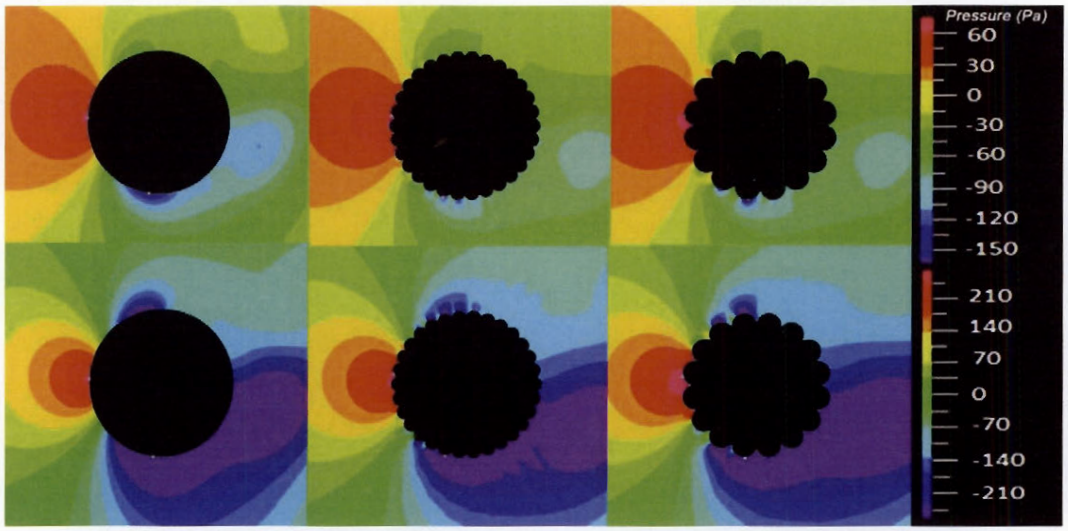

Figure 5.6Pressure field developed around conductors for V=10 m/s and V= 20 m/s

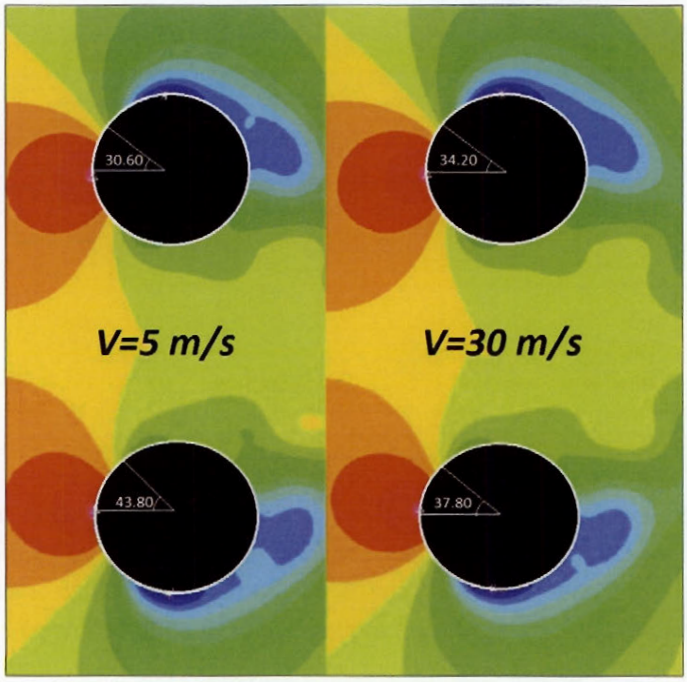

Figure 5.7Displacement of stagnation point for V = 5 m/s and V = 30 m/s

Figure 5.8 depicts the variation of lift coefficient with velocity and, as expected, the amplitude of this variation decreases considerably by increasing the wind velocity. As previously discussed, the smooth cylinder experiences the largest drop in negative pressure when the wind velocity increases, unlike the stranded cable models.

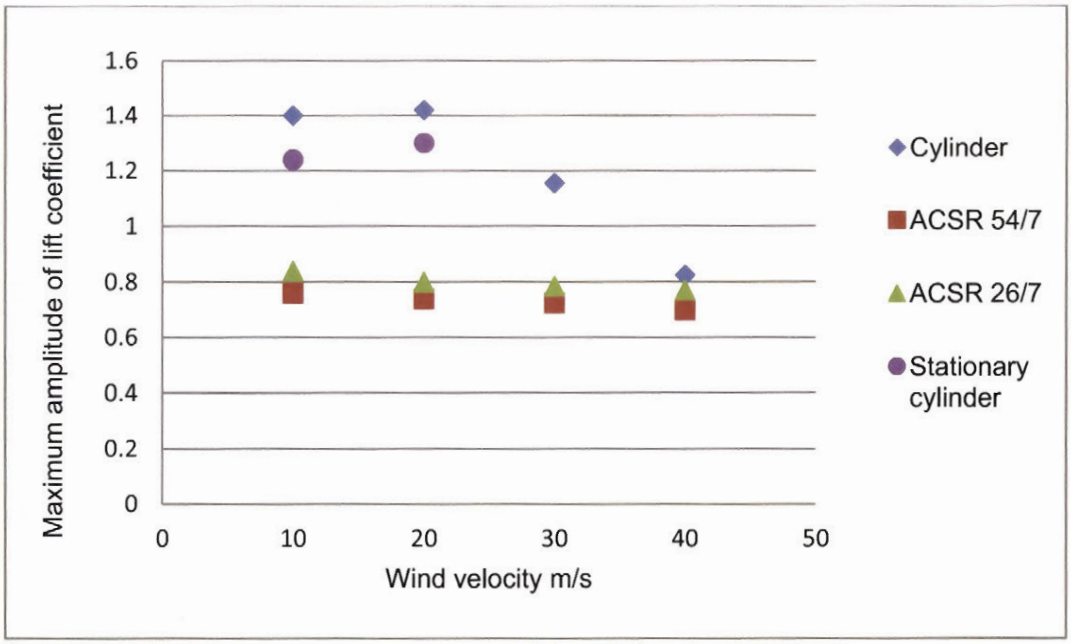

Figure 5.8Variation of lift coefficient with incident wind velocity

Another explanation of the higher lift coefficient in smooth cylinders compared to stranded surfaces is obtained from observing differences in the pressure fields developed around the two cross sections (Figure 5.9). While the area of positive pressure in the smooth cylinder is covering a sector of about 72° *to* 74° at the stagnation point, the sector size is increased to 80° in ACSR 26/7 and 83.5° in ACSR 54/7. Having a smaller area with positive pressure thus leaves a larger portion of the cable surface exposed to negative pressure, hence increasing lift. The average lift coefficient for all models remains zero, as also reported in most experimental studies [2, 3, 6], but no published wind tunnel test results could be found to compare with the fluctuations of the lift coefficient amplitude found in the numerical simulations. Such high frequency and low amplitude fluctuations of lift are very hard to capture in physical measurements. Instantaneous lift is also affected by several parameters, such as the cylinder's natural frequency, its velocity and Reynolds number of the incident air flow.

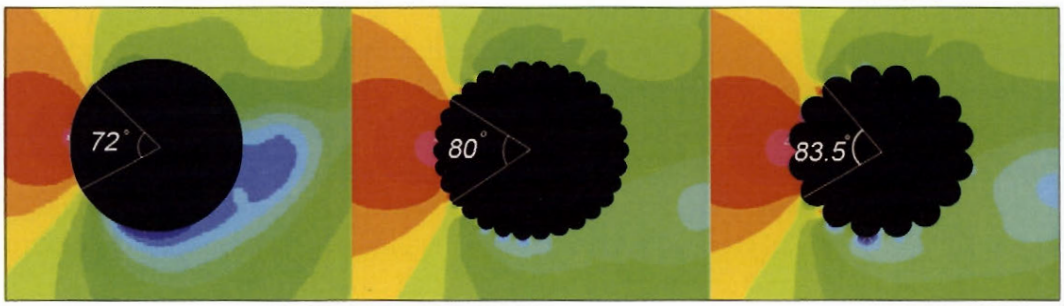

Figure 5.9Comparison of cable area exposed to positive pressure in three surface roughness conditions

5.4.4 *Effects of surface strand geometry on conductor drag and lift coefficients*

Comparing the drag and lift coefficients presented in Figure 5.5 and Figure 5.5 reveals that the smooth circular cylinder is not the best profile to predict the cable aerodynamic properties at wind speeds and Reynolds numbers in the range used in transmission line design. Despite this fact, many numerical and experimental studies use the circular fixed cylinder to predict stranded conductor response to wind loads. The differences in drag shown in Figure 5.5are significant. At the relatively low wind velocity of 10 m/s (Re = 21100) the difference is less than 15% but it increases to 40% when the wind velocity is increased to 20 m/s. At higher wind velocity, the smooth cylinder goes into critical flow and experiences a large drop in drag, while the stranded cables are experiencing higher drag than the smooth cylinder. Figure 5.5 and Figure 5.8 also indicate that the number (size) of the outer layer strands affects lift even more than drag forces. It is seen in Figure 5.8 that the differences in lift coefficient are more pronounced at lower wind speeds and decrease with wind speed; all models experience almost the same lift coefficient at V = 40 m/s. An extrapolation of the trend (not verified with simulations) suggests that above 40 m/s the lift coefficient for stranded cables will be higher than for smooth cylinders. In practice, these observations mean that predicting the time-accurate buffeting response of overhead line conductors at high wind speed may prove quite difficult.

5.4.5 *Effects of ice accretion on conductor drag and lift coefficients*

The effects of atmospheric ice accretion have been studied in more details for the aerodynamic properties of the ACSR 26/7 conductor. As indicated in Table 5.1 and Figure 5.1, three different levels of glaze ice accumulation (with density of 917 kg/m^3) are considered on the bottom face: a layer of ice with thickness equal to 10% of the cable diameter in model (e) where the corrugated surface is not covered on the top portion; a slightly larger accretion of 20% of cable diameter in model (f), and finally the ice thickness is increased to 40% of cable diameter in model (g). An important assumption is that the ice accreted in models (f) and (g) completely covers the corrugations of the strands and provides smooth oval shapes. Figure 5.10 reports the variation of drag coefficient with accreted ice thickness. It is seen that the general trend is for the drag coefficient to increase with ice thickness, regardless of wind speed except for the conductor with thin ice. In the latter case, the ice thickness is increasing the wind catching areas (both windward and leeward) but this effect is not significant and the overall the drag coefficient remains as in the bare case with small changes related to cable surface roughness at different wind velocities. In particular, at V =20m/s and above, the drag coefficient of the smooth cylinder drops considerably (see also Figure 5.5). The cross-sectional shape with corrugations at the top and smooth surface at the bottom behaves differently at higher wind speed (drag is reduced compared to the bare cable), while this is not seen at 10 and 20 m/s. Clearly, increasing the ice thickness to 20% and 40% of cable diameter increases the drag, due to the increased wind-catching area of the modified cross section.

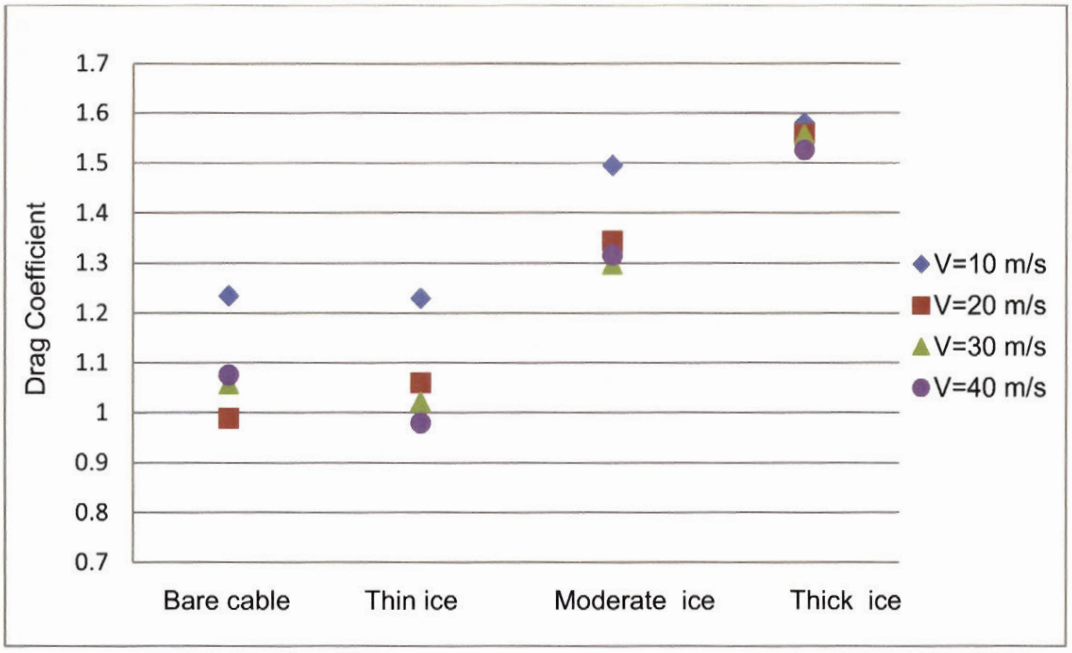

Figure 5.10Drag coefficients for ACSR 26/7 with different ice accretions at the bottom face

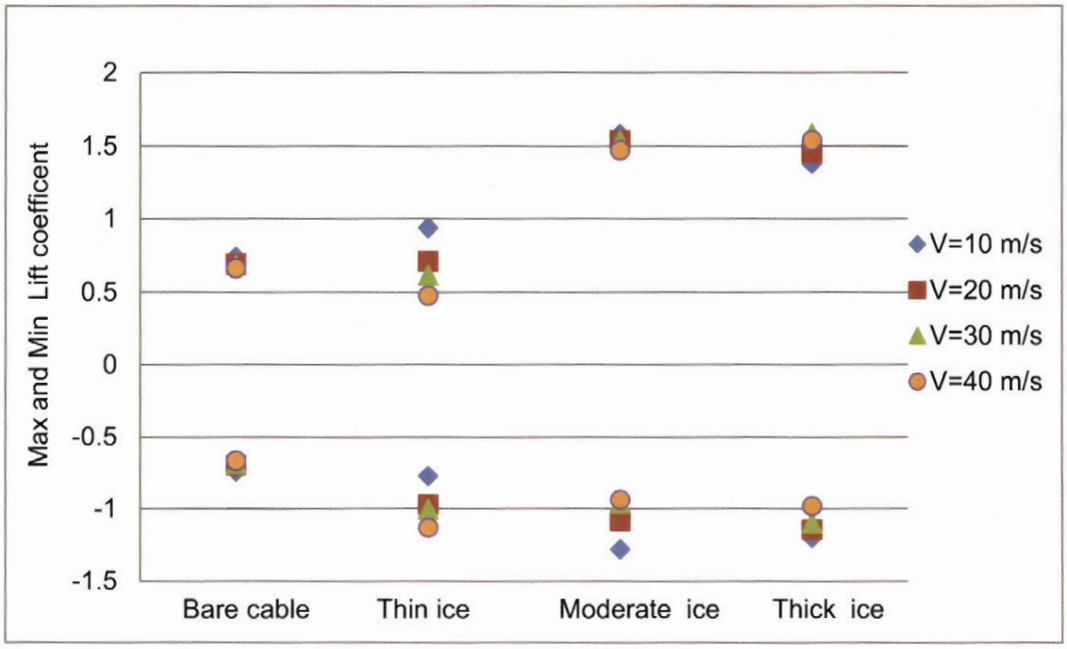

Figure 5.11Lift coefficients for ACSR 26/7 with different ice accretions at the bottom face

Figure 5.11 shows the effects of ice accretion and wind speed on the lift coefficient amplitude for ACSR 26/7. The maximum lift tends to increase with ice accretion, but this effect tapers off after moderate icing, yielding a smooth oval shape. It is also observed that the lift coefficient, which oscillates

with frequency of about 65 Hz (at V = 10 m/s), is not symmetric in the iced profiles since an upward resultant lift force is obtained.

The effect of lift force on cable motion is depicted in Figure 5.12 for V = 20 m/s and two cross-sections. The iced cable moves up to 50 mm in the cross-flow (vertical) direction and approximately 400 mm along the flow (horizontal), whereas the bare cable movement in the cross-flow direction is, while not zero, negligible due to oscillating lift, as shown in the bottom right insert of Figure 5.12. So the important effect of the asymmetric ice accretion on the mean lift coefficient is confirmed for this particular case of ice accreted at the bottom face.

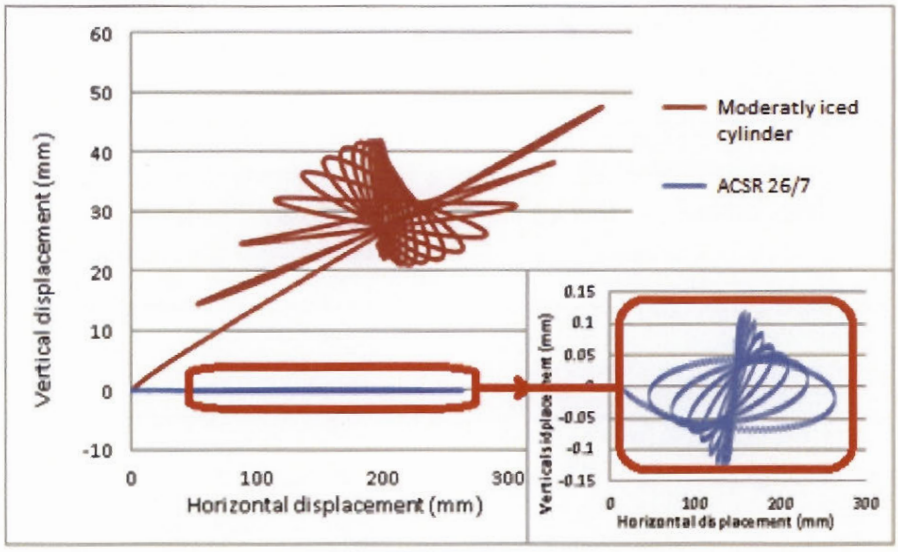

Figure 5.12Cable displacement in bare and moderately iced conditions at V = 20m/s

5.4.6 Effects of angle of attack on conductor aerodynamics

The effects of angle of attack have also been studied in more details for two series of models with low ice accretion; the first series considers the ACSR 26/7 conductor, while the other is for a smooth cylinder, as indicated in Table 5.1 and Figure 5.1. Each model is subjected to 5 angles of attack, from 0 to 180 degrees, for the studied range of wind speeds. The results of these simulations are reported in Figure 5.13 to Figure 5.19 and are discussed next.

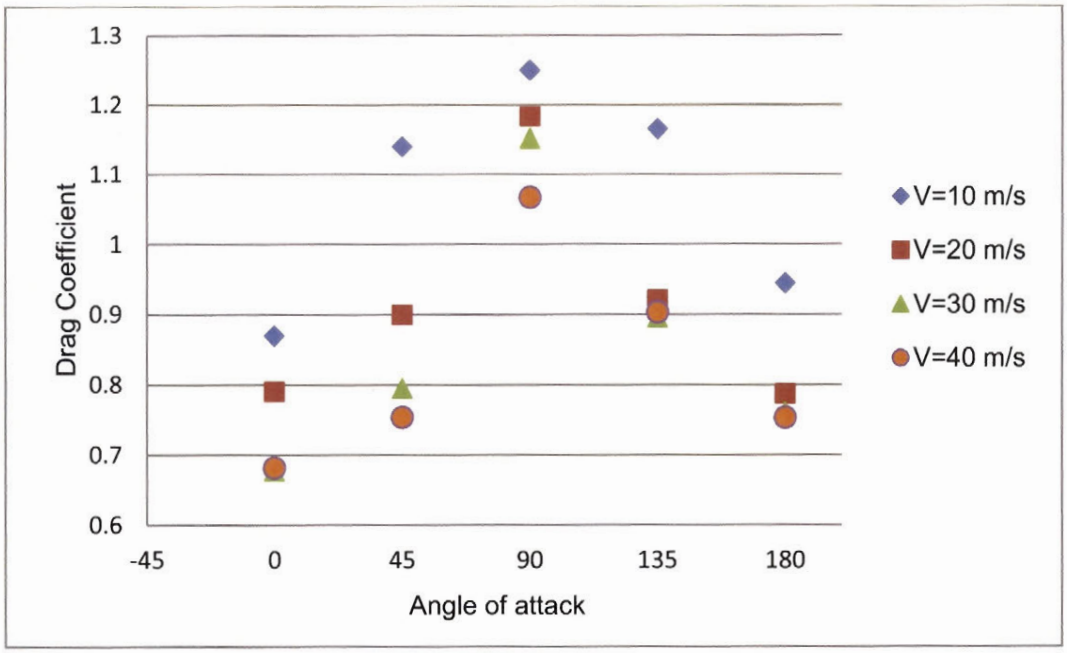

Figure 5.13Drag coefficient for iced smooth cylinder exposed to wind with different angles of attack

Figure 5.13 to Figure 5.16 relate to the first series of simulations with the smooth cylinder. As expected, the cable cross-section experiences the largest drag at an angle of attack of 90°, since this condition maximizes the area exposed to wind. Increasing the wind velocity (see Figure 5.13) will decrease the drag coefficient, which agrees with the results of Figure 5.5. Of course, increasing wind velocity will increase the net drag force but the drag coefficient will decrease. Figure 5.13 also indicates that the drag coefficients are in the same range for the angles of attack of 45° and 135°, and are considerably lower than the 90° case. The main explanation for this is the lower wind-catching area when the angle of attack is oblique. The drag coefficients in the model with angle of attack of 45° are slightly lower than those with 135° especially at higher wind speeds, and this is due to the difference in the wind pressure flow induced by the shape of the iced conductor which no longer occupies a symmetric position. A similar trend is observed at 0° and 180°.

As shown in Figure 5.14, the angle of attack is affecting the lift coefficient significantly. Those models with angles of 0° and 180° experience a balanced lift force and therefore do not undergo notable cross-flow movement. Oscillations of the lift coefficient have a frequency of about 70 Hz (for Re = 22400) and in this case the lift force applied in each half cycle has the same magnitude, so the resultant cross flow force on the cable is negligible. As illustrated in Figure 5.15, the high-frequency low-magnitude lift forces cause a very small cross-flow motion. Similar trends in the results have been observed for models with angle of attack of 180°, but with a slightly different value of lift coefficient and a vortex shedding frequency of 65 Hz. The small difference in lift coefficient amplitude in the case of 0° and 180° is related to the position of the ice shape in the flow (leeward or windward), as also experimentally observed in.(Zdero and Turan, 2010)

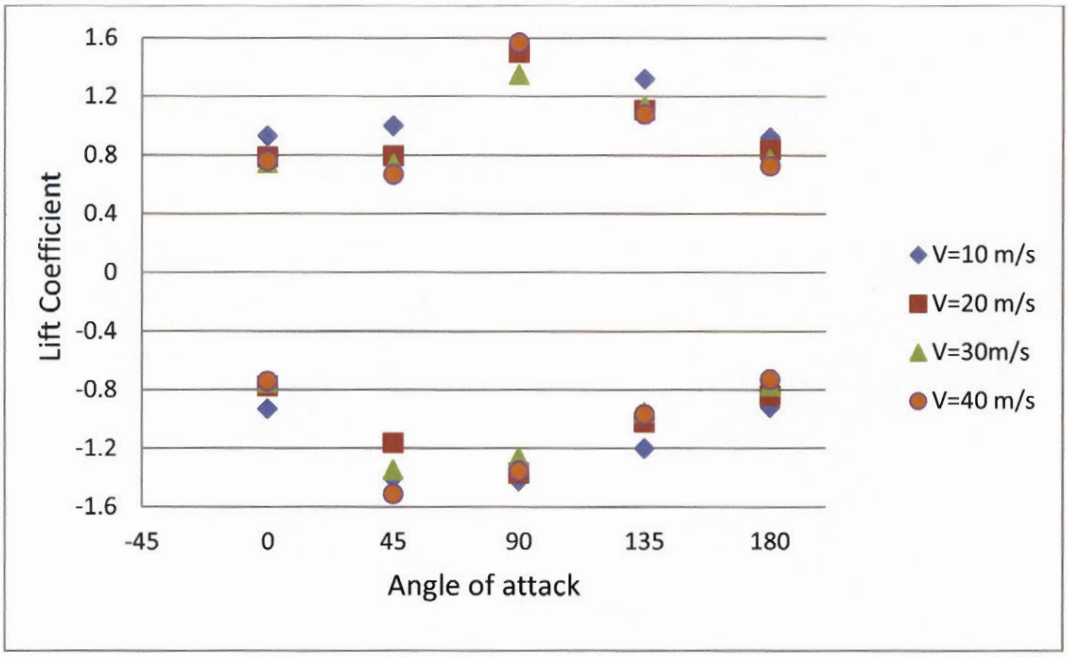

Figure 5.14Lift coefficient for iced smooth cylinder exposed to wind with different angles of attack

Figure 5.14 further indicates that the lift coefficient applied on the cable with the angle of attack of 45° is not balanced, which results in a net downward cross-flow displacement of a few millimetres, as shown in Figure 5.16. A similar trend is observed at 135°, but with an upward resultant force and displacement. These effects are illustrated schematically in Figure 5.17 where the orientation of the net forces in action is shown for these two directions.

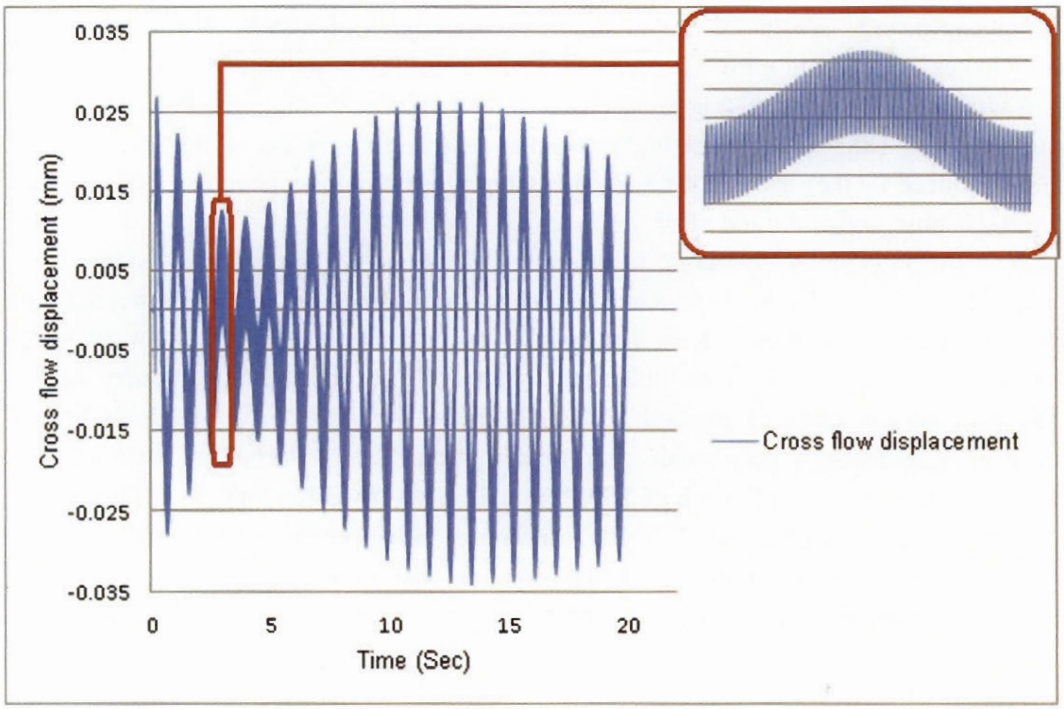

Figure 5.15Cross-flow displacement of iced smooth cylinder with angle of attack of 0°.

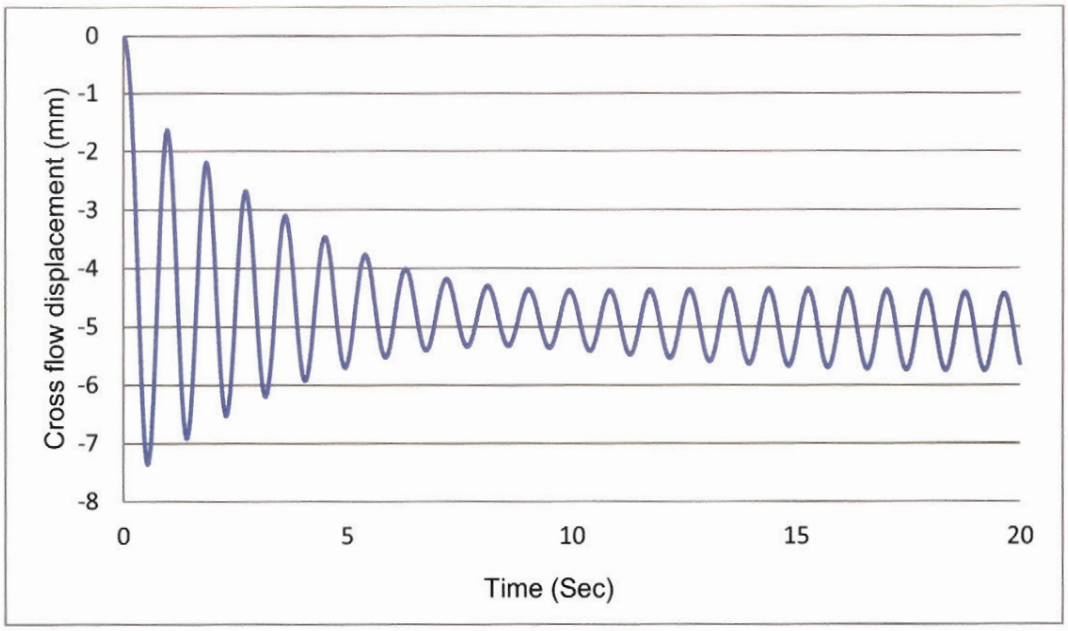

Figure 5.16Cross-flow displacement of iced smooth cylinder with angle of attack of 45°.

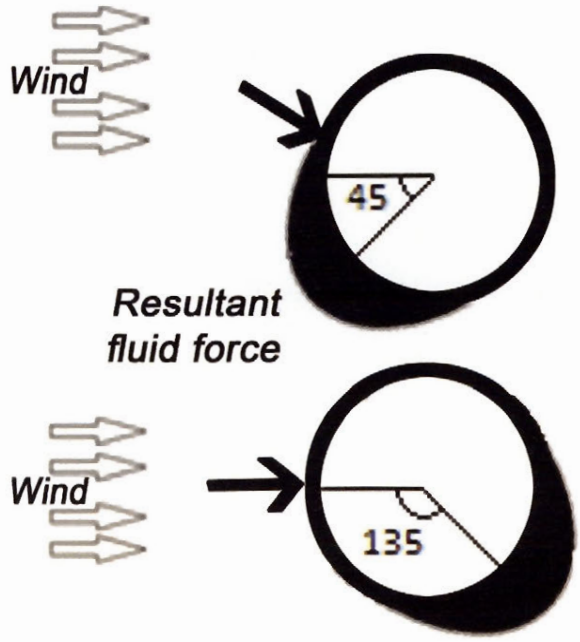

Figure 5.17Net aerodynamic force applied on the leeward side of the iced smooth cylinder for angles of attack of 45° and 135°

A second series of numerical simulations serve to study the effect of angle of attack on a more realistic case, and the ACSR 26/7 iced conductor is subjected to the same incident wind flow conditions as the iced smooth cylinder model.

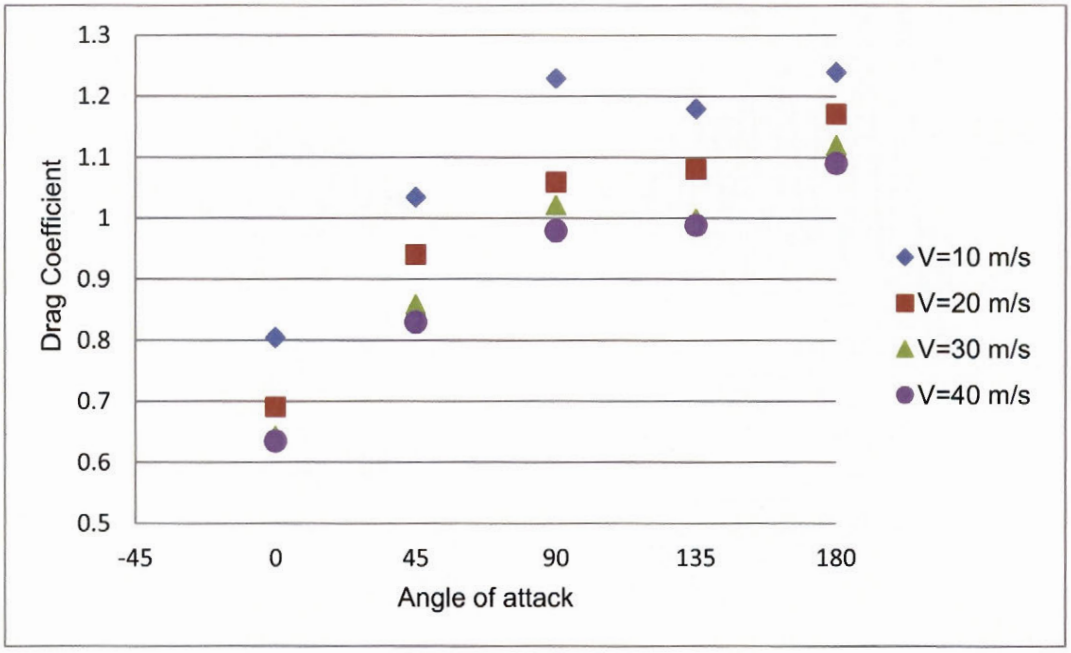

Figure 5.18Drag coefficient for iced ACSR 26/7 exposed to wind with different angles of attack

A comparison of Figure 5.13 and Figure 5.18 shows considerable differences in the drag coefficients obtained from the two series of models. The surface roughness and presence of strands dominate over the effect of angle of attack. The most striking difference in drag coefficient is observed when the angle of attack is 180°; this is because in the iced smooth cylinder model the flow first meets a smooth surface, while for the iced ACSR 26/7 conductor the flow first meets the corrugated bare cable surface. The vortex shedding frequency for the smooth cylinder is 75 Hz and reduces to 64 Hz in the latter case (for V=10 m/s); it has also been reported in experimental studies (Zdero and Turan, 2010) that when the vortex shedding frequency decreases the drag coefficient increases and the lift coefficient decreases slightly. By increasing the angle of attack from 0° to 45° and 90° the drag coefficient in Figure 5.18 increases as the wind-catching area of the conductor grows, but further increasing the angle of attack from 90° to 135°, and then 180° , the drag rise tapers off. Similar observations can be made for the lift coefficient in Figure 5.19. The iced conductor does not experience notable lift in the case of 0° *and* 180°, but experiences maximum lift at 135°.

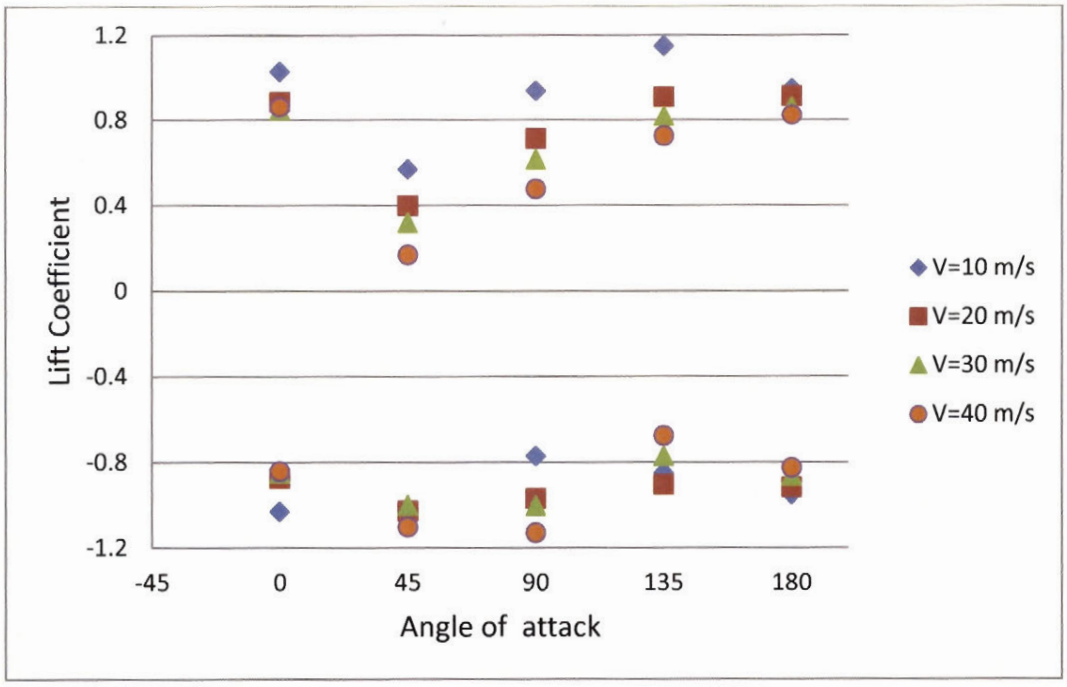

Figure 5.19Lift coefficient for iced ACSR 26/7 exposed to wind at different angles of attack

5.5 Wind Load Model

Using the calculated lift and drag forces obtained from FSI analysis, the effect of a time-varying horizontal wind speed (see the time-history record in Figure 5.20) is simulated on a 355-m span of transmission line with ACSR 57/7 (model d)(Keyhan et al, 2011b). The FSI analysis is conducted along different sections of the span to determine the resultant wind force acting on the cable's cross-section: the wind forces vary span wise, while the variations in wind intensity remain synchronous. The results of this nonlinear dynamic analysis are compared to the predictions of the simplified methods adopted in most transmission line design codes (ASCE, 2010; IEC60826, 2003) based on Bernoulli's equation. Figure 5.21 shows that the wind loads predicted by the two methods agree better at the cross-section closer the support than at midspan, due to a conductor motion of smaller amplitude and therefore lower wind-cable interaction. Figure 5.22 shows that the cable horizontal displacement at midspan, predicted by two different methods, is significantly different and that dynamic analysis based on Bernoulli's equation predicts conservative values.

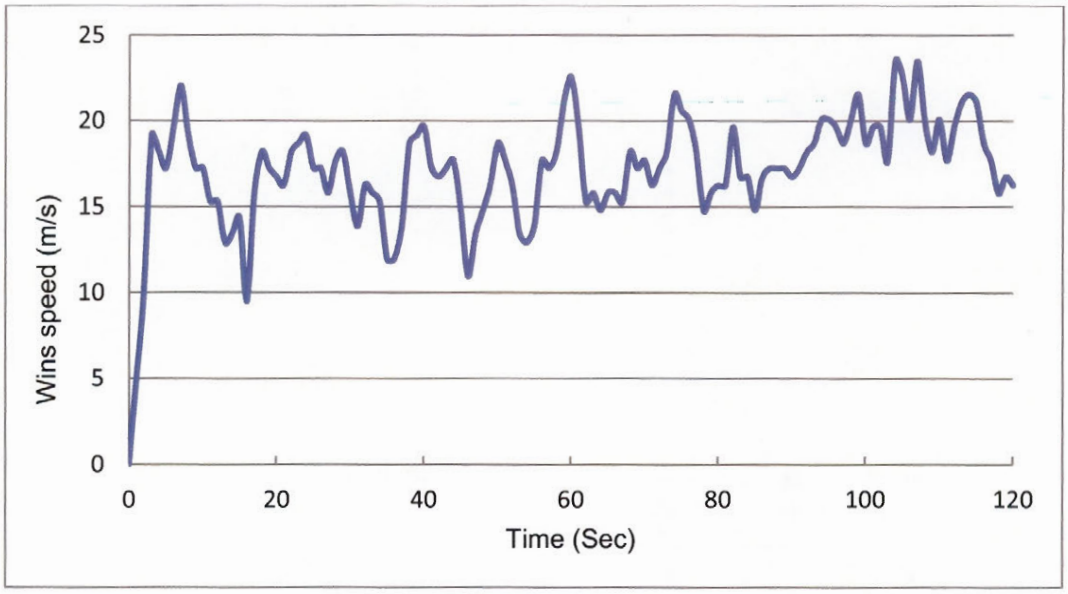

Figure 5.20Wind speed time history from a natural wind record

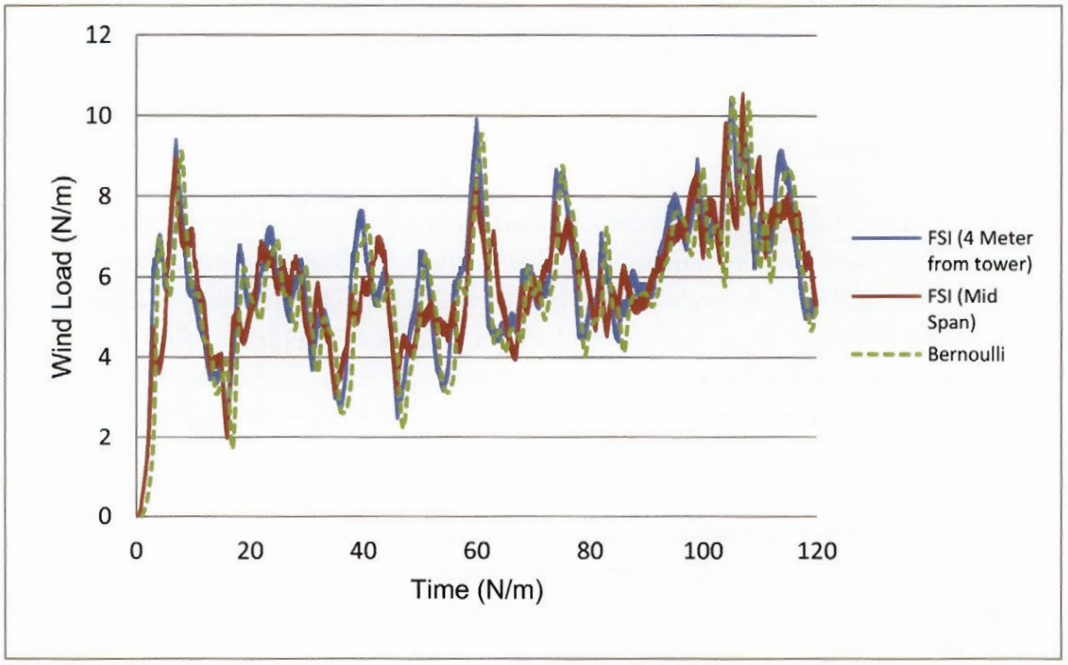

Figure 5.21Wind force applied on conductor predicted by FSI and Bernoulli's equation

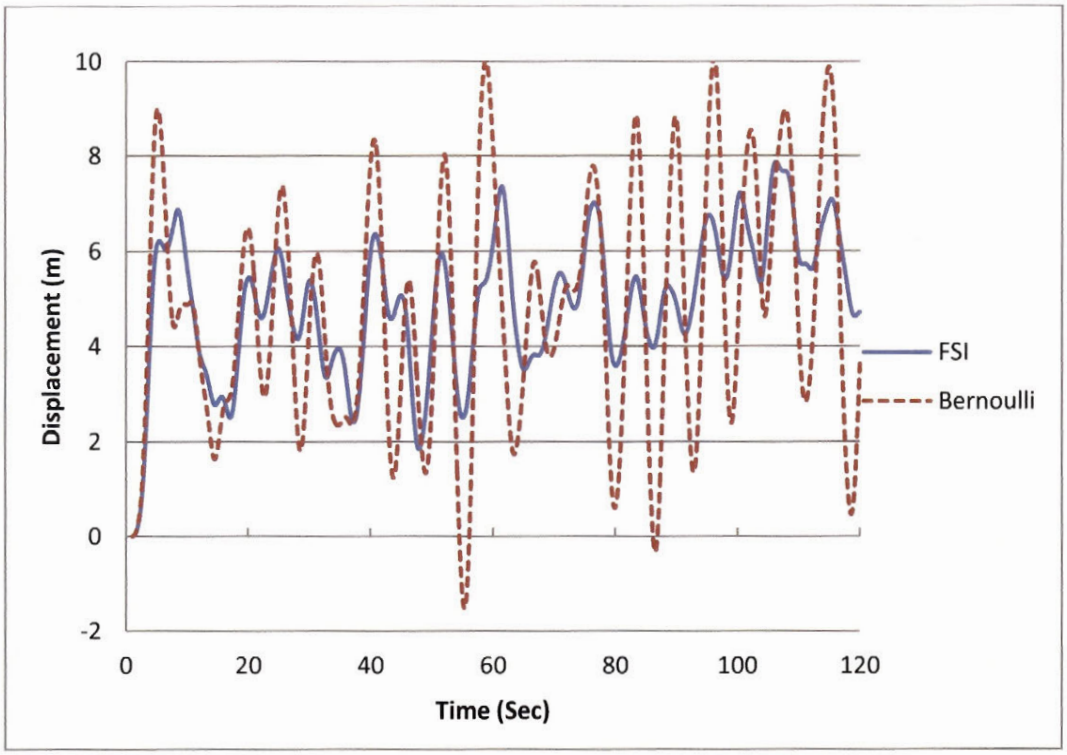

Figure 5.22 Conductor horizontal motion at the mid span

5.6 Conclusions

The paper presents the salient features of a computational study of wind-structure interaction effects on overhead transmission line conductors in various 2-D flow conditions. The main findings confirm some of the previous experimental observations made by other researchers, while bringing new insight in iced cable dynamics by showing some response effects that are difficult, if not impossible, to measure in physical experiments.

The main conclusions of the computational study for overhead line engineering are summarised as follows:

- The drag and lift coefficients of a moving cylinder (on elastic supports) are slightly higher than those of a fixed cylinder.
- The drag and lift coefficients generally decrease with increasing incident wind speed, but at different rates depending on cable surface roughness and cross-section geometry.
- Stranded cables with increased surface roughness experience their drag crisis at $20{,}000 < Re < 40{,}000$, compared to $70{,}000 < Re < 100{,}000$ for cylindrical cables. Stranded cables experience higher drag and lift coefficients than the smooth cylinder for Reynolds number above the critical range.
- Non-symmetric ice accretion with respect to incident wind makes the conductor more susceptible to cross-flow oscillations. This can be simulated in detail in computational models

- The effect of angle of attack on the loading of the iced conductor is such that the minimum drag and lift were obtained for $0°$ *and* $180°$. The drag coefficient is maximum for $90°$ and the lift coefficient, for $45°$.
- The effect of surface roughness dominates the calculated load at various angles of attack.

The FSI analysis procedure described in this paper was used to generate equivalent wind loads applied along a single span of overhead conductor subjected to a turbulent natural wind speed record. Dynamic analysis of the conductor span in different loading scenarios indicates that wind-conductor interactions are prominent when the conductor is experiencing large motions. These effects are to be studied in more details in future work.

Acknowledgement

This research was funded by the *Fonds québécois de la recherche sur la nature et les technologies (FQRNT)* research team grant program, and by the Natural Sciences and Engineering Research Council of Canada (NSERC). The CLUMEQ (https://www.clumeq.ca/) Supercomputer Centre provided the computational platform.

References

ADINA R&D Inc, 2009. ADINA Systems online Manuals, 71 Elton Ave, Watertown, MA 02472, USA.

ASCE, 2010. Guidelines for Elecrical Transmission Line Structural Loading, in: C. Jerry Wong, M.D.M. (Ed.), 3rd ed. ASCE, p. 191.

Bathe, K.-J., Zhang, H., 2002. A flow-condition-based interpolation finite element procedure for incompressible fluid flows. Computers & Structures 80, 1267-1277.

Davenport, A.G., 1979. Gust response factors for transmission line loading, in: Proceedings of the Fifth International Conference on Wind Engineering. Pergamon Press.

Hughes, T.J.R., Liu, W.K., Zimmermann, T.K., 1981. Lagrangian-Eulerian finite element formulation for incompressible viscous flows. Computer Methods in Applied Mechanics and Engineering 29, 329-349.

IEC60826, 2003. Design criteria of overhead transmission lines, International Standard, 3rd ed. International standard, Geneva.

Kadab, R.R., 1998. Response of electrical transmission conductors to extreme wind using field data., Civil Engineering. Texas Tech Universit, Texas.

Keyhan, H., McClure, G., Habashi, W.G., 2011a. Computational study of surface roughness and ice accumulation effects on wind loading of overhead line conductors. International Review of Civil Engineering Vol. 2 N.4, 208-214.

Keyhan, H., McClure, G., Habashi, W.G., 2011b. A fluid structure interaction-based wind load model for dynamic analysis of overhead transmission lines, 9th International Symposium on Cable Dynamics, Shanghai, China, pp. 86-94.

Keyhan, H., McClure, G., Habashi, W.G., 2011c. On computational modelling of interactive wind and icing effects on overhead line conductors, 14th International workshop on atmospheric icing of structures, Chongqing, China, pp. 8-13, B-15-11-28.

Shan, L., Jenke, L.M., Cannon, D.D., 1992. Field determination of conductor drag coefficients. Journal of Wind Engineering and Industrial Aerodynamics 41, 835-846.

Shih, W.C.L., Wang, C., Coles, D., Roshko, A., 1993. Experiments on flow past rough circular cylinders at large Reynolds numbers. Journal of Wind Engineering and Industrial Aerodynamics 49, 351-368.

Tabatabai, M., Krishnasamy, S.G., Meale, J., Cooper, K.R., 1992. Response of smooth body, trapezoidal wire overhead (compact) conductors to wind loading. Journal of Wind Engineering and Industrial Aerodynamics 41, 825-834.

Zdero, R., Turan, O.F., 2010. The effect of surface strands, angle of attack, and ice accretion on the flow field around electrical power cables. Journal of Wind Engineering and Industrial Aerodynamics 98, 672-678.

Zdravkovich, M.M., 1997. Flow around circular cylinders: a comprehensive guide through flow phenomena, experiments, applications, mathematical models, and computer simulations. Oxford University Press.

6 Dynamic analysis of transmission line subject to gusty wind based on wind pressure predicted by full wind-conductor interaction

In this part of the research results from wind-conductor interaction analysis explained in previous chapters are integrated and used for wind load modeling of overhead transmission line conductors. The procedure of the new wind load modeling approach is described in detail, from 2-D FSI analysis of the wind-conductor domains to complete nonlinear dynamic analysis of a 3-D transmission line model. The method is demonstrated using a case study of a 5-span transmission line section where the latticed suspension towers and conductors are modeled in details. Four different natural wind records are used to derive wind loading scenarios accounting for dynamic interactions between the moving conductor and the air flow. The results obtained from these analyses are compared against another set of dynamic analysis results which were based on pressure loads predicted by Bernoulli's equation. This comparison shows how including FSI can affect the predicted stress and deflection levels and consequently transmission line structural design. The main results of this part of the research are summarised into a manuscript that is currently under review:

Keyhan, H., McClure G., Habashi W.G. (2012). "Dynamic analysis of an overhead transmission line subject to gusty wind loading predicted by wind-conductor interaction" Computers & Structures, Manuscript number: CAS-D-12-00549, submitted on June 20th 2012. (Keyhan H. et al. 2012b). Review comments on the manuscript were received on 17 August 2012 and the text included in the thesis is the original manuscript version without revisions.

Dynamic analysis of an overhead transmission line subject to gusty wind loading predicted by wind-conductor interaction

Hooman Keyhan [a,1], Ghyslaine McClure [a], Wagdi G. Habashi [b]

[a] McGill University, Department of Civil Engineering and Applied Mechanics, Montreal, QC, Canada,
[b] McGill University, Computational Fluid Dynamics Laboratory, Department of Mechanical Engineering, Montreal, QC, Canada

6.1 Introduction

Transmission line structures are designed to withstand several different load cases they may experience during their service life. Among these load cases, those involving extreme wind and combined wind and icing in cold climates are typically governing the design for lateral loads. In design practice wind loading on transmission line conductors is applied following simplified static procedures that are meant to be conservative. Such procedures, described in national and international codes and standards or in utility guidelines, are very similar and essentially based on Bernoulli equation. Referring to Equation (6.1) provided by Canadian standards CSA-C22.3 No. 60826-10, Design criteria of overhead transmission lines[1], the wind pressure on towers and conductors, q, is obtained by multiplying the reference dynamic wind pressure, q_o - actually the equivalent pseudo-static pressure predicted by Bernoulli equation, by a gust effect factor proposed by Davenport in the late 1970s [2] to account for tower resonant response and wind gustiness. The incident wind speed nominally specified at 10 m elevation is also modified to account for terrain roughness and height according to the classical boundary layer wind model.

[1] Corresponding author. Tel: +1 604 782-3053
E-mail address: Hooman.keyhan@mail.mcgill.ca

Journal of Computers & Structures, Manuscript number: CAS-D-12-00549

Finally, a span coefficient is used to consider the random unevenness of wind gust speed along the span.

$$q = q_0 C_{xc} G_c G_L \qquad (6.1)$$

Where, C_{xc} is the drag coefficient of the conductor (considered in the un-iced condition), G_c is the combined wind factor for the conductors, which depends on height above ground and terrain roughness categories, and G_L is the span factor. Other standards such as IEC 60826, Design criteria of overhead transmission lines issued by International Electrotechnical Commission [3] and ASCE Manual No. 74 [4]use similar approaches.

Among the different mechanical components of transmission lines, conductors have the largest area exposed to wind, especially in high and ultra high voltage lines where bundles of four or more conductors are used. Line conductors are particularly sensitive to wind effects as they are long and relatively flexible compared to their supports. Because of their flexibility, conductors may experience large motions under wind loading: depending on wind speed, line parameters and span length, horizontal (swinging) displacements at the mid span may reach 10 m to 20 m in high voltage lines. In cold climates, atmospheric ice accretions of various types, from light rime to dense glaze, further increase the effects of wind loads on lines and give rise to the most severe design loading conditions. Although simplified static methods are expected to be conservative for design, economy brings other incentives to better understand and quantify the effects of wind loads on line conductors, especially in the context of older line assessment where overly conservative load estimates may lead to costly retrofit measures that are not necessary. It is clear that in extreme wind conditions conductors experience large displacements and interact with the wind flow: is this interaction contributing to increasing or decreasing the net pressures on the conductor span and consequently the loads transferred to their supporting towers? This is

the main question that motivated this research. A refined computational model of the conductor cross section on flexible supports in surrounding moving air is used to investigate the dynamic interaction between wind and conductor motion. The net wind load resulting from fluid-structure interaction (FSI) analysis is then applied to detailed three-dimensional models of a line section to determine the loads transferred to line supports.

6.2 Fluid-Structure Interaction Analysis

Considering the conductor motion in the wind flow, an accurate computational evaluation of wind pressure on overhead conductors requires FSI analysis. In this analysis, a two-dimensional model of the conductor cross section is coupled to its surrounding air flow (fluid) domain, as illustrated in Fig. 6.*1*. In the solid domain, the outer cable boundary is modeled using rigid two-dimensional Bernoulli beam elements with appropriate tributary mass. The cross section is assumed mounted of flexible springs with equivalent vertical and horizontal linearized stiffnesses that can be adjusted for various line parameters. In the application presented here, these equivalent stiffness properties were determined for a mid-span cross section using a detailed large kinematics nonlinear static analysis of a level 355-m span suspended in still air, with a horizontal tension of 19.2 kN in the bare condition (cable self-weight 14.9 N/m). A viscous damping constant equivalent to 1% of critical is also assigned at the support in each orthogonal direction to approximate internal material damping in the conductor. These two-dimensional models provide a tool to evaluate the effects of several parameters such as the magnitude of incident wind speeds, conductor shape, surface roughness and ice accretion on resultant wind loading of overhead line conductors.[5]

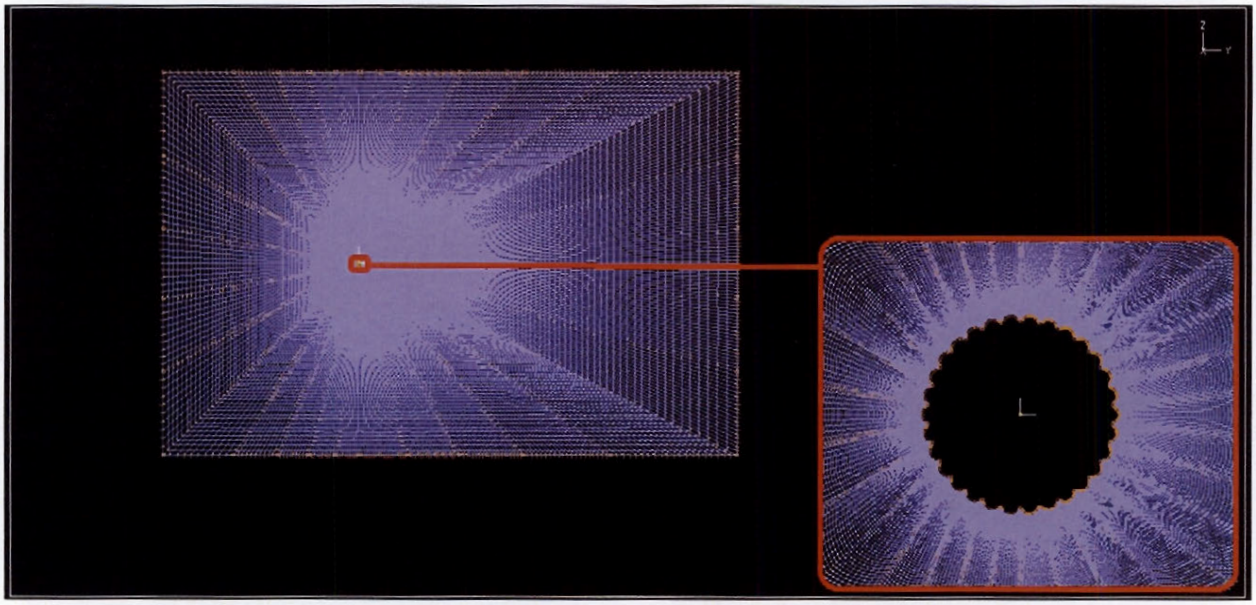

Fig. 6.*1. Two-dimensional model of stranded conductor cross section coupled to its surrounding air flow.*

In the solid domain, direct time-step integration is used to solve the incremental form of the nonlinear equations of motion (equation 6.2) of the cable cross section on spring supports and dashpots, and the equilibrium iterations are carried using the Full Newton method for stiffness updates. In the following equation u is the cable displacement vector; K, M and C are stiffness, mass and damping matrices respectively, and $F_{t+\Delta t}$ represents the fluid force applied on the conductor nodes at time $t + \Delta t$.

$$M\Delta\ddot{u} + C\Delta\dot{u} + K\Delta u = F_{t+\Delta t} - M\ddot{u} - C\dot{u} - Ku \tag{6.2}$$

For computational fluid dynamics, the modelling parameters that were found to have the most influence on accuracy are the fluid domain dimensions and the mesh fineness. Thereafter, these were iteratively adjusted with several numerical experiments until the computational domain was found adequate to minimize blockage and boundary effects on cable response while keeping the computational cost reasonable. The fluid domain is discretized with quadrilateral FCBI-C elements[6], using a structured "O" shape mesh (See Fig. 6.*1*). To capture the fluid response with reasonable accuracy 450 elements are used at the fluid-solid interface. The fluid elements' thickness is reduced when approaching the interface and a refined mesh is used in a ring zone of

about 1xD thickness around the cable surface of diameter D. The CFD analysis is based on the direct time-step integration of the unsteady Reynolds-averaged Navier-Stokes equations (Equation 6.3) using the Euler α - method of first order, and a constant time-step size of 0.1 ms was found optimal for the problem at hand.

$$\rho\bar{u}_j \left.\partial\bar{u}_i\right/_{\partial x_j} = \rho\bar{f}_i + \left.\partial\right/_{\partial x_i}\left[-\bar{p}\delta_{ij} + \mu\left(\left.\partial\bar{u}_i\right/_{\partial x_j} + \left.\partial\bar{u}_j\right/_{\partial x_i}\right) - \rho\overline{\acute{u}_i\acute{u}_j}\right] \tag{6.3}$$

In Equation 6.3, ρ is the air density, $\bar{u}_i and\ \acute{u}_i$ are the mean and fluctuating components of i-th component of the fluid velocity, $\bar{p}$ is the mean static pressure, μ is the air viscosity and $\bar{f}_i$ is a vector representing the mean external forces applied on the control fluid domain. The iterative solver for the linearized incremental equations is the Algebraic Multi-Grid method (AMG). Airflow turbulence is modeled with the Spalart-Allmaras one-equation approach and vortex-shedding effects are introduced with the Detached Eddy Simulation (DES) algorithm. In FSI analysis, the Arbitrary-Lagrangian-Eulerian (ALE) formulation is used to allow for compatible mesh deformations and displacements for the air surrounding the cable in motion in each solution step. Note that these features are available in commercial software ADINA which was used in the study. [7]

The evaluation of the wind pressure field on the conductor proceeds by CFD analysis of the fluid domain in each time step, and the resultant load on the air-cable interface is obtained by integration of the pressure field on the cable contour. This net wind load is calculated at each time step and acts as an external load on the conductor in the solid domain. Based on this calculated load, the solid domain is solved and the cable displacement is determined which updates the position of the fluid boundary subsequently in each time step. This two-dimensional

FSI analysis serves to construct wind loading time histories to be used in nonlinear dynamic analysis of three-dimensional line section models assumed in still air conditions (i.e. solid models only). To illustrate the process, the results obtained from FSI analysis for four different wind velocity time histories are presented in section III where the conductor is assumed in the bare (non iced) condition, i.e. its surface shows the corrugations of a stranded construction.

6.3 Transmission Line model

A three-dimensional computational model of a 120 kV double-circuit line section owned and operated by Hydro-Québec is built in ADINA (See Fig. 6.2) to illustrate the application of the proposed wind load model on conductors and its effects on the forces transferred to supporting towers. A detailed finite element model comprising five spans and four intermediate lattice supports was available from a previous structural dynamics study presented in [8] and following a methodology described in [9]. In the present study, the model was truncated to three spans and two suspension towers for simplicity; the wind load is applied only to the central span of 355 m. The boundary conditions provided by the suspension insulator strings at the both ends of the loaded span are quite realistic in allowing conductor motions under wind. The far ends of the conductors in the adjacent spans are assumed perfectly fixed to represent a strain tower condition where conductors are directly anchored to the structure instead of being suspended. Although the strain towers experience some deflection under load and the conductors' attachment points and are not perfectly rigid, this flexibility has negligible effects in this study dominated by transverse conductor displacements in swinging mode. Detailed properties of the stranded 54/7 CONDOR ACSR conductor used in this example are available in [10]. Each conductor span is discretized with 30 two-node isoparametric truss elements with three translational degrees of freedom at

each node. To account for the cable's slackening in the dynamic analysis, tension-only linear elastic material is modeled for the conductor with the equivalent composite modulus of elasticity, which accounts for compatibility of cable strand deformations and layering effects. The catenary equation of an inextensible cable is employed to position the conductor nodes in the initial condition and a geometrically nonlinear static analysis under self weight provides a realistic equilibrium configuration. Dynamic wind loading analyses are restarted from the line at rest. To avoid singularities in the initial stiffness matrix of the cable elements in the initial run, a pre-stressing value corresponding to the initial tension is assigned to each element. The conductors are attached to suspension towers by 1.4-m long insulator strings, which are modeled with a two-node isoparametric truss element of high axial rigidity. [8, 9]

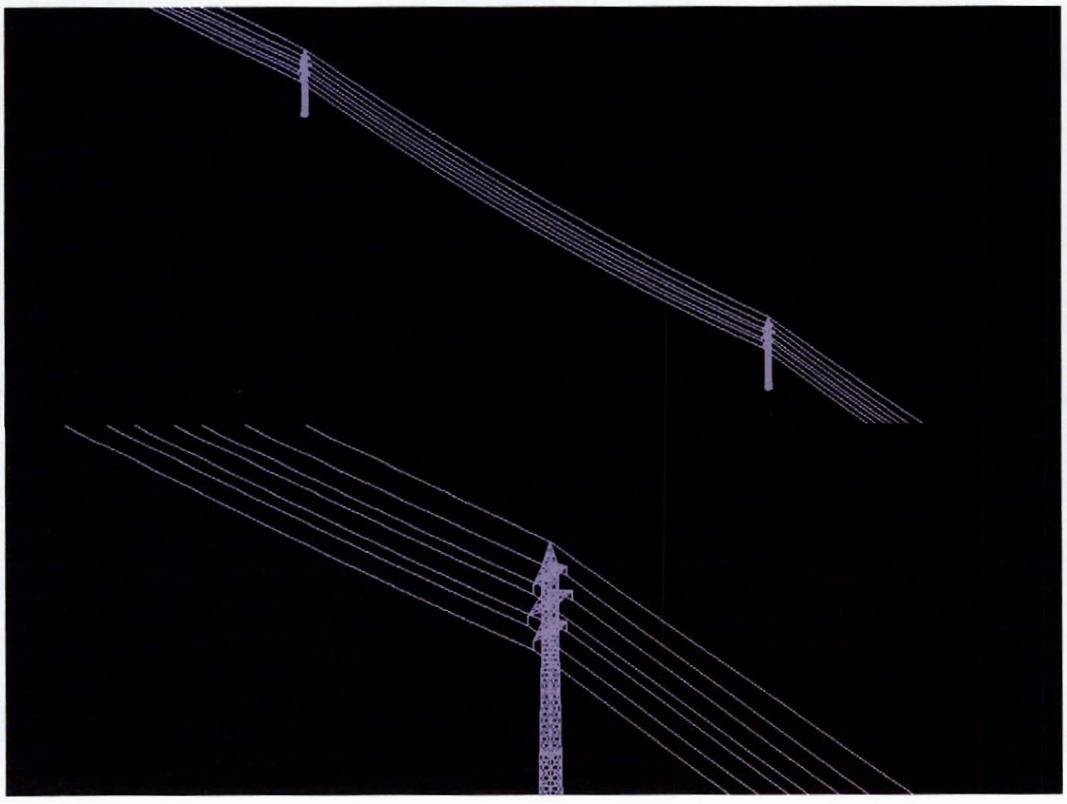

Fig. 6.2. Computational model of double circuit overhead transmission line section on steel lattice supports.

In the numerical model of the line, damping is introduced with discrete viscous dashpots defined between the two end nodes of each cable element. For the gusty wind loading condition where the conductor experiences several meters of sway displacement in the mid span region, damping has two main sources: internal and aerodynamic. Internal damping is mainly caused by friction between the strands in contact and friction induced by bending of the wires. The values suggested for internal damping ratio of non iced aluminum-steel conductors can vary from about 0.5% to 2% of equivalent critical viscous values. [9, 11] Aerodynamic damping can be evaluated from FSI analysis and the results obtained in the study indicate a reasonable range of 3% to 5% of critical damping. Considering both sources of damping, a total damping ratio equivalent to 5% of critical damping is modeled with the viscous dashpot elements. Introducing damping is also beneficial to filter out the spurious high frequency response of the finite element model that is not representative of the behavior of the physical system.[10]

The geometrically nonlinear dynamic analysis of the line section model subjected to wind is conducted by direct time integration of the incremental equations of motion (Equation 6.4). Newmark's classical trapezoidal rule is employed for integration and equilibrium iterations are performed in each time step until convergence is reached according to set threshold residual errors. The convergence criteria are selected based on displacement and energy error norms. [12]

$$M\Delta\ddot{U}_t + C\Delta\dot{U}_t + K\Delta U_t = F_{t+\Delta t} - M\ddot{U}_t - C\dot{U}_t - KU_t \qquad (6.4)$$

In this equation $\Delta\ddot{U}_t$, $\Delta\dot{U}_t$, ΔU_t are the incremental acceleration, velocity and displacement vectors respectively and, M is the mass matrix, C the damping matrix and K is the stiffness matrix, and $F_{t+\Delta t}$ is the prescribed wind load at the conductor nodes.

6.4 Wind Load Model

In this section the proposed new method for transmission line wind loading is described. It proceeds in five main steps illustrated in Fig. 6.3. The first step is to evaluate the horizontal transverse stiffness of the conductor under horizontal load at different positions along the span, using nonlinear static analysis. As expected, the analysis results show that the stiffness varies with higher rate near the end support points of the span while a few meters away from suspension point the horizontal stiffness is only slightly larger than at the mid span. In the example selected as a case study, nine sections of conductor are selected to be representative of the whole span and their lateral and vertical stiffness values are used in the FSI model.

In Step 2, FSI analysis is performed with the different cable support stiffness values determined in Step 1. The resultant wind load history on each cable section is computed and the results from this analysis are applied as input to the 3-D line model in Step 3 for nonlinear dynamic analysis.

Because this loading differs from the static loading used in Step 1 to evaluate the lateral stiffness of the cable, the conductor will experience slightly different displacements which in turn provide different values of conductor lateral stiffness. So the FSI analysis of Step 2 is repeated with the new stiffness values and after a few iterations a very good estimate of lateral stiffness of the conductor is obtained.

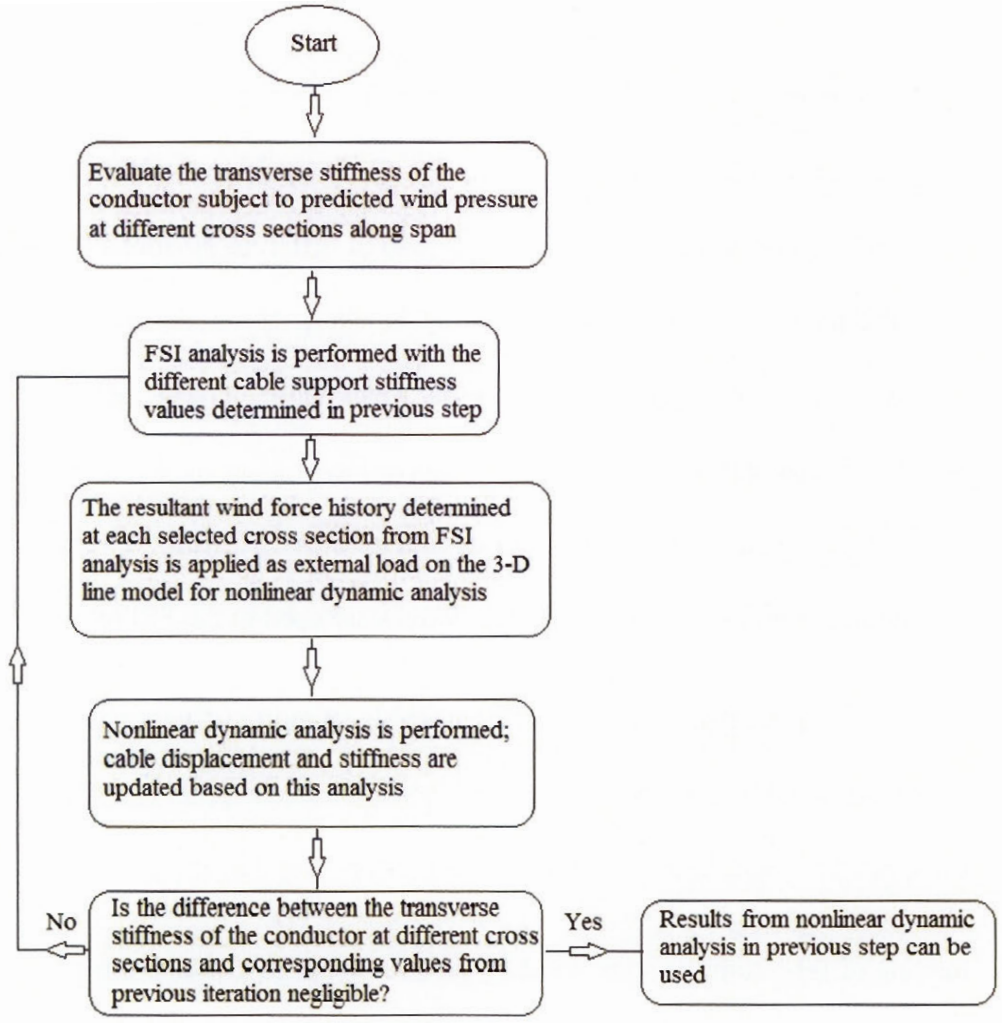

Fig. 6.3. Wind load modeling and dynamic analysis procedure.

The results from FSI analysis on all selected sections along the span for each wind case are transferred to the 3-D line model (see Fig. 6.8) and nonlinear dynamic analysis is performed in Step 4 to predict the response of the transmission line components. Results of the dynamic analysis of Step 4 for the four wind load cases are discussed next.

In Fig. 6.4 to 6.7 , the results from FSI analysis performed in Step 2, at three different cross sections along the span are compared against the wind pressure predicted by Bernoulli's equation (neglecting wind-conductor interaction) for all four incident wind load cases used in this study. The results confirm that the wind load predicted by FSI analysis at different sections of the span differs from the prediction made using Bernoulli's equation. As expected, the equivalent quasi-static pressure predicted by Bernoulli's equation shows better general agreement with the computed dynamic wind pressure applied on cable sections closer to end supports: these sections undergo smaller cable displacements, and subsequently lower wind-structure interaction when compared to conductor cross sections further away from the supports.

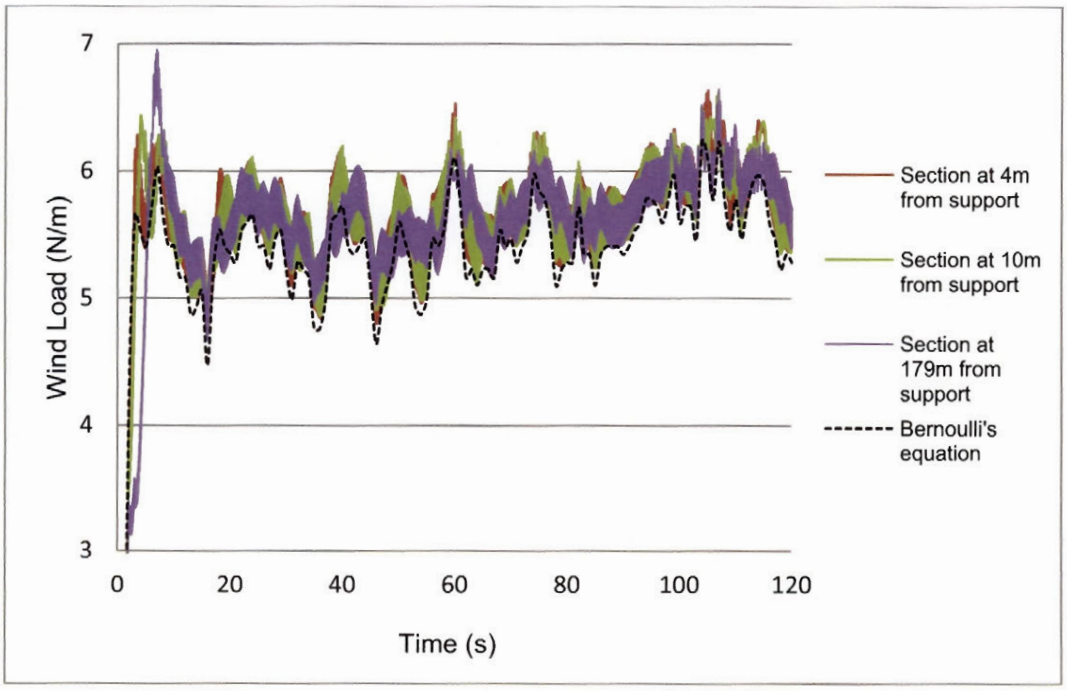

Fig. 6.4. Calculated wind load on conductor at three different positions along the span (Wind record 1).

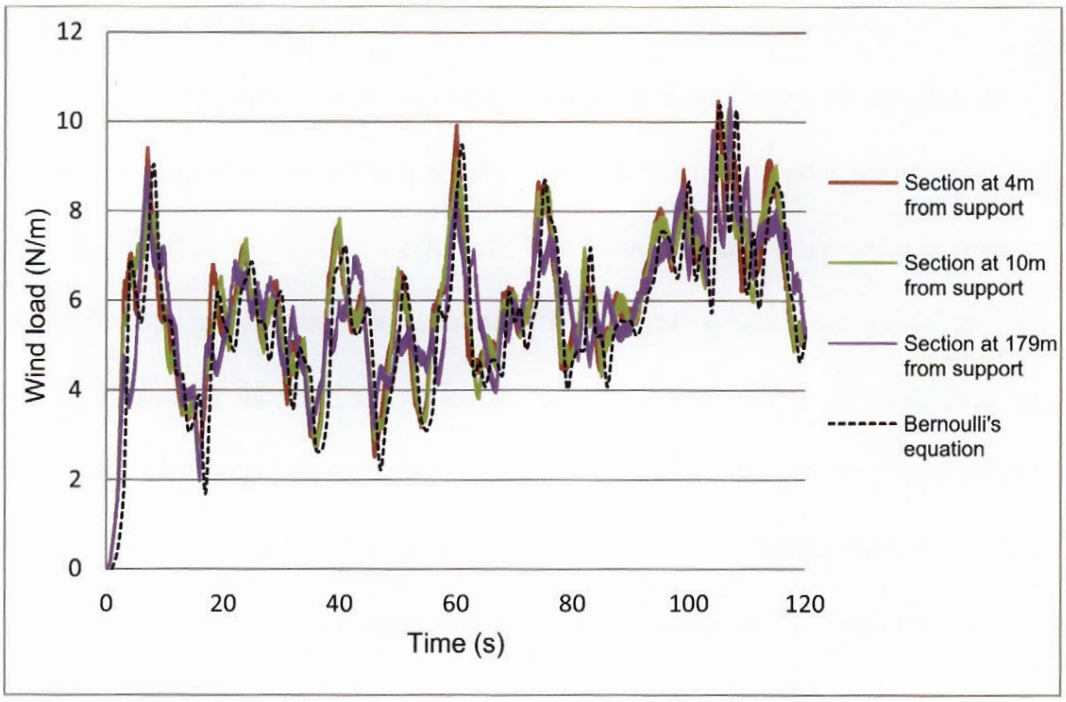

Fig. 6.5. Calculated wind load on conductor at three different positions along the span (Wind record 2).

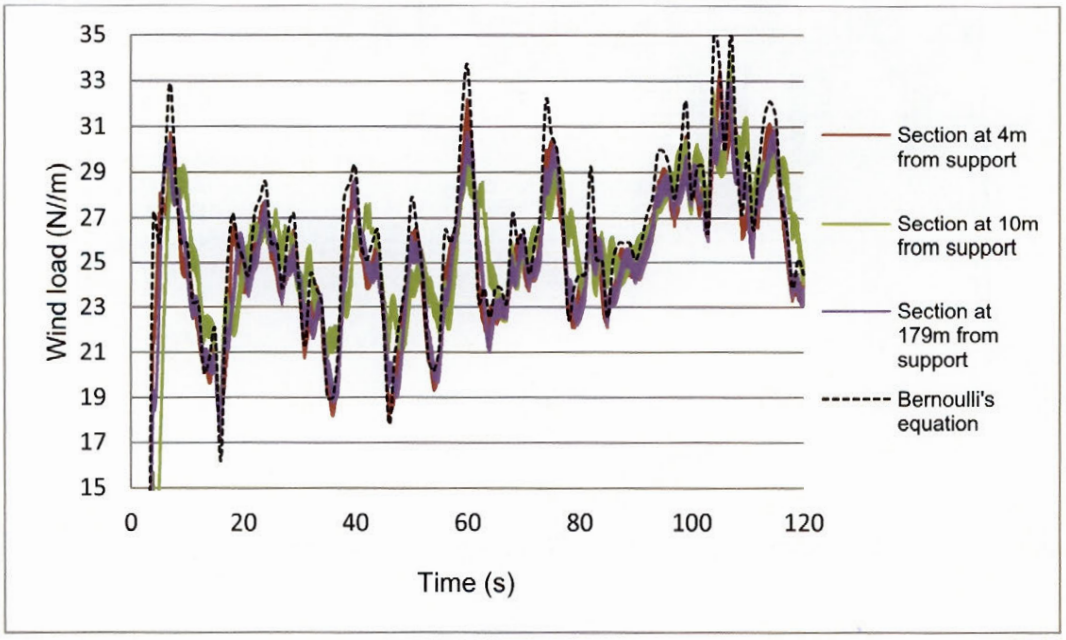

Fig. 6.6. Calculated wind load on conductor at three different positions along the span (Wind record 3).

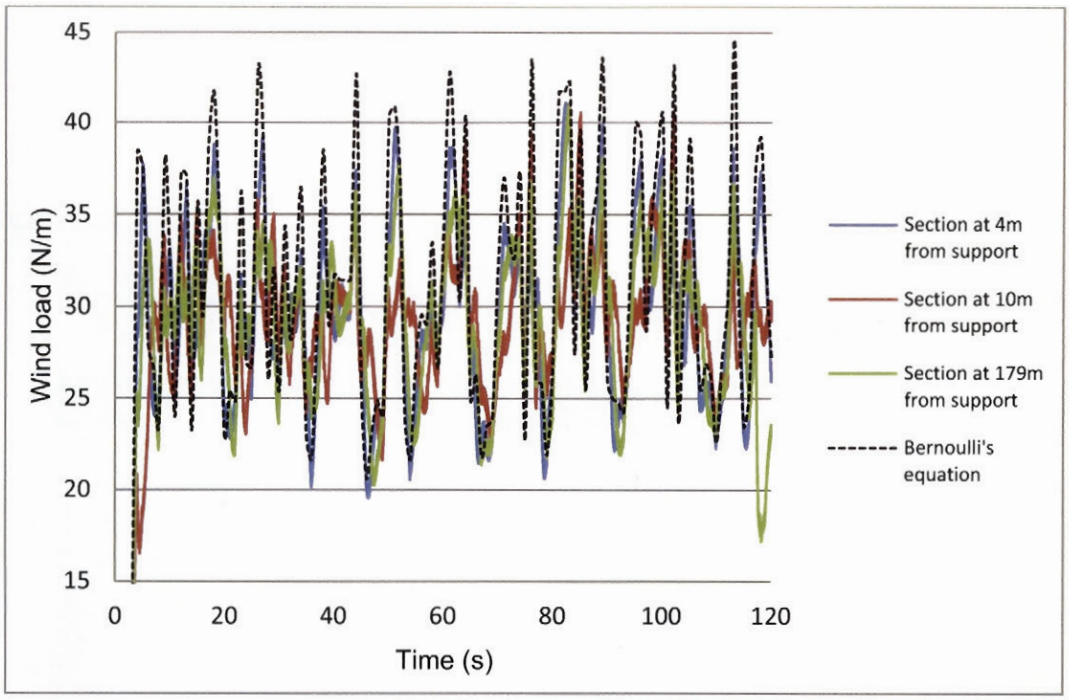

Fig. 6.7. Calculated wind load on conductor at three different positions along the span (Wind record 4).

Another observation is the oscillatory character (high frequency, low amplitude) of the wind load from FSI analysis which makes the plots appear as thick lines: this is caused by the oscillation in drag force due to vortex shedding. Such an oscillation in wind load (of rather small amplitude) will not significantly affect the lateral displacement of the conductor, which is the main parameter that will influence FSI analysis results. Comparing Fig. 6.4 and 6.5, fluctuations in the loads determined along the span by FSI analysis (i.e. at cross sections of varying support stiffness) are more important when incident wind has higher turbulence intensity. Figure 6.7 displays similar results but for the wind record with higher speed and turbulence intensity: differences between FSI-based wind loads and the wind load values predicted by Bernoulli's equation are much larger in this case because of the higher degree of cable wind interaction.

6.5 Dynamic analysis of wind-loaded line section

To illustrate the proposed methodology and assess the effects of this new wind load model on the line response calculation, the line section model is studied under the four wind load models derived by FSI analysis (See Fig. 6.8).

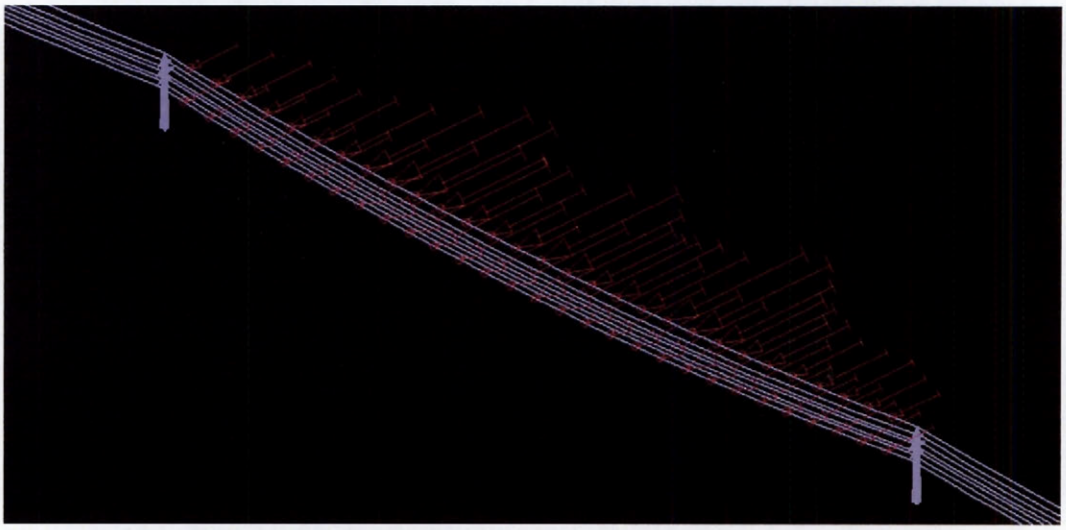

Fig. 6.8. 3-D transmission line model with wind load determined from FSI analysis.

Fig. 6.9 displays the four wind speed records used in the study, which are based on natural wind measurements in Quebec. The sampling rate of the available wind records is 1/s. The power spectral density functions of these wind records are displayed in the bottom right insert of the graph.

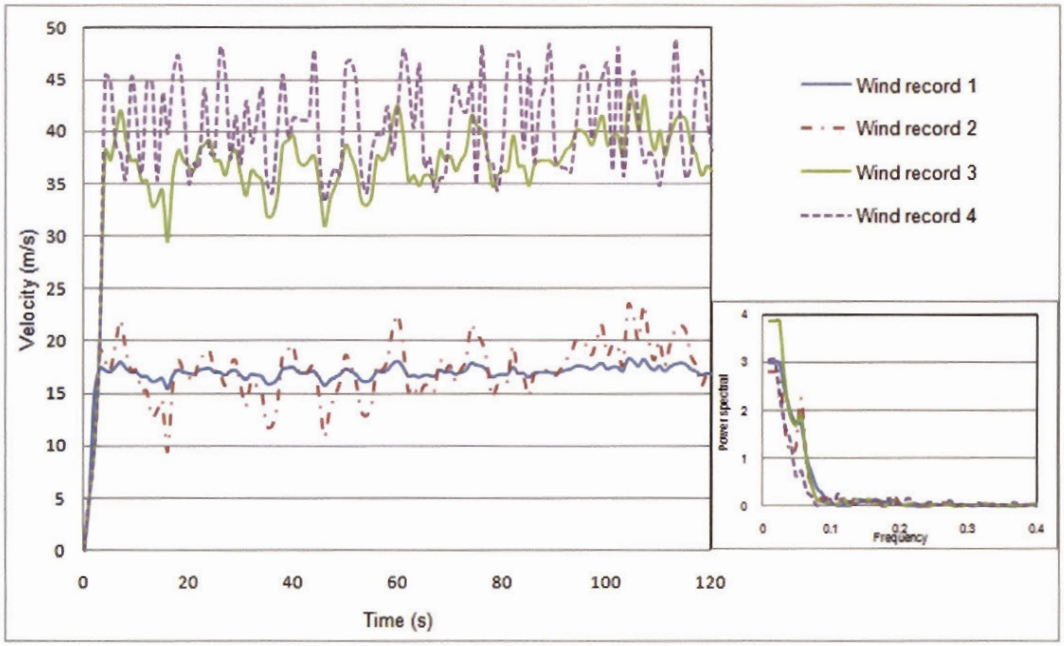

Fig. 6.9. Four incident wind velocity time histories used in this study.

Results from nonlinear dynamic analysis of the short line section subject to wind loading obtained from both the proposed method and using Bernoulli's equation are compared next. Among the many response indicators computed by nonlinear dynamic analysis, a selection was made to highlight the salient features of the results and illustrate the differences predicted by the (FSI-based and Bernoulli wind loading methods). The conductor displacements and tension are first examined, followed by internal forces such as the horizontal shear and axial force in one of the tower legs. For the sake of brevity, conductor tensions and horizontal displacements for wind record 4 are displayed in Fig. 6.11 and 6.10 while the numerical results for all four wind records are summarized in Table 6.1.

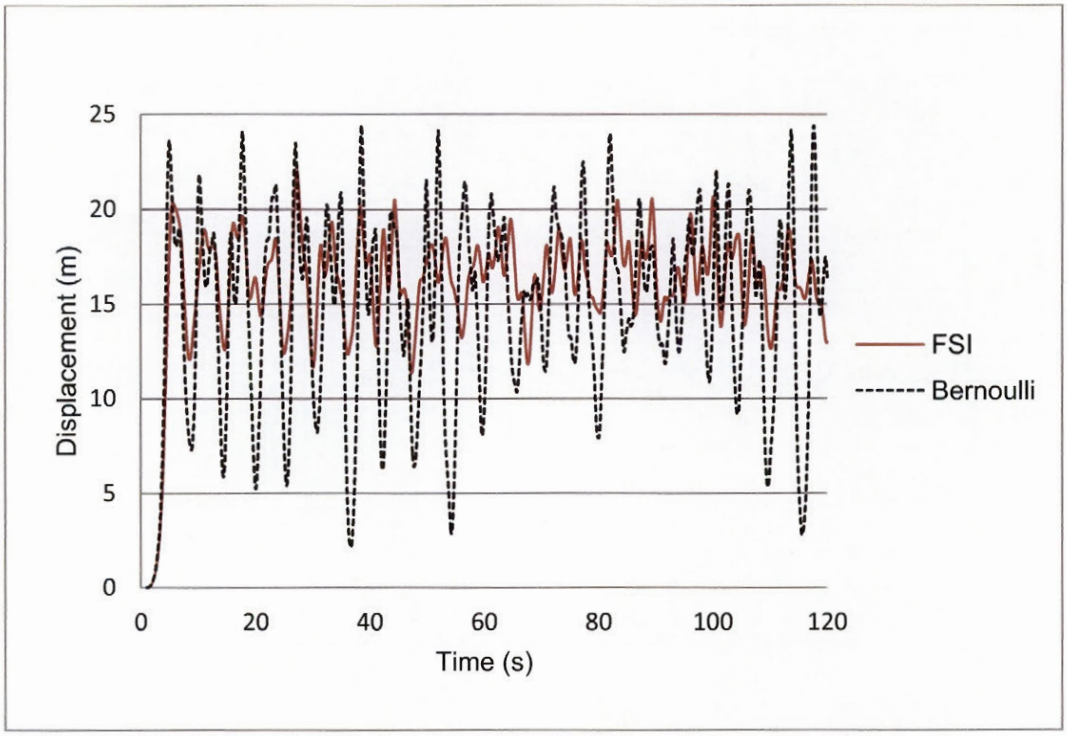

Fig. 6.10. Conductor horizontal displacement at the mid span subject to Wind record 4.

Table 6.1 *Conductor response to different wind loadings.*

Wind Record Time History	Average wind speed (m/s)	Turbulence intensity (%)	Conductor maximum horizontal displacement at mid span (m)		Conductor horizontal tension (kN)	
			FSI	Bernoulli	FSI	Bernoulli
1	16.8	8.7	6.0	8.1	20.0	20.4
2	17.1	37.2	7.8	10.1	21.1	21.5
3	36.5	19.3	20.5	21.4	38.3	44.1
4	39.8	23.2	22.1	24.5	45.0	71.0

Table 6.1summarizes the conductor response results. It is seen that for lower wind speeds (Records 1 and 2) the FSI-based loading yields significantly smaller displacements (by 26% and 23%, respectively) than Bernoulli's approach although the conductor tensions are comparable with differences less than 2%. For the two stronger wind records (3 and 4), the displacements

obtained with FSI-based loading are still smaller but the differences are less important (4% and 9% respectively). However, the differences in conductor tensions are very significant, with 13% and 37%, respectively. These results suggest that the Bernoulli method is overly conservative at high wind speed and turbulence intensities that characterize wind storm events that likely govern the design.

Horizontal displacement of conductors is an important parameter in transmission line design and in selecting tower top geometry: underestimating it can result in clearance violations while overestimating it can make the line construction very expensive by increasing required clearances as well as the right of way, which can have significant environmental impacts. It is seen from Fig. 6.10 and Table 6.1 that the benefits of wind-conductor interaction analysis become more important in higher wind speed with high turbulence intensity.

In Fig. 6.11 the horizontal tension in the conductor predicted with the two load models is compared for Wind record 4. Conductor tension is the most important factors in determining the structural loading of towers. Overestimating it can greatly penalize tower design, especially in angle suspension towers and in strain towers. Results in Table 6.1 indicate that conductor tension is overestimated when wind-conductor interaction is neglected, and this overestimation will increase with conductor motion: For FSI-based Wind record 1, the overestimation is of approximately 2% only while it increases to 55% for Wind record 4. Comparing the effects of wind turbulence intensity and average wind speed of the wind records shows that the peak tension is more affected by wind speed than turbulence intensity.

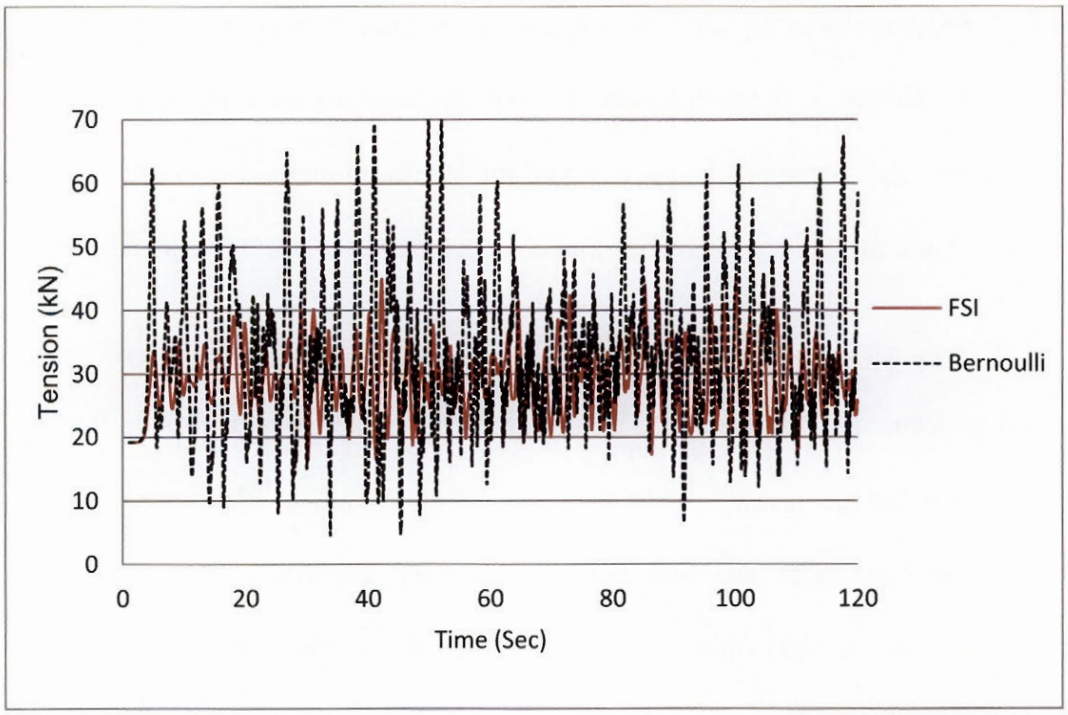

Fig. 6.11. Conductor horizontal tension in the span subject to Wind record 4.

As mentioned previously, the difference in the wind pressure evaluation not only affects the conductor tension and mid span displacement predictions but it also greatly affects the loads transferred to the tower attachment points, which affect the internal forces in all the tower members and line components. To illustrate these effects on the tower internal forces, time histories of the transverse shear force and axial force in one of the tower legs obtained from dynamic analysis are compared in Fig. 6.13 and 6.14 for Wind record 2. Despite the small difference in the predicted conductor tension (by approximately 2% only), the magnitudes of the swing angle of the suspension insulating strings predicted by the two wind load models are considerably different as shown in Fig. 6.12. This explains why the Bernoulli load model overestimates the shear force and axial force in the tower leg by as much as 21% and 19% respectively.

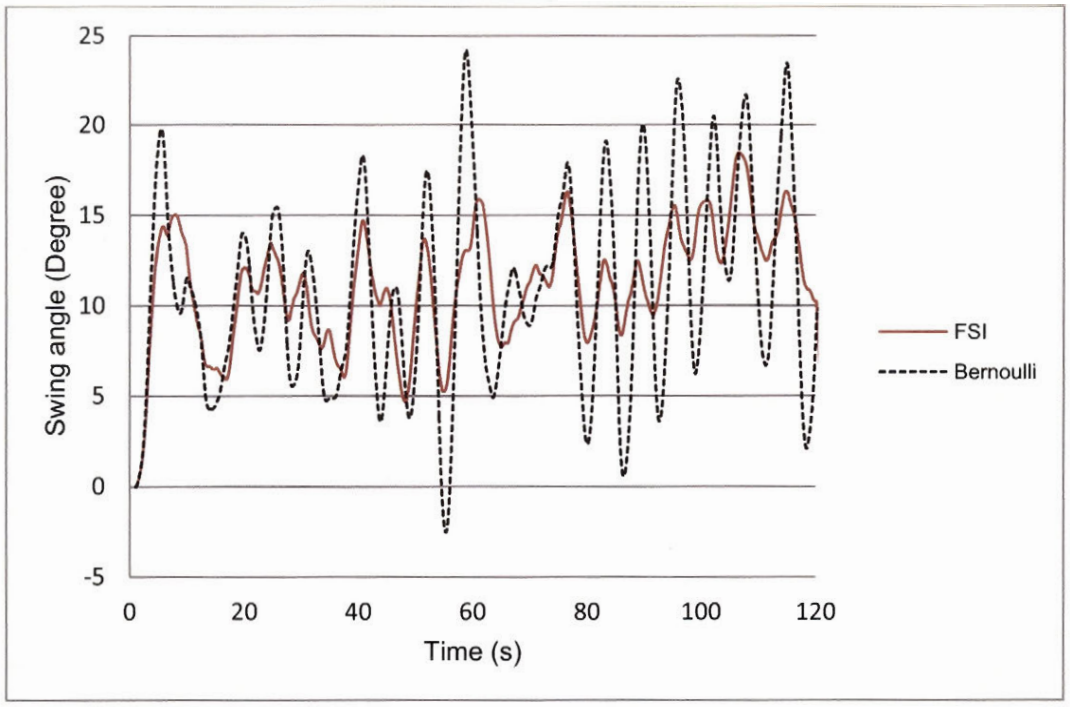

Fig. 6.12. Insulator swing angle in suspension tower supporting the loaded span subject to Wind record 2

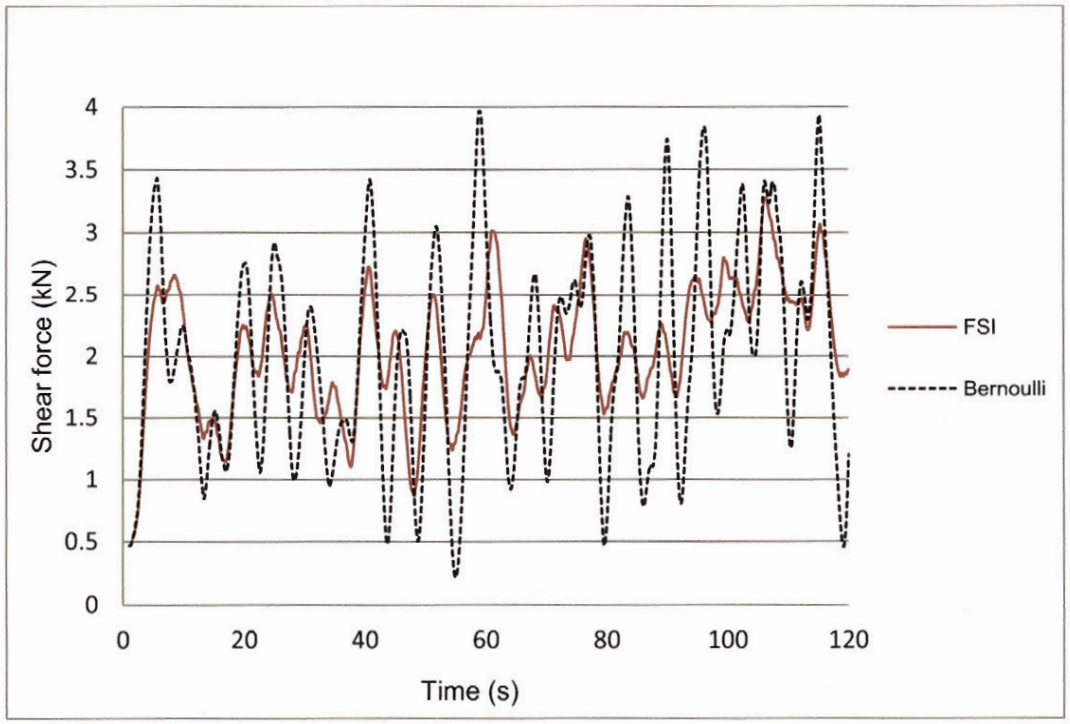

Fig. 6.13. Transverse shear force in tower leg supporting the loaded span subject to Wind record 2.

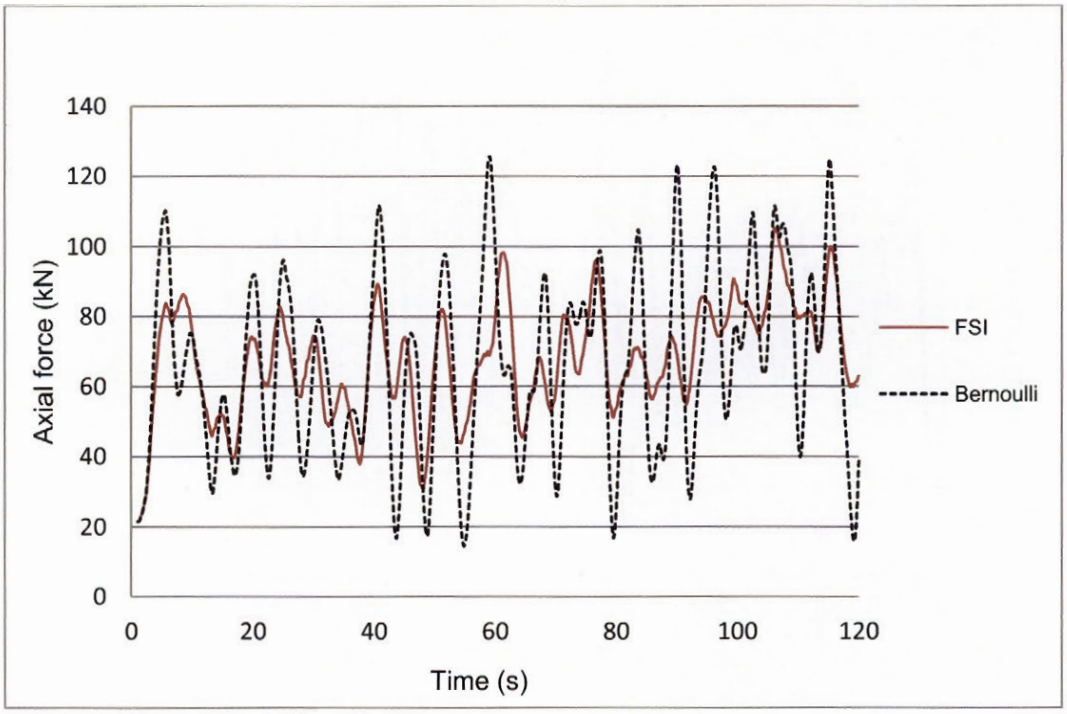

Fig. 6.14. Axial force in tower leg supporting the loaded span subject to Wind record 2.

6.6 Conclusions

In this paper a new method is proposed to determine wind loading of transmission lines with a view to obtain a more accurate representation of pressure loads acting on moving line conductors than provided by the pseudo-static pressure calculation based on Bernoulli's equation which neglects any fluid-structure interaction. It combines two-dimensional CFD and FSI analyses on conductor sections moving in their surrounding wind flow, which yield the resultant wind load on the conductor. The wind load time histories are then used as input in a three-dimensional finite element model of a line section for nonlinear dynamic analysis.

Four different natural wind records are used to generate the conductor load cases using the proposed FSI-based method and the Bernoulli's equation method prescribed in most overhead line design standards [1, 3, 4]. For the sake of brevity, only a few line response parameters are

presented which show that the current method neglecting wind-conductor interaction overestimates the wind pressure on the conductor within the span where it experiences large displacements. Owing to conductor flexibility, a large portion of the span experiences sizeable horizontal displacements especially in the suspension spans where the conductor is attached to suspension insulator strings. Thereafter in the gusty wind condition, where conductors experience large displacements, the Bernoulli method overestimates the total wind load on the line and the conductor tensions, which results in higher internal forces in tower members. These results clearly show that wind-conductor interaction should be considered in wind pressure evaluation on conductors, especially in gusty conditions where conductors experience notable displacements.

It is understood that the procedure is meant to assess the degree of conservatism of current simplified wind load models based on static methods, and is not recommended for direct design applications as it requires specialized expertise to guarantee good results and their correct interpretation. This study is pioneering the field of computational mechanics analysis of overhead power lines: The proposed procedure is of general applicability for conductor types, line geometry, and input wind and icing conditions, which announces great potential to study the response of overhead lines to realistic climatic loading scenarios. Subsequent computational studies are planned to help improve the accuracy range of the simplified methods currently in used: a direct application is the assessment of the effect of approximations on the assumed conductor drag coefficient for various wind and ice loading conditions.

Acknowledgements

A research team grant from the *Fonds québécois de la recherche sur la nature et les technologies* (FQRNT) is gratefully acknowledged.

References

[1] Canadian Standards Association. CSA-C22.3 No. 60826-10, Design criteria of overhead transmission lines. Canadian Standards Association; 2010. p. 350.
[2] Davenport AG. Gust response factors for transmission line loading. Fifth International Conference on Wind Engineering. Colorado State University: Pergamon Press; 1979. p. 899 - 909.
[3] International Electrotechnical Commission. Design criteria of overhead transmission lines. International Standard. 3rd ed. Geneva: International Electrotechnical Commission; 2003. p. 252.
[4] ASCE. Guidelines for Elecrical Transmission Line Structural Loading. 3rd ed: ASCE; 2010.
[5] Keyhan H, McClure G, Habashi WG. Computational study of surface roughness and ice accumulation effects on wind loading of overhead line conductors. International review of Civil Engineering. 2011;2:207-14.
[6] Bathe K-J, Zhang H. A flow-condition-based interpolation finite element procedure for incompressible fluid flows. Computers & Structures. 2002;80:1267-77.
[7] ADINA R&D Inc. Automatic Dynamic Incremental Nonlinear Analysis (ADINA). Theory and Modeling Guide, 2000. Report ARD 00-7, Watertown, MA. 2009.
[8] Lapointe M. Dynamic analysis of a power line subjected to longitudinal loads: McGill University,Montréal, Canada; 2003.
[9] McClure G, Lapointe M. Modeling the structural dynamic response of overhead transmission lines. Computers & Structures. 2003;81:825-34.
[10] Keyhan H, McClure G., Habashi W.G. A fluid structure interaction-based wind load model for dynamic analysis of overhead transmission lines,. 9th International Symposium on Cable Dynamics. Shanghai, China2011. p. 86-94.
[11] Roshan Fekr M, McClure G. Numerical modelling of the dynamic response of ice-shedding on electrical transmission lines. Atmospheric Research. 1998;46:1-11.
[12] Bathe Kj. Finite Element Procedures: Prentice Hall, Pearson Education Inc.; 2006.

7 Advances in wind load modelling on overhead transmission lines

This chapter presents the concluding part of this research by comparing the results predicted by the wind loading method developed in this research against those from the design method used in engineering practice. The case study of chapter 6 is used to compare response predictions that are most relevant in overhead transmission line design, such as the peak dynamic tension developed in the conductor, the maximum conductor displacement and the internal forces in selected tower members. The comparison shows that FSI can significantly affect the predicted stresses and displacements, and consequently transmission line structural design.

This part of the work is to be presented by the author at the Cigré Canada conference in Montreal: Keyhan H., McClure G. and Habashi W.G. (2012). Advances in wind load modelling on overhead transmission lines. 2012 CIGRÉ Canada (International Council on Large Electric Systems), 24-26 September 2012, Montreal, Canada: 166.(Keyhan H. et al. 2012a)

21, rue d'Artois, F-75008 PARIS
http : //www.cigre.org

CIGRÉ-166

2012 CIGRÉ Canada Conference
Hilton Montréal Bonaventure
Montréal, Québec, September 24-26, 2012

Advances in wind load modelling on overhead transmission lines

H. KEYHAN*[1], G. MCCLURE[1], W.G. HABASHI[2]

[1]Department of Civil Engineering and Applied Mechanics, McGill University, Canada
[2]Department of Mechanical Engineering, Computational Fluid Dynamics Laboratory, McGill University, Canada

SUMMARY

All overhead transmission lines are exposed to wind effects. Wind loads on conductors are also predominant in cold climates where their combination with atmospheric icing may create very severe loading conditions on the supporting towers. Therefore accurate prediction of the wind pressure on overhead conductors is essential to conduct a reliable assessment of the line response, in terms of both electrical clearances and conductor loads transferred to supports. Spatial randomness of wind loads on overhead lines has already been addressed by stochastic analysis methods and is currently taken into account with the use of so-called span factors. Further important gains in accuracy can be obtained by examining the physics of wind effects on conductors, in both non-iced and iced conditions, with improved predictions of lift and drag forces determined from fluid-structure interaction (FSI) analysis[1].

In current overhead transmission line design codes [2, 3], it is prescribed to consider the wind load on conductors and towers as an equivalent static pressure for routine analysis, although it is understood that during wind storms the wind flow around conductors is complex and generates dynamic loads. The goal of this computational study is to provide more insight in the dynamic nature of the wind loads transferred from conductors to supporting towers with a view to assess and improve the accuracy of static design approaches. The study examines wind effects on conductors only.

In gusty wind conditions with high turbulence intensity, conductors may experience large horizontal displacements that affect their surrounding wind flow. A physically accurate wind load evaluation on conductors is possible by computational wind-structure interaction analysis. To date, largely due to its high computational cost and the lack of experimental data to validate computational models, an advanced fluid-structure analysis framework for wind-cable interaction has not been developed.

Hooman.keyhan@mail.Mcgill.ca.

This paper presents a new approach based on FSI analysis to evaluate equivalent wind loads on overhead conductors. The FSI analysis is carried in two dimensions where the detailed conductor section geometry and surrounding air flow are modelled, considering a given incident wind speed. The conductor cross section is assumed to be supported on flexible supports to study the interaction between the conductor motion and the air flow. For this purpose the conductor's horizontal and vertical stiffness terms are evaluated along the span: cross sections closer to the anchor and suspension points are therefore assigned stiffer support conditions than cross sections further inside the span. FSI analysis yields both the fluid and structure response. Of particular interest is the wind pressure field on the conductor section, which allows the computation of the resultant drag and lift forces. This contour integration process is repeated for several cross sections along the span and the resulting forces provide the effective span-wise wind load distribution on the conductor.[4, 5] This wind loading is then used as input in a separate 3-D computational nonlinear dynamic analysis model to predict the line response. This dynamic analysis of the line section can be detailed to represent very realistic line sections including conductors, suspension links and supporting towers.

KEYWORDS

Fluid-structure interaction- Overhead line conductor- Wind load- Dynamic analysis

7.1 Wind Load Model

In this study four different natural wind records have been applied on ACSR 54/7 conductor to evaluate wind lift and drag forces that account for wind-cable interaction (see figure 7.1). The wind pressures obtained from this analysis are compared against pressures predicted by standard OHL wind calculation practice based on Bernoulli's equation [2, 3]. The resultant wind forces on the conductor cross section obtained from different methods employed in this study are presented in figure 7.2. These resultant forces are then used as input load for dynamic analysis of a detailed numerical model of a 120 kV double-circuit line section comprising five spans supported by tangent suspension lattice supports and two straining towers at both ends. The suspension towers have been modeled in detail while the straining towers are simply represented by fixed support points. The results obtained from these analyses are compared to assess the influence of wind-conductor interactions on the line response. A static analysis is also conducted based on the simplified static wind loading method employed in Canadian design criteria of overhead transmission lines [2] and the predicted dynamic responses from both methods are compared. In the static method the ten-minute average wind speed is used as required by CSA-C22.3 No. 60826-10 [2] and a span factor of 1.00 is used because of the complete correlation in wind pressure used along the span. To obtain the combined wind factor in the simplified static method, conductor heights are assumed to be constant at 10 m above ground to exclude height adjustment effects and different terrain categories are used based on wind record turbulence intensity. A drag coefficient of 1.12 is used in the static method based on previous detailed computational studies conducted on ACSR54/7.[4, 5]

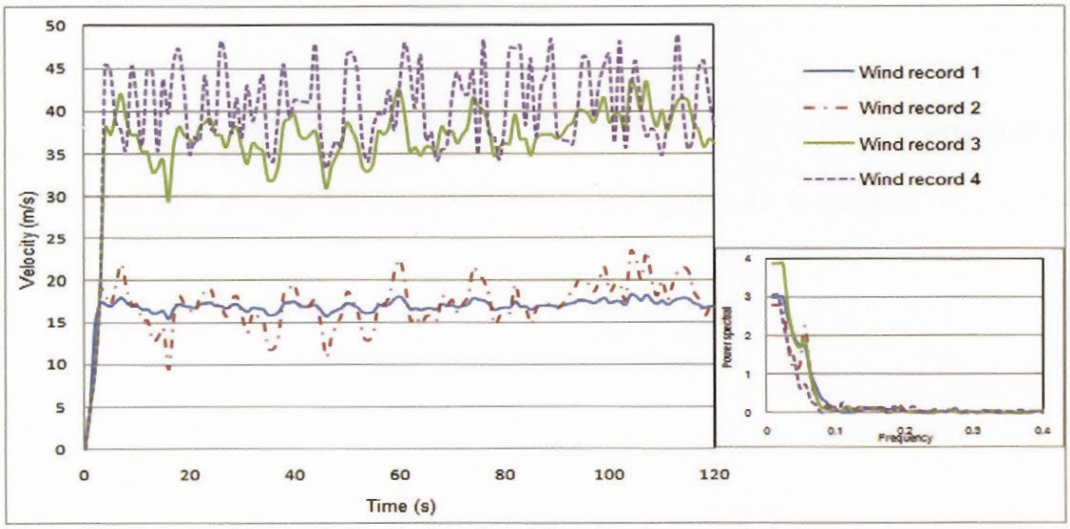

Figure-7.1Four incident wind velocity time histories (spectra in insert) used in this study.

7.2 Results

The computational results indicate that neglecting wind-cable dynamic interactions overestimates the line response to wind load. The level of over estimation depends on the magnitude and frequency content of the wind speed time history and the natural frequencies of the oscillating conductor in its wind flow. In Table 7.1 results from all three methods are presented for conductor tension, maximum horizontal conductor displacement, insulator

swing angle, as well as axial force in one of the tower legs. Because of the limited space available, only the results for the second wind record are presented in figures 7.3 to 7.6. This wind record is deemed representative of every day conditions.

In the case study presented it is observed that for the average wind speed of 16.8 m/s with moderate turbulence intensity, neglecting wind-conductor interactions (CSA quasi static approach) does not affect the maximum conductor tension significantly (the over prediction is of only 2 % on the maximum amplitude - see table 7.1), while the horizontal displacement at mid span is over predicted by 35% and insulator swing angle by 7%. Comparing the internal force in one of the tower legs shows about 55% over estimation by the static method compared to FSI-based dynamic analysis. For the second wind record with average wind speed of 17.2 and turbulence intensity, neglecting wind-conductor interactions does not affect conductor tension notably (see figure 7.4) but the horizontal displacement is over predicted by 27% (see figure 7.3) and insulator swing by 20%. In this load case the tower leg axial force is over predicted by 38% (see figure 7.5). In these first two load cases which are representing moderate wind effects, the difference in the wind load model results is directly reflected in the insulator swing angle and hence conductor displacement rather than conductor tension. A larger swing angle will lead to larger horizontal load transfer from conductor to tower and that will result in larger internal forces in the tower leg members.

Considering the results obtained with the third wind record of average wind speed of 36.5 m/s and fairly high turbulence intensity, the conductor tension is over predicted by the static method only by about 5% while the conductor displacement and insulator swing obtained from both methods are practically the same. Nonetheless, the difference in the tower leg axial force reaches 25%. Considering the last wind record with average wind speed of 39.8 m/s and high turbulence intensity, (record 4 in table 7.1), the computational results indicate that neglecting wind-cable interactions leads to a considerable over prediction of the maximum conductor tension (12%) while the horizontal displacement at mid span is over predicted by only 1%. For cable tensions, it is seen that this potentially large over estimation has a strong incidence on over predicting tower loading, especially in straining towers in such a high conductor tension range. In the case of wind records 3 and 4, the insulator swing angles are so large that the difference in wind pressure predicted by different methods cannot considerably add to swing angles and displacements but the difference is rather reflected in the conductor tension as well as internal forces in tower members.

Table 7.1. Results obtained from different wind load models.

		Wind record 1	Wind record 2	Wind record 3	Wind record 4
Two minutes Average wind speed (m/s)		16.8	17.2	36.5	39.8
Turbulence intensity (%)		8.7	37.2	19.3	23.2
Conductor maximum horizontal displacement at mid span (m)	FSI	6.0	7.8	20.5	22.1
	Bernoulli	8.1	10.1	21.4	24.5
	CSA	8.2	9.92	20.6	22.3
Maximum conductor horizontal tension (kN)	FSI	20.0	21.1	38.8	45
	Bernoulli	20.4	21.5	44.1	71
	CSA	20.7	21.6	40.8	50.3
Maximum leg axial force (kN)	FSI	38.9	60.7	355.5	462.0
	Bernoulli	75.1	81.6	621	1160
	CSA	60.54	83.8	444.9	678.7
Maximum insulator swing (degree)	FSI	14.2	19.2	60.0	64.0
	Bernoulli	19.7	25.1	69.8	84.0
	CSA	19.7	24.2	59.6	64.4

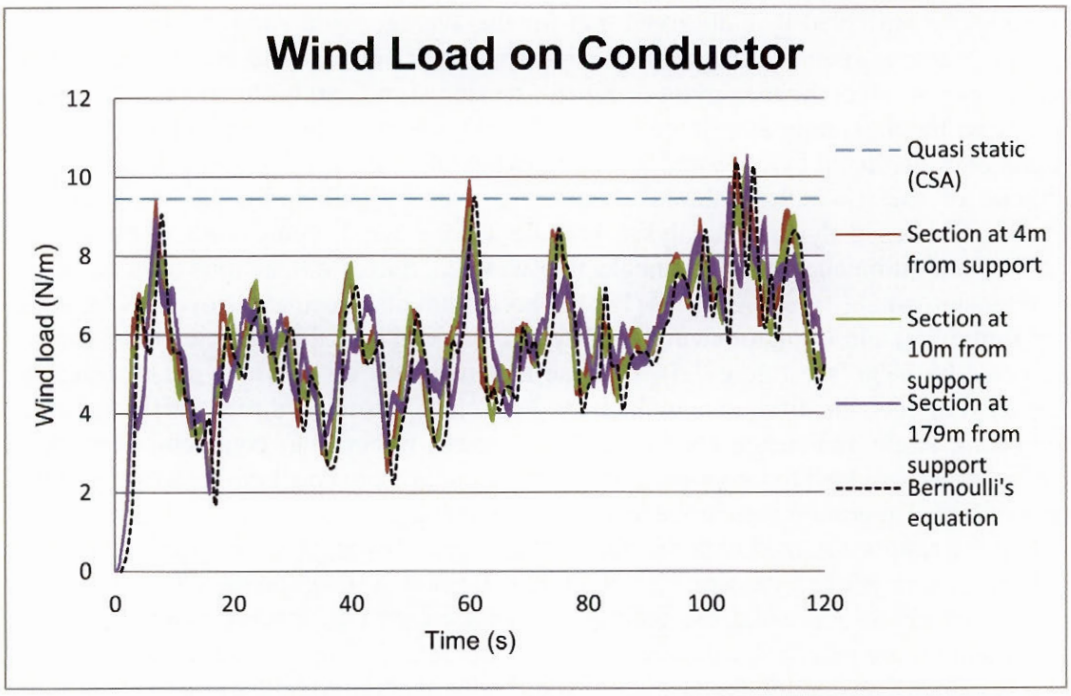

Figure-7.2Calculated wind load on conductor at three different positions along the span (Wind record 2).

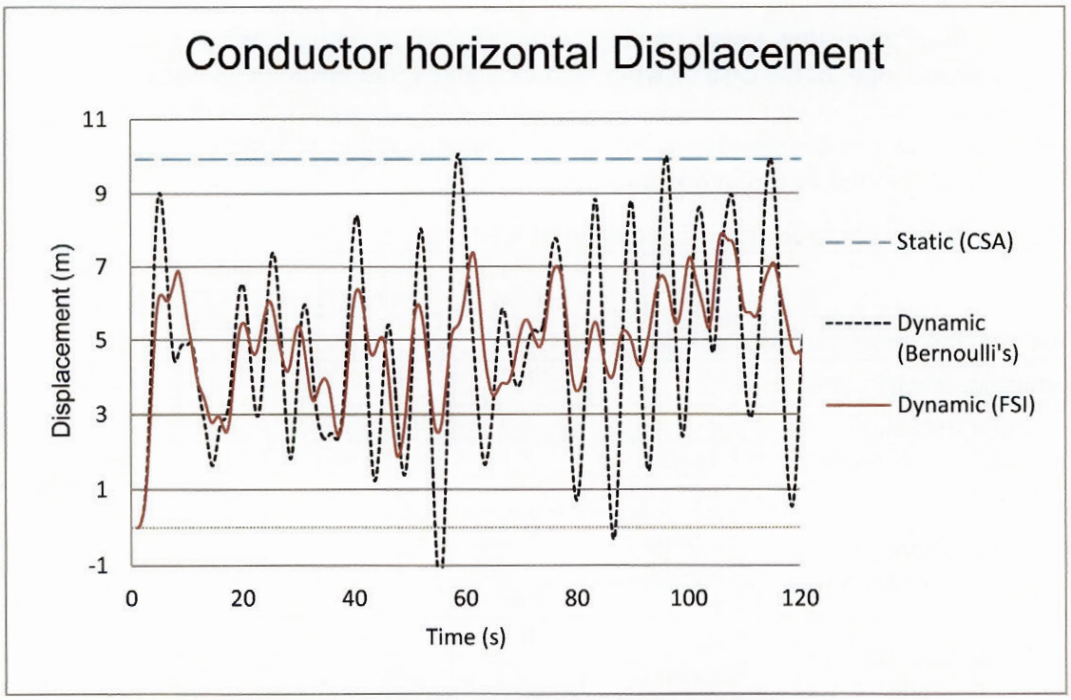

Figure-7.3 Conductor horizontal displacement at the mid span (Wind record 2)

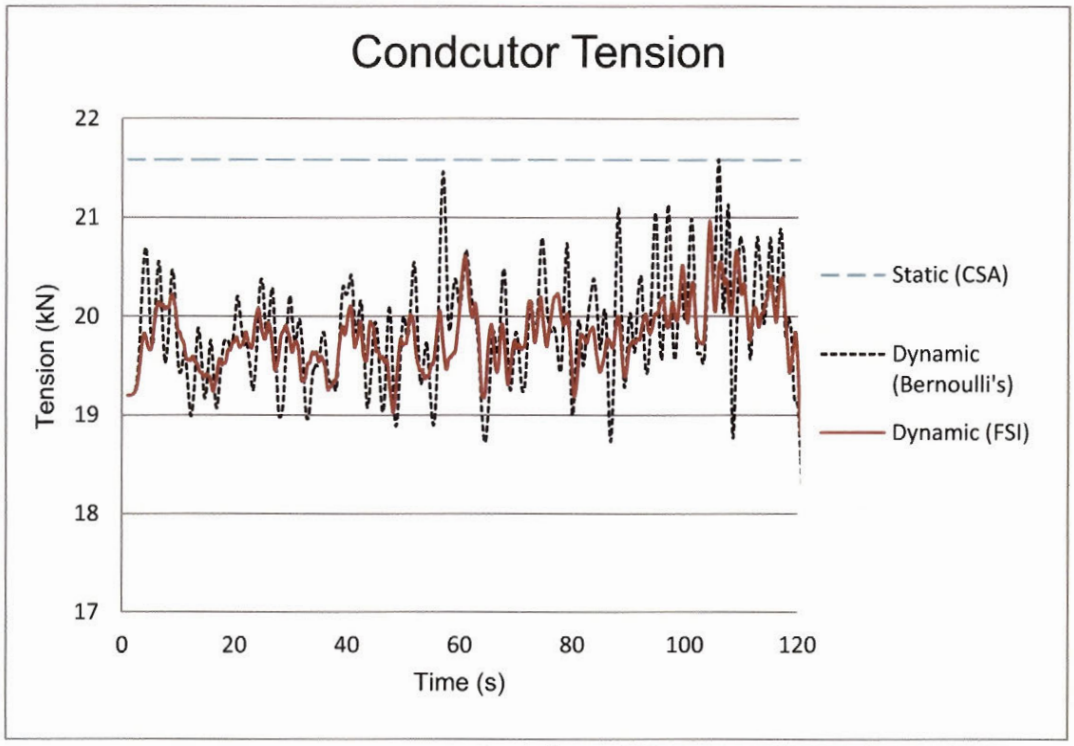

Figure-7.4 Mid span conductor tension in the loaded span (Wind record 2)

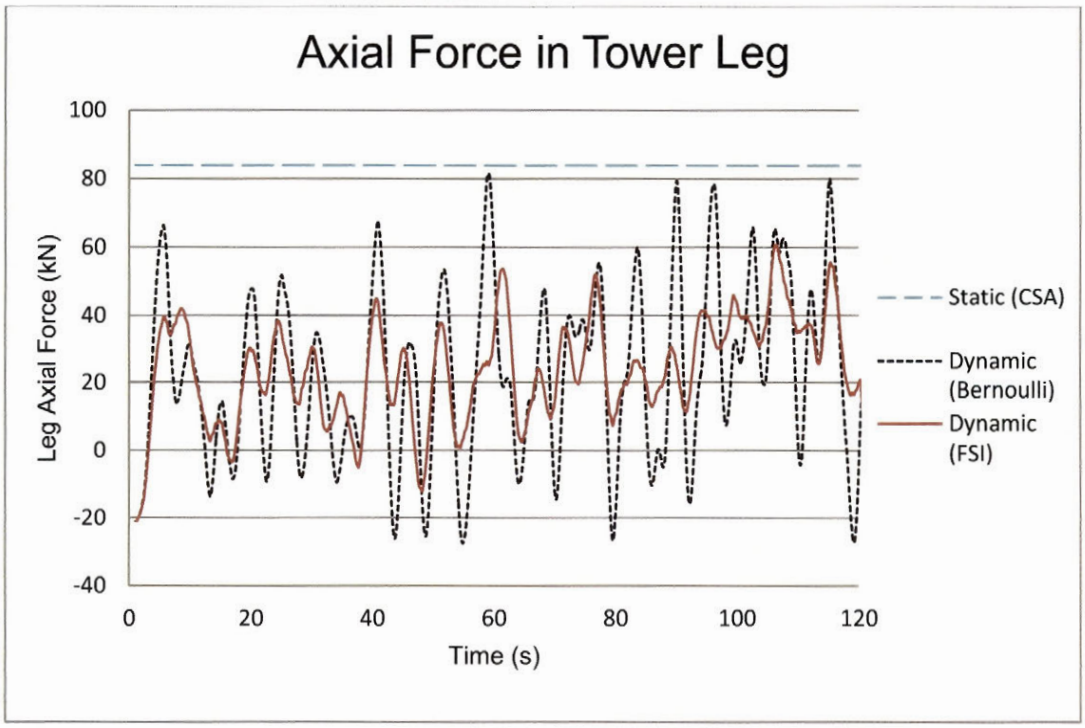

Figure-7.5 Axial force in the suspension tower leg subject to wind load (Wind record 2)

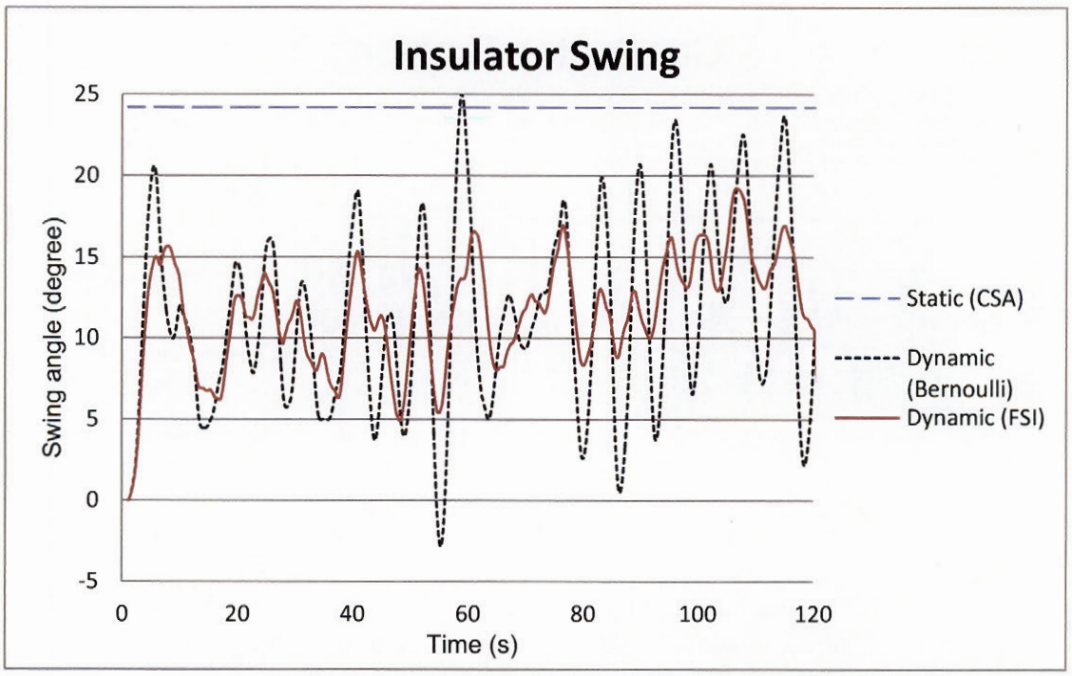

Figure-7.6 Insulator swing in the tower adjacent to the span subjected to the wind load (Wind record 2)

7.3 Conclusions

In this study a new method is proposed to determine wind loading of transmission lines with a view to obtain a more accurate representation of pressure loads acting on moving line conductors than provided by the pseudo-static pressure calculation based on Bernoulli's equation, which neglects any fluid-structure interaction. Results from this study indicate that neglecting wind-cable interactions leads to over prediction of several line design parameters such as conductor displacement and internal forces in tower members.

It should be emphasized that the writers do not advocate the "complexification" of overhead line wind analysis with the introduction of FSI and dynamic computational simulations in engineering offices. They rather propose to use these advanced computational methods in a research and development context, to evaluate and possibly improve current wind analysis methods. Another very interesting application of this computational technique relates to optimized cross-sectional design of conductors, in terms of geometry and surface roughness. Detailed FSI analysis also enables the evaluation of aerodynamic damping of various cable geometries.

As many Canadian utilities are reassessing the reliability levels of their transmission infrastructure and making difficult investment decisions, a more realistic wind loading model could be of high value.

Acknowledgements
A research team grant from the Fonds québécois de la recherche sur la nature et les technologies (FQRNT) is gratefully acknowledged.

BIBLIOGRAPHY

[1] Bathe K.J. "Finite Element Procedures."(Prentice Hall, Pearson Education Inc.; 2006 1037 p.)
[2] Canadian Standards Association. "CSA-C22.3 No. 60826-10, Design criteria of overhead transmission lines." (Canadian Standards Association; 2010. 350 p.)
[3] ASCE. "Guidelines for Elecrical Transmission Line Structural Loading." (3rd ed: ASCE; 2010. 191 p.)
[4] Keyhan H., McClure G., Habashi W.G." Computational study of surface roughness and ice accumulation effects on wind loading of overhead line conductors."(International Review of Civil Engineering. 2011 vol.2 pages 207-214.)
[5] Keyhan H., McClure G., Habashi W.G. "A fluid structure interaction-based wind load model for dynamic analysis of overhead transmission lines." (Proceedings of the 9th International Symposium on Cable Dynamics. Shanghai, China. 2011. pages 86-94)

8 Conclusions

8.1 Summary and main conclusions

The doctoral research presented in this dissertation has achieved its main goal: to develop a wind load model for overhead transmission line that takes wind-conductor interactions into account.

A new methodology was proposed and tested to determine wind loading of transmission lines based on a more accurate representation of aerodynamic forces acting on moving conductors than provided by the pseudo-static pressure calculation based on Bernoulli's equation which neglects any fluid-structure interaction. It combines two-dimensional CFD and FSI analyses on conductor sections moving in their surrounding wind flow, which yield the resultant wind load on the conductor. The wind load time histories are then used as input in a three-dimensional finite element model of a line section for nonlinear dynamic analysis.

In the first part, the research concentrated on the study of conductor aerodynamic properties and the wind pressure flow acting on the conductor for different conductor geometries (icing conditions) and incident wind velocities. The next step was to integrate these results on the conductor interface to obtain net section forces and use them as a basis for the proposed wind load model. In the last step a 3-D numerical line model is used to compare the line response predictions from the proposed wind load method and existing methods used in practice, which neglect wind-conductor interaction effects.

Results from FSI analysis show that the wind pressure on the conductor is far from uniform and depends on the conductor cross-sectional shape, surface roughness, wind velocity and turbulence, and also on wind-conductor interactions due to conductor motion. The numerical examples selected to demonstrate the approach are based on realistic transmission line data and the results indicate that including wind-conductor

interactions in wind loading predictions on line conductors has considerable effect on overhead transmission line response to wind load.

The line response parameters which are discussed in the thesis show that the current method based on Bernoulli's static pressure equation, which neglects wind-conductor interaction, overestimates the wind pressure on the conductor within the span where it experiences large displacements. Owing to conductor flexibility, a large portion of the span experiences sizeable horizontal displacements especially in the suspension spans where the conductor is attached to suspension insulator strings. Thereafter in the gusty wind condition, where conductors experience large displacements, the Bernoulli method overestimates the total wind load on the line and the conductor tensions, which results in higher internal forces in tower members. These results clearly show that wind-conductor interaction should be considered in wind pressure evaluation on conductors, especially in gusty conditions where conductors experience notable displacements.

8.2 Research limitations

There have been two major constraints that have limited the outcome of this research: 1) restrictions on computational resources, and 2) the lack of available results from physical experiments. The research was essentially based on the numerical modeling of fluid-structure interactions and required extensive numerical modeling and lengthy computations, both in the fluid and solid domains and at the conductor surface. Because of the complexity of the wind flow around the conductor, a very fine mesh and small time step were needed to capture the response in the fluid domain.

The research was carried out using the CLUMEQ Supercomputer Center with supercomputing platforms, initially at Krylov and later at Guillimin. However, the efficiency of the parallel computation was limited because the academic version of ADINA has a set limit of a single node which amounted to 8 CPUs on the Guillemin server. Note that the full commercial version of ADINA that is now available allows for multiple nodes so at CLUMEQ it could be run with a maximum of 128 CPUs. With this

limitation, the numerical FSI analysis of each model took about one calendar month to process. We were also limited in the number of jobs to be submitted in CLUMEQ. With the improved version, the computation time could be reduced to 5 to six days.

Another limitation in this research was related to the lack of experimental results available for comparison with the computational results. Most of existing wind tunnel test results could not be used because they have been affected by the size and boundary conditions of the tunnel, which are not present in natural conditions. Also in the reported field measurements, variations in parameters like wind direction and turbulence intensity as well as air temperature do affect the reported results considerably.

8.3 Application of the proposed method in engineering practice

In this research a new method is proposed to determine wind loading of transmission lines with a view to obtain a more accurate representation of pressure loads acting on moving line conductors than provided by the pseudo-static pressure calculation based on Bernoulli's equation, which neglects any fluid-structure interaction. Because of its complexification and high computational demand, this method is not proposed to be used directly in the engineering office rather it is proposed to be used as a tool with high accuracy during reassessing the reliability levels of transmission infrastructure. Many utilities in Canada and around the world need a reliable and precise method to reassess their existing transmission line reliability levels before making difficult investment decisions.

The author also proposes to use the advanced computational method in a research and development context, to evaluate and possibly improve current wind analysis methods. Another very interesting application of this computational technique relates to optimized cross-sectional design of conductors, in terms of geometry and surface roughness.

9 References

ADINA R&D Inc (2009). ADINA Systems online Manuals. 71 Elton Ave, Watertown, MA 02472, USA.

ADINA R&D Inc. (2009). "Automatic Dynamic Incremental Nonlinear Analysis (ADINA). Theory and Modeling Guide. Report ARD 00-7, Watertown, MA.".

ASCE (2010). Guidelines for Elecrical Transmission Line Structural Loading, ASCE Manuals and Reports on engineering Practice No. 74. 1801 Alexander Bell Drive, Roston, Virginia 20191, ASCE.

Ball, N. G., Rawlins, C. B. and Renowden, J. D. (1992). "Wind tunnel errors in drag measurements of power conductors." *Journal of Wind Engineering and Industrial Aerodynamics* **41**(1–3): 847-857.

Bartoli, G., Cluni, F., Gusella, V. and Procino, L. (2006). "Dynamics of cable under wind action: Wind tunnel experimental analysis." *Journal of Wind Engineering and Industrial Aerodynamics* **94**(5): 259-273.

Battista, R. C., Rodrigues, R. S. and Pfeil, M. S. (2003). "Dynamic behavior and stability of transmission line towers under wind forces." *Journal of Wind Engineering and Industrial Aerodynamics* **91**(8): 1051-1067.

Canadian Standards Association (CSA) (2010). CSA-C22.3 No. 60826-10, Design criteria of overhead transmission lines, Canadian Standards Association**:** 350.

Cluni, F., Gusella, V. and Bartoli, G. (2008). "Wind tunnel scale model testing of suspended cables and numerical comparison." *Journal of Wind Engineering and Industrial Aerodynamics* **96**(6–7): 1134-1140.

Davenport, A. G. (1979a). Gust response factors for transmission line loading. Fifth International Conference on Wind Engineering. Colorado State University, Pergamon Press.

Davenport, A. G. (1979b). Gust response factors for transmission line loading. Fifth International Conference on Wind Engineering, 1979, Colorado State University, Pergamon Press**:** 899-909.

El-Attar, M. M. (1997). Nonlinear Dynamics and Seismic Response of power Transmission Lines. Ph.D. thesis, McMaster University,Hamilton, Canada., 254.

EPRI (2006). Transmission line design reference book: Wind-induced conductor motion Palo Alto, California, Electric Power Research Institute.

Farzaneh, M. (2008). Atmospheric Icing of Power Networks. Université du Québec à Chicoutimi, Canada., Springer.

Fikke, S., Rolfseng, L. and Ghonnoun, E. (2005). Collecting and using weather data for the design of overhead lines according to IEC 60826. 11th International Workshop on Atmospheric Icing of Structures, June 2005, Montreal, Canada.**:** 105-111.

Forster, C. (2007). Robust methods for fluid-structure interaction with stabilised finite elements. Ph.D. Thesis, University of Stuttgart,Stuttgart, Germany., 184.

Glück, M., Breuer, M., Durst, F., Halfmann, A. and Rank, E. (2001). "Computation of fluid-structure interaction on lightweight structures." *Journal of Wind Engineering and Industrial Aerodynamics* **89**(14-15): 1351-1368.

Guruswamy, G. P. (1990). "A multidisciplinary program for fluid/structural interaction studies of aerospace vehicles." *Computing Systems in Engineering* **1**(2-4): 237-256.

International Electrotechnical Commission (IEC) (2003). Design criteria of overhead transmission lines (IEC 60826). International Standard. Geneva, International Electrotechnical Commission**:** 252.

Joel H, F. (1990). "Approaches to turbulent flow computation: Applications to flow over obstacles." *Journal of Wind Engineering and Industrial Aerodynamics* **35**(0): 1-19.

Kálmán, T., Farzaneh, M. and McClure, G. (2007). "Numerical analysis of the dynamic effects of shock-load-induced ice shedding on overhead ground wires." *Computers & Structures* **85**(7–8): 375-384.

Keyhan H., McClure G. and Habashi W.G. (2011a). "Computational study of surface roughness and ice accumulation effects on wind loading of overhead line conductors." *International Review of Civil Engineering* **2**(2): 207-214.

Keyhan H., McClure G. and Habashi W.G. (2011b). On computational modeling of interactive wind and icing effects on overhead line conductors. International Workshop on Atmospheric Icing of Structures (IWAIS), May 8-13, 2011, Chongqing, China**:** B-5-1-28.

Keyhan H., McClure G. and Habashi W.G. (2012a). Advances in wind load modelling on overhead transmission lines. 2012 CIGRÉ Canada (International Council on Large Electric Systems), 24-26 September 2012, Montreal, Canada.**:** 166.

Keyhan H., McClure G. and Habashi W.G. (2012b). "Dynamic analysis of an overhead transmission line subject to gusty wind loading predicted by wind-conductor interaction." *Computers & Structures (CAS-D-12-00549, submitted in 12 June 2012).*

Keyhan H., McClure G. and Habashi W.G. (2012c). "Fluid-Structure Interaction analysis of wind effects on overhead transmission line conductors." *Wind Engineering & Industrial Aerodynamics (Manuscript number: INDAER-D-12-00062, submitted in 22 March 2012).*

Khedr, M. A. H. (1998). Seismic analysis of lattice towers. Ph.D. Thesis, Department of Civil Engineering and Applied Mechanics, McGill University, Montreal, Canada, 269.

Krishnan, A. G. (2006). Orbital Dynamics Analysis and Scale Model Testing of Galloping Transmission Lines. Ph.D., Concordia University, Montreal, Canada, 215.

Lee, C. J. K., Noguchi, H. and Koshizuka, S. (2007). "Fluid-shell structure interaction analysis by coupled particle and finite element method." *Computers & Structures* **85**(11-14): 688-697.

Liao, M. (1996). Galloping of Bundle Transmission Lines. Ph.D., University of Manitoba, Winnipeg, Canada., 116.

Loredo-Souza, A. M. (1996). The behavior of transmission line under high wind. Ph.D. Thesis, University of Western Ontario, Londoon, Canada, 223.

Loredo-Souza, A. M. and Davenport, A. G. (2003). "The influence of the design methodology in the response of transmission towers to wind loading." *Journal of Wind Engineering and Industrial Aerodynamics* **91**(8): 995-1005.

Lozowski, E., Musilek, P. and Pytlak, P. (2009). Wind and Ice Load Model Using Numerical Weather Prediction. 13th International Workshop on Atmospheric Icing on Structures & Final Workshop of COST Action 727. Andermat Switzerland**:** 108-117.

McClure, G., Langlois, S. and Rogier, J. (2008). Understanding how overhead lines respond to high intensity wind storms. Proceedings of the 2008 ASCE SEI Structures Congress,Crossing Borders. Vancouver, Canada**:** 10p.

McClure, G. and Lapointe, M. (2003). "Modeling the structural dynamic response of overhead transmission lines." *Computers & Structures* **81**(8–11): 825-834.

McClure, G. and Tinawi, R. (1987). "Mathematical modeling of the transient response of electric transmission lines due to conductor breakage." *Computers & Structures* **26**(1-2): 41-56.

Panneer, S. R. and Paterson, D. A. (1993). "Computation of conductor drag coefficients." *Journal of Wind Engineering and Industrial Aerodynamics* **50**(0): 1-8.

Rodi, W. (1993). "On the simulation of turbulent flow past bluff bodies." *Journal of Wind Engineering and Industrial Aerodynamics* **46–47**(0): 3-19.

Roshan Fekr, M. and McClure, G. (1998). "Numerical modelling of the dynamic response of ice-shedding on electrical transmission lines." *Atmospheric Research* **46**(1–2): 1-11.

Shan, L., Jenke, L. M. and Cannon Jr, D. D. (1992). "Field determination of conductor drag coefficients." *Journal of Wind Engineering and Industrial Aerodynamics* **41**(1–3): 835-846.

Tabatabai M., Krishnasamy S. G., Meale J. and Cooper K. R. (1992). "Response of smooth body, trapezoidal wire overhead (compact) conductors to wind loading." *Journal of Wind Engineering and Industrial Aerodynamics* **41**(1–3): 825-834.

Tambaca, J., Canic, S. and Mikelic, A. (2005). "A two-dimensional effective model describing fluid-structure interaction in blood flow: analysis, simulation and experimental validation." *Comptes Rendus Mécanique* **333**(12): 867-883.

Wall, W. A., Genkinger, S. and Ramm, E. (2007). "A strong coupling partitioned approach for fluid-structure interaction with free surfaces." *Computers & Fluids* **36**(1): 169-183.

Wu, Y., Sun, X. and Shen, S. (2008). "Computation of wind-structure interaction on tension structures." *Journal of Wind Engineering and Industrial Aerodynamics* **96**(10-11): 2019-2032.

Zhan, S., Xu, Y. L., Zhou, H. J. and Shum, K. M. (2008). "Experimental study of wind-rain-induced cable vibration using a new model setup scheme." *Journal of Wind Engineering and Industrial Aerodynamics* **96**(12): 2438-2451.